CHAPTER 1

Introduction

1.1 Motivation

Laser-induced fluorescence detection is an invaluable tool and has been widely applied in the fields of biology and medicine. The two most important and widely used applications of fluorescence in biomedical research are fluorescence microscopy and flow cytometry. However, because of the highly scattering and absorptive nature of biological tissue and blood, current techniques can only quantify fluorescence signals near the tissue surface. Therefore, most of the analysis can only be conducted *in vitro* or *ex vivo*. Even with multiphoton excitation using a near-infrared (NIR) pulsed laser, the penetration depth is only limited to a few hundred micrometers [1-3]. There has been a long quest to develop an optical technique to quantify fluorescence signals in deep tissue *in vivo*. Although visualization of localized fluorescence from internal regions of animal models has been demonstrated by whole-body imaging [4], such analysis is not quantitative and requires a large amount fluorescent markers to achieve enough brightness for detection. The requirement of large amount to fluorescent labeling limits its application for clinical use. Current available techniques for the analysis of fluorescently labeled molecules in tumors require invasive procedures such as surgery or biopsy. The excised tissue samples are then analyzed by microscope or flow cytometry [5-8]. However, it is critical to be able to quantify the fluorescence biomarkers in the native environment of the cells to

understand cancer biology or to monitor drug activity on specific tumors on the cellular level [9].

In order to conduct fluorescence biosensing *in vivo*, our group has developed a two-photon optical fiber fluorescence (TPOFF) probe. The use of an optical fiber circumvents the notorious problems of tissue scattering and absorption [10, 11]. In the previous version, a single-mode fiber (SMF) is used to delivery the excitation femtosecond pulses and to collect the two-photon excited (2PE) fluorescence. This simple detection configuration is essential and critical for constructing a compact *in vivo* biosensing system. Two-photon excitation provides several advantages, such as localized excitation volume at the immediate vicinity of the fiber core, reduced background, minimized photo-toxicity to the specimen, and the ability to excite multiple fluorophores by a single NIR laser [1, 12-14]. The probe was first used by Myaing *et al*. to quantify the uptake of biocompatible fluorescent dendrimer conjugates and antibodies in tumors in live mice on a real-time basis [15].

Nevertheless, because of the low numerical aperture (NA) of the SMF, the detection sensitivity is limited. In order to increase the sensitivity of the TPOFF probe, a double-clad fiber (DCF) is used. The DCF has the unique features of allowing single-mode propagation in the core to optimize the 2PE efficiency and the large NA of the multimode inner cladding to increase the fluorescence signal collection efficiency. The large NA of the inner cladding greatly enhances the two-photon fluorescence (TPF) collection efficiency. Enhanced detection sensitivity of TPOFF probe was demonstrated by Myaing *et al.* with a double-clad photonic crystal fiber (DCPCF) [16, 17]. The sensitivity was enhanced by more than one order of magnitude. However, because of the air holes in the photonic crystal structure, liquid uptake due to capillary action limited its biological applications.

In this dissertation, a solid DCF is used and the DCF-TPOFF probe is applied to aqueous environments for biological studies, as will be demonstrated in the following

chapters. The signal collection efficiency is on the same order as an objective lens-based microscope. The high sensitivity and the small 2PE probe volume open up the possibility to implement a range of molecular fluorescence spectroscopy techniques with the probe, such as fluorescence lifetime spectroscopy, fluorescence correlation spectroscopy (FCS), and fluorescence resonance energy transfer (FRET). Using the DCF- TPOFF probe, these analytic fluorescence techniques can be conducted quantitatively in real time in deep tissue to assist clinical diagnosis.

One of the biomedical challenges that may be addressed by the TPOFF probe is cell circulation dynamics. Cancer metastases rather than primary tumors are responsible for most cancer mortality. Circulating tumor cells (CTCs) in the bloodstream has been reported as a sensitive biomarker in cancer progression and metastasis [18-20]. Therefore, the quantification of CTCs is important for disease prognosis and treatment surveillance [21, 22]. Traditional assays require extraction of blood samples followed by flow cytometry analysis. However, because the blood can only be sampled intermittently, the assay cannot reflect the patient's condition in real time [23]. Use of microscope-based approaches to monitor the circulating cells *in vivo* has been demonstrated recently [24-27]. However, a serious shortcoming of current *in vivo* flow cytometry techniques is the low blood sampling rate because of the difficulty of accessing large blood vessels noninvasively. In order to practically enumerate the number of rare circulating cells (less than one cell per milliliter), a large blood volume has to be sampled. With the TPOFF probe, we can insert the fiber intravenously into large blood vessels deeper inside the body to increase the sampling rate. In addition, no anesthesia will be required for intravenous measurements in human patients, thus long-term monitoring is feasible. The high sensitivity provided by the DCF and the single-cell resolution ensured by 2PE make the DCF-TPOFF probe a suitable tool for conducting *in vivo* flow cytometry. Furthermore, with the ability to excite multiple fluorophores with a single NIR laser by 2PE, we can detect multiple cell populations simultaneously [26, 27].

1.2 Dissertation overview

In this dissertation, we use solid double-clad fibers to increase the detection sensitivity of the TPOFF system, which enables a range of new applications for *in vivo* studies.

In Chapter 2, the operating principle of the TPOFF probe system is described. The instrumentation and system parameters are described in detail. The methods and difficulty of delivery of ultrafast pulses through optical fibers are reviewed. The trade-off between the excitation and collection efficiencies is discussed. The enhanced detection sensitivity by a DCF is demonstrated. The operating principle of a time-correlation single-photon counting system for time-resolved measurements is described. Through-fiber fluorescence lifetime spectroscopy is demonstrated.

In Chapter 3, the sensitive DCF probe is used to conduct biological measurements. The results are compared to SMF probes. Both DCF and SMF probes are used to measure the targeting of dendrimer conjugates in folic acid receptor (FAR)-expressing tumor cells. Simultaneous detection of fluorescent antibody conjugates with different emission wavelengths is demonstrated.

In Chapter 4, two-photon excitation fiber fluorescence correlation spectroscopy (2PE-FFCS) is demonstrated with the DCF-TPOFF probe. The theory of 2PE FCS is presented. The 2PE-FFCS system is used to measure the diffusion of fluorescent nanoparticles and quantum dots. The feasibility of using the technique to measure flow velocity and particle size is explored.

In Chapter 5, we use the TPOFF probe to conduct flow cytometry both *in vitro* and *in vivo*. The ability to detect circulating cells in live mice is demonstrated. The two-photon excitation and detection efficiencies of various fluorescent markers and fluorescent proteins are compared. The advantages and limitations of the technique are also discussed.

In Chapter 6, a summary of the dissertation is given. The major contributions of this doctoral work are outlined and related publications are listed. Possible application and future research directions are presented and discussed.

1.3 Reference

1. K. Konig, "Multiphoton microscopy in life sciences," J Microsc 200, 83-104 (2000).
2. W. R. Zipfel, R. M. Williams, and W. W. Webb, "Nonlinear magic: multiphoton microscopy in the biosciences," Nature Biotechnology 21, 1368-1376 (2003).
3. R. Weissleder, and V. Ntziachristos, "Shedding light onto live molecular targets," Nat Med 9, 123-128 (2003).
4. C. S. Mitsiades, N. S. Mitsiades, R. T. Bronson, D. Chauhan, N. Munshi, S. P. Treon, C. A. Maxwell, L. Pilarski, T. Hideshima, R. M. Hoffman, and K. C. Anderson, "Fluorescence imaging of multiple myeloma cells in a clinically relevant SCID/NOD in vivo model: biologic and clinical implications," Cancer Res 63, 6689-6696 (2003).
5. M. J. Bellmunt, M. Portero, R. Pamplona, L. Cosso, P. Odetti, and J. Prat, "Evidence for the Maillard Reaction in Rat Lung Collagen and Its Relationship with Solubility and Age," Biochimica Et Biophysica Acta-Molecular Basis of Disease 1272, 53-60 (1995).
6. D. R. Braichotte, G. A. Wagnieres, R. Bays, P. Monnier, and H. E. Vandenbergh, "Clinical Pharmacokinetic Studies of Photofrin by Fluorescence Spectroscopy in the Oral Cavity, the Esophagus, and the Bronchi," Cancer 75, 2768-2778 (1995).
7. J. K. Frisoli, E. G. Tudor, T. J. Flotte, T. Hasan, T. F. Deutsch, and K. T. Schomacker, "Pharmacokinetics of a Fluorescent Drug Using Laser-Induced Fluorescence," Cancer Research 53, 5954-5961 (1993).
8. M. Kriegmair, R. Baumgartner, R. Knuchel, H. Stepp, F. Hofstadter, and A. Hostetter, "Detection of early bladder cancer by 5-aminolevulinic acid induced porphyrin fluorescence," Journal of Urology 155, 105-109 (1996).
9. A. Petrovsky, E. Schellenberger, L. Josephson, R. Weissleder, and A. Bogdanov, Jr., "Near-infrared fluorescent imaging of tumor apoptosis," Cancer Res 63, 1936-1942 (2003).
10. J. Y. Ye, M. T. Myaing, T. B. Norris, T. Thomas, and J. Baker, "Biosensing based on two-photon fluorescence measurements through optical fibers," Optics Letters 27, 1412-1414 (2002).
11. L. Fu, and M. Gu, "Fibre-optic nonlinear optical microscopy and endoscopy," J Microsc 226, 195-206 (2007).
12. W. Denk, J. H. Strickler, and W. W. Webb, "Two-photon laser scanning fluorescence microscopy," Science 248, 73-76 (1990).

13. W. Denk, and K. Svoboda, "Photon upmanship: why multiphoton imaging is more than a gimmick," Neuron 18, 351-357 (1997).

14. C. Xu, W. Zipfel, J. B. Shear, R. M. Williams, and W. W. Webb, "Multiphoton fluorescence excitation: new spectral windows for biological nonlinear microscopy," Proc Natl Acad Sci U S A 93, 10763-10768 (1996).

15. T. P. Thomas, M. T. Myaing, J. Y. Ye, K. Candido, A. Kotlyar, J. Beals, P. Cao, B. Keszler, A. K. Patri, T. B. Norris, and J. R. Baker, Jr., "Detection and analysis of tumor fluorescence using a two-photon optical fiber probe," Biophys J 86, 3959-3965 (2004).

16. M. T. Myaing, J. Y. Ye, T. B. Norris, T. Thomas, J. R. Baker, W. J. Wadsworth, G. Bouwmans, J. C. Knight, and P. S. J. Russell, "Enhanced two-photon biosensing with double-clad photonic crystal fibers," Optics Letters 28, 1224-1226 (2003).

17. M. T. Myaing, J. Y. Ye, T. B. Norris, T. P. Thomas, J. R. Baker, W. J. Wadsworth, G. Bouwmans, J. C. Knight, and P. S. J. Russell, "Two-photon fluorescence biosensing with conventional and photonic crystal fibers," in Conference on Optical Fibers and Sensors for Medical Applictions IV, I. Gannot, ed. (Spie-Int Soc Optical Engineering, San Jose, CA, 2004), pp. 151-157.

18. R. Weissleder, and M. J. Pittet, "Imaging in the era of molecular oncology," Nature 452, 580-589 (2008).

19. A. F. Chambers, A. C. Groom, and I. C. MacDonald, "Dissemination and growth of cancer cells in metastatic sites," Nat Rev Cancer 2, 563-572 (2002).

20. K. Pantel, R. H. Brakenhoff, and B. Brandt, "Detection, clinical relevance and specific biological properties of disseminating tumour cells," Nat Rev Cancer 8, 329-340 (2008).

21. P. Mancuso, M. Colleoni, A. Calleri, L. Orlando, P. Maisonneuve, G. Pruneri, A. Agliano, A. Goldhirsch, Y. Shaked, R. S. Kerbel, and F. Bertolini, "Circulating endothelial-cell kinetics and viability predict survival in breast cancer patients receiving metronomic chemotherapy," Blood 108, 452-459 (2006).

22. M. Cristofanilli, G. T. Budd, M. J. Ellis, A. Stopeck, J. Matera, M. C. Miller, J. M. Reuben, G. V. Doyle, W. J. Allard, L. W. Terstappen, and D. F. Hayes, "Circulating tumor cells, disease progression, and survival in metastatic breast cancer," N Engl J Med 351, 781-791 (2004).

23. E. R. Tkaczyk, J. Y. Ye, A. Myc, S. Katnik, K. E. Luker, G. D. Luker, J. R. Baker, and T. B. Norris, "In Vivo Extended Cavity Laser Enhanced Two-Photon Flow Cytometry," Journal of Biomedical Optics 13 (2008).

24. J. Novak, I. Georgakoudi, X. Wei, A. Prossin, and C. P. Lin, "In vivo flow cytometer for real-time detection and quantification of circulating cells," Optics Letters 29, 77-79 (2004).

25. V. Zharov, E. Galanzha, and V. Tuchin, "Integrated photothermal flow cytometry in vivo," Journal of Biomedical Optics 10 (2005).

26. C. F. Zhong, E. R. Tkaczyk, T. Thomas, J. Y. Ye, A. Myc, A. Bielinska, Z. Cao, I. Majoros, K. Balazs, J. R. Baker, and T. B. Norris, "Quantitative Two-Photon Flow Cytometry – in Vitro and in Vivo," Journal of Biomedical Optics 13 (2008).

27. E. R. Tkaczyk, C. F. Zhong, J. Y. Ye, A. Myc, T. Thomas, Z. Cao, R. Duran-Struuck, K. E. Luker, G. D. Luker, T. B. Norris, and J. R. Baker Jr, "In vivo monitoring of multiple circulating cell populations using two-photon flow cytometry," Optics Communications 281, 888-894 (2008).

CHAPTER 2
Two-photon Optical Fiber Fluorescence Probe

2.1 Introduction

Quantification of fluorescence signals in deep tissue using conventional techniques is complicated by the strong scattering and absorption of light. Although multi-photon excitation with ultrafast near-infrared pulses provides greater penetration into tissue samples, the depth is limited to only a few hundred microns due to the scattering and absorption of the turbid tissue [1].Whole-body fluorescence imaging or fluorescence molecular tomography techniques are limited in their ability to provide accurate quantitative information on the distribution of a fluorescently tagged molecule in tissues because of the requirement of large fluorescent signals for penetration through tissue barriers; hence, these techniques lack sensitivity for detection of low concentrations of drug uptake [2, 3].

Use of a fiber to deliver the excitation light to the desired location enables deep tissue fluorescence measurements *in vivo*. Fiber probes are widely used in biomedical spectroscopy applications. Because of their compact and minimally invasive nature, they are ideal for clinical uses and can easily be incorporated into current techniques. There are basically two types of detection schemes in fiber probes. One is to use separate fibers for excitation and collection. However, this would make the size of the probe larger, thus reducing the viability for *in vivo* clinical use. In addition, because the excitation region of two-photon excitation is only at a close proximity around the core of the fiber, using a

separate fiber to collect would greatly reduce the collection efficiency. Because of the back scattering and autofluorescence from the fiber, it was generally considered difficult to use the same fiber for light delivery and fluorescence collection [4]. However, because of the two-photon excitation scheme we employed here, the problems of back scattering and autofluorescence can be effectively suppressed.

We have developed a two-photon optical fiber fluorescence (TPOFF) probe as a minimally invasive technique for quantifying fluorescence in deep tissues in live mice on a real-time basis [5-7]. In our system, the pulses produced by a mode-locked Ti:sapphire laser are delivered through the single-mode core of the fiber to excite two-photon-induced fluorescence (TPF). The collection of the TPF signal was accomplished by either the single-mode core or the inner cladding of a dual-clad fiber (DCF) through the same fiber [8, 9]. The concept of employing a DCF to enhance the detection sensitivity will be presented in Section 2.4. Experimental demonstrations of using a DCF for biological applications will be discussed in Chapter 3. The DCF has more than an order of magnitude higher sensitivity when compared to a SMF under the same experimental conditions. The employment of a DCF in our single-fiber probe scheme is important and critical for the feasibility of the applications we will further discuss in the following chapters.

2.2 The experimental method and apparatus

The experimental setup is shown in Figure 2.1. The Ti:sapphire oscillator (Coherent Inc., Mira 900) generates 50-fs pulses at 800 nm with a 76-MHz repetition rate. The pulse is first double-passed through a 2000 line/mm reflection grating (PC 2000, Spectrogon, Parsippany, NJ) in a pulse stretcher geometry to give the pulse a negative chirp of about -35000 fs^2 to pre-compensate the linear dispersion in the fiber (about 1 meter) and the objective. The peak intensity of the output pulse is thus

optimized, which ensures maximum fluorescence intensity from the two-photon excitation (TPE) [10]. The beam is then coupled into the core of the fiber with a 40X microscope objective of numerical aperture (NA) 0.65 (Newport, M-40X). The size of the beam at the back aperture of the objective is adjusted by a telescope so that the focal spot after the objective matches the mode field diameter (MFD) of the fiber core. The fluorescence signal is collected back by the same fiber and the objective and separated from the excitation beam by a dichroic mirror. The fluorescence signal is then focused into a 0.25m monochromator (250is/sm Imaging Spectrograph, Chromex). The wavelength-resolved output spectrum is further filtered with a short-pass filter to reject the excitation laser light. The fluorescence signal is detected by a photomultiplier tube (PMT, Hamamatsu, H7422-40). This PMT sends the electrical signal to the time-correlated single-photon counting (TCSPC) module (SPC630, Becker and Hickl, GmbH) in a computer. The TCSPC module enables our system to implement steady-state wavelength-resolved or dynamic time-resolved measurements.

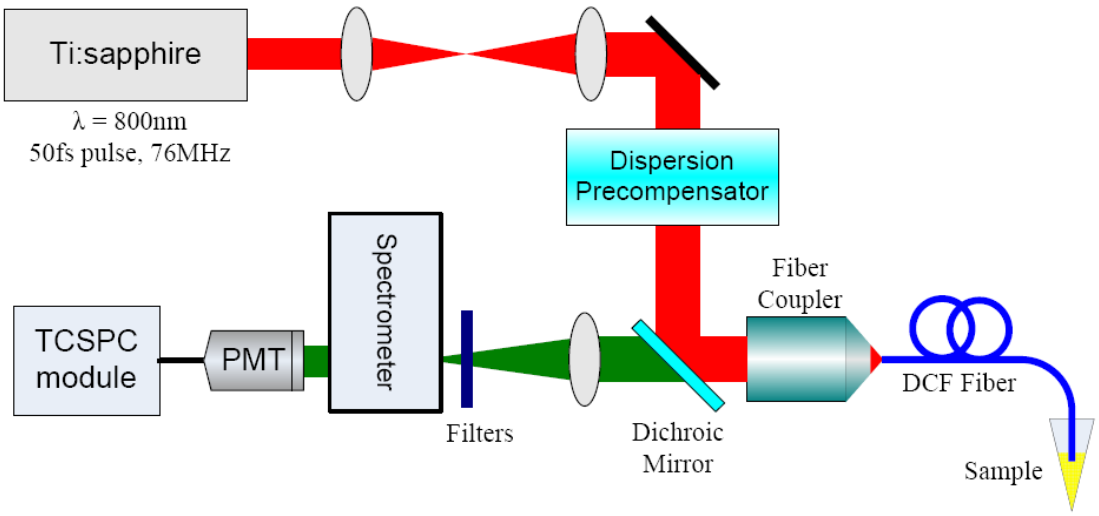

Figure 2.1 Experimental setup of two-photon excitation optical fiber fluorescence (TPOFF) probe.

The fiber length for our studies is typically 1 m (for either SMF or DCF). The dispersion in different kinds of fibers is usually different. The dispersion compensation is determined by adjusting the distance between the grating and the mirror as illustrated in Figure 2.2. It is essential to characterize the excitation pulses for future data analysis. Figure 2.3 (a) and (b) are the spectrogram of the pulses measured by the GRENOUILLE pulse measurement system (Swamp Optics Inc.). The pulse generated by the Mira has a temporal pulse width of 50~80 fs with a spectral bandwidth of the pulses at about 20 nm. The spectrogram in Figure 2.3 (b) is the pulse after being propagated through a double-clad fiber with a core size of 6 μm in diameter (P6-123DC, Liekki Corp.). The pulse duration is about 150 fs with energy of about 0.3 nJ as shown in Figure 2.3 (d). The pulse is longer than the output pulse from the Mira. However, this is because the pulse has traveled through multiple optical components, such as the isolator, lenses and coatings on the mirrors. The pulse duration does not increase much after traveling through the fiber when the pre-compensator is optimized. However, without the pre-compensation, the pulse duration would be on the order of pico-second.

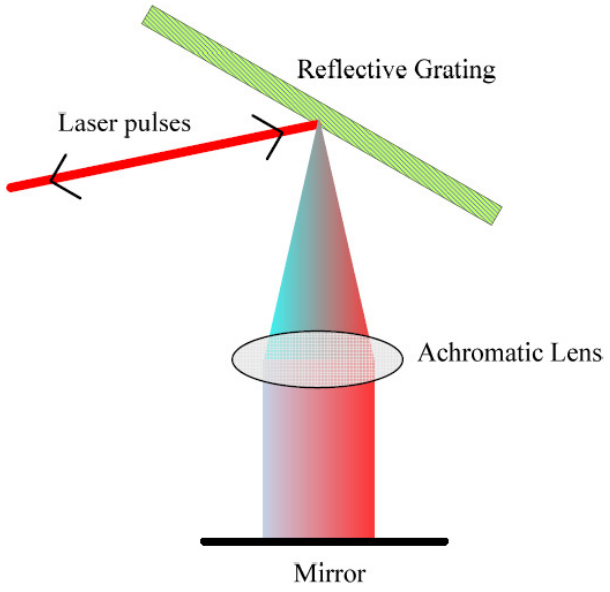

Figure 2.2 Schematic diagram of the dispersion precompensator. The grating has a groove density of 2000 lines/mm. The achromatic lens has a focal length of 12.5 cm.

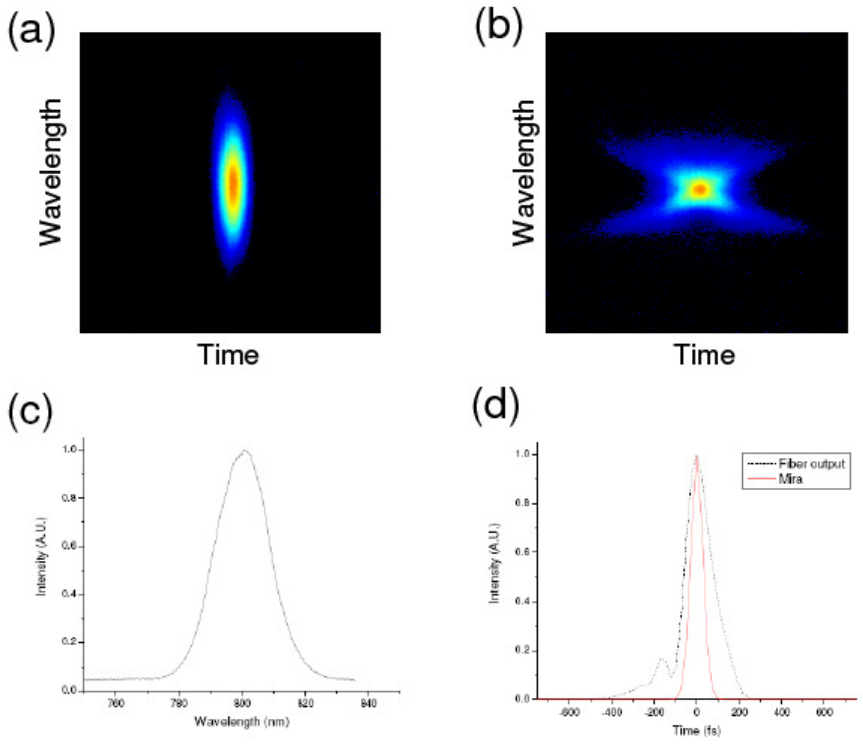

Figure 2.3 (a) Spectrogram of Mira output measured by GRENOUILLE. **(b)** Spectrogram of the pulse at the output of the TPOFF probe. **(c)** Spectrum of the pulses generated by the Mira, measured by a spectrometer (Ocean Optics Inc.). **(d)** Temporal pulse profile right after the Mira (red solid line) and at the output of the TPOFF probe (black dashed line), measured by GRENOUILLE.

2.3 Delivery of femtosecond pulses through optical fibers

As discussed in Chapter 1, the excitation efficiency of two-photon fluorescence (TPF) depends on the peak intensity of the pulse. Because of the ultrashort temporal duration of the femtosecond pulse, the spectral width of the pulse in the frequency domain is rather wide. Different frequency components of the pulse propagate at different speeds in the fiber due to group velocity dispersion (GVD). For pulses of wavelengths centered at 800 nm traveling in conventional silica glass fibers, the pulses will experience normal dispersion, which makes the longer wavelength components travel faster than

shorter wavelength components. The pulse will thus become longer as it travels through the fiber and acquires a positive chirp. Such linear dispersion does not affect the pulse spectrum. Thus the pulse stretching effect can be overcome by introducing a negative chirp before the pulse is delivered through the fiber. A grating pair can produce the negative chirp we need to compensate for the positive dispersion in the fiber [10, 11]. By launching a negatively pre-chirped pulse into the fiber, the pulses will acquire a positive chirp during the propagation and we will have close to transform-limited pulses at the output of the fiber.

However, because of the high peak power of the pulses and small core diameter of single mode fibers, the high peak intensity in the fiber makes nonlinear effects, such as self-phase modulation (SPM), significant even at moderate pulse energy (less than 1 nJ). For transform-limited or positively-chirped pulses, SPM will broaden the pulse spectrum. However, for negatively-chirped pulses, SPM narrows the spectral width of the pulses, causing the pulse width to increase. If the nonlinear effects are severe, the pulse width at the output of the fiber can no longer be compensated to the original transform-limited pulse width, which would cause non-quadratic dependence of the two-photon excited fluorescence signal [12].

Figure 2.4 shows the power dependence of the TPF signal versus the excitation power at the output of a SMF. The SMF was put in a 100-nM 6-Tamra dye solution. At low power the two-photon excited fluorescence signal follows the quadratic law. However, when the power is higher than 28 mW (pulse energy of ~0.35 nJ), the dependence starts to deviate from the quadratic law and showed sub-quadratic increasing of the signal. The TPF signal will still increase until pulse break-up occurs at higher energy. Our previous studies showed that pulse break-up happened at about 4 nJ in our system [10, 12].

Nevertheless, for *in vivo* studies, the output power from the SMF was always kept less than or around 20 mW because we found that when the laser power was higher than

20 mW, the biological tissue could be damaged as burning spot could be identified. Therefore, for the purpose of using the TPOFF probe as an *in vivo* biosensing probe, we only need to consider the linear regime of operation.

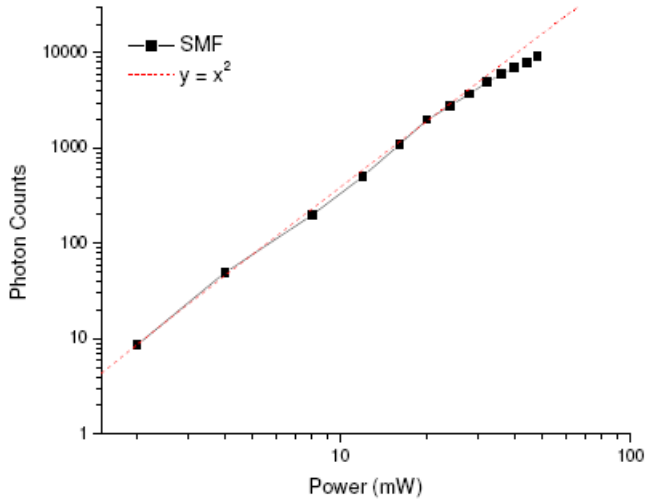

Figure 2.4 Power dependence of the TPF photon counts when dipping a SMF in 100nM 6T. The black squares are measured TPF. The dashed red line is the fit of the measurement using the points before 20mW. The deviation from the quadratic dependence law expected in two-photon-induced fluorescence is seen for laser power higher than 24mW.

2.4 Excitation and collection of two-photon-induced fluorescence through the same fiber

2.4.1 Trade-off between excitation efficiency and collection efficiency

The TPOFF probe presented in this dissertation uses the same optical fiber for both excitation and collection of the TPF. This simple and compact configuration is essential and critical for implementing the technique for *in vivo* biosensing application as compared to other detection schemes, such as 90^{o} detection geometry [13] or detecting

with an additional multi-mode fiber [14]. With this scheme, there is a trade-off between the high excitation efficiency of a single mode fiber (SMF) and the high collection efficiency of a multimode fiber (MMF). We found that the SMF gave orders of magnitude higher signal levels than the MMF [5, 15, 16].

It is not immediately obvious that the SMF should lead to larger signals; the SMF enables higher peak intensity at the fiber exit tip than the MMF, which increases the two-photon excitation rate. The lower numerical aperture (NA) of the SMF would imply, however, that the fluorescence collection efficiency is superior for the MMF.

In order to understand the trade-off between the SMF and the MMF, we performed the following analyses [5, 12].

Power of the detected TPF signal is given by,

$$P_f = \kappa \int_0^\infty \eta \phi(z) I_{out}^2(z) \tau_{out} R \pi W^2(z) dz \tag{1}$$

where κ denotes the overall detection efficiency of the detection system, η is the quantum yield of the fluorophore, $\phi(z)$ is the fluorescence collection efficiency determined by the NA of the fiber, $I_{out}(z) = CP_L/[R\tau_{out}\pi W^2(z)]$ is the laser peak intensity at a distance z from the fiber tip, C is the fiber coupling efficient, P_L is the average incident laser power, R is the repetition rate of the laser pulses, τ_{out} is the excitation pulse duration after propagating through the fiber, and $W(z)$ is the laser beam radius at position z. For a single-core (clad) fiber, the analytical solution of Eq. (1) can be calculated as [5, 12]:

$$P_f = \frac{\kappa \eta C^2 P_L^2}{R \tau_{out} \lambda} \left[\arctan \frac{n\lambda}{\pi a (NA)} - \sqrt{1-(NA/n)^2} \arctan \frac{n\lambda \sqrt{1-(NA/n)^2}}{\pi a (NA)} \right] \tag{2}$$

where n is the refractive index of the sample, λ the laser wavelength, and a the radius of the fiber core.

For a SMF, material dispersion stretches the pulse at the output to τ_{out}

$$\tau_{out} = \tau_{in}\sqrt{1+(L/L_D)^2} \tag{3}$$

where L is the fiber length, τ_{in} the incident pulse duration, and $L_D = \tau_{in}^2/\beta_2$ is the dispersion length with β_2 representing the dispersion of group velocity. On the other hand, for a step-index MMF, multimode distortion is normally much larger than material dispersion, which therefore is neglected in the following calculation. The broadened pulse duration at the output end of the fiber is given by [17]

$$\tau_{out} = n_{core}(NA)^2 L/[cn_{clad}(n_{core}+n_{clad})] \tag{4}$$

Substituting Eqs. (3) and (4) into Eq. (2), we calculated the relative TPF power detected with a SMF or a step-index MMF. Figure 2.5 indicates that a SMF is more efficient than a step-index MMF for TPF detection. The reason is that the lower collection efficiency (NA) of the SMF is more than offset by the high peak power in the sample. This result is consistent with our experimental findings. Therefore it is advisable to use fibers with a single-mode core for TPF excitation [13, 18].

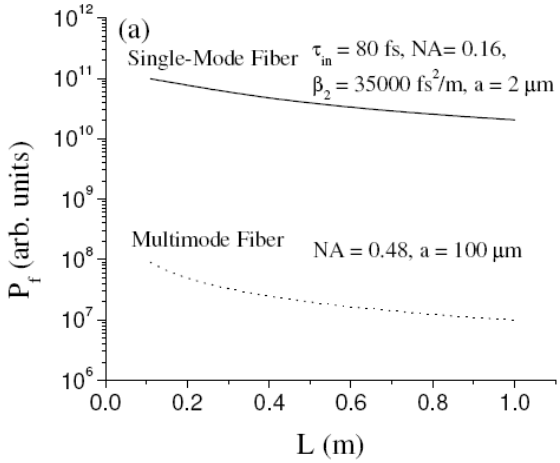

Figure 2.5 A comparison of calculated TPF detection efficiency between a single-mode fiber and a step-index multimode fiber. The parameters used in the calculation are τ_{in} = 80 fs, β_2 = 35000 fs^2/m. The single-mode fiber has a mode field diameter of 4.1 μm and NA of 0.16. The step-index multimode fiber has a core size of 200 μm and NA of 0.48 [5].

2.4.2 Double-clad fibers

A double-clad (or dual-clad) fiber (DCF) has two cladding layers surrounding a smaller diameter core. The schematic diagram of the cross-section of a double-clad fiber is illustrated in Figure 2.6. Both cladding layers have a lower refractive index than the core, and the inner cladding layer has a lower refractive index than the outer cladding so the light can be confined in both the core and the inner cladding. The DCF was originally developed for high-power fiber lasers [19] because the core can be doped to act as the gain medium and the pump beam can be efficiently coupled into the inner cladding due to its higher NA. The size and the NA of the core are usually designed such that it only supports single-mode operation at a certain wavelength. Therefore the NA of the core is usually small (~0.1). The size and the NA of the inner cladding layer are usually large to ensure optimum coupling of the pump beam. For example, for the fibers we used in this work, the diameter is 125μm and the NA is 0.46. Therefore, the inner cladding can carry multimode light with different wavelengths. Here we take advantage of the unique feature of the DCF by delivering ultrafast pulses through the single-mode core to achieve high two-photon excitation efficiency and collecting the fluorescence signal through the higher NA inner cladding. The working principle is illustrated in Figure 2.6.

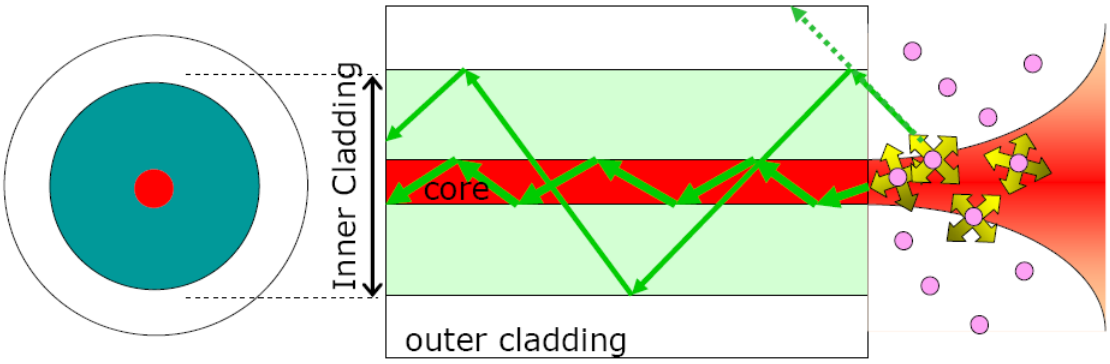

Figure 2.6 Schematic diagram to illustrate the structure of a double-clad fiber (DCF) and the use of a DCF for simultaneous excitation light delivery (red) and fluorescence light collection (green). The excitation light is propagating from left to right in the core and the fluorophores are excited at the end of the fiber. The excited two-photon

fluorescence can be collected back through both the core and the inner cladding of the fiber, as illustrated in the diagram by green arrows.

2.4.3 Enhanced sensitivity with dual-clad fibers

It is clear from the discussion in the previous section that a SMF is better when used to conduct two-photon excitation. However, the low collection efficiency because of the small NA (~0.1) of the SMF implies a low signal-to-noise ratio. It is desirable to exploit the high collection efficiency that accompanies the high NA of the MMF.

Since the last decade, there has been an enormous advance in fiber technology; this includes high-numerical-aperture double-clad fibers and novel photonic crystal fibers. Fluorescence signals enhanced through the use of a dual-clad photonic crystal fiber (DCPCF) compared to a SMF have been demonstrated [8]. A high excitation rate is achieved by propagating short pulses down an inner single-mode core, and the collection efficiency is improved by the high-NA multimode inner cladding. We show that the fluorescence signal level obtained with the dual-clad fiber is higher by over an order of magnitude than that obtained with even the sensor-grade SMF with a relatively larger NA (0.16).

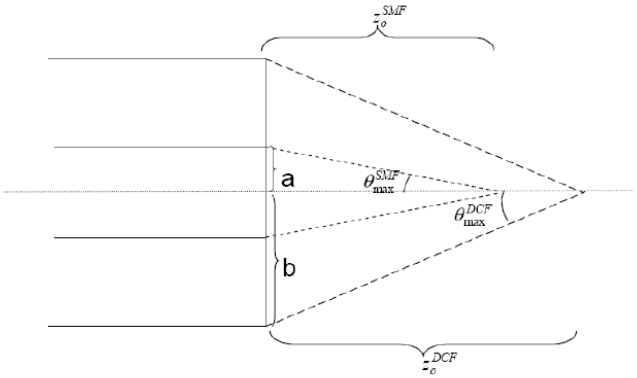

Figure 2.7 Geometry diagram for the calculation of collection efficiency.

We can estimate the enhanced collection efficiency of the DCF compared to the SMF by following the analysis carried out in Myaing's Ph.D. Thesis [12]. We denote the

core and the inner cladding radii by parameters a and b, respectively (for the DCF we used in the following chapters, a=3 μm and b= 62.5 μm). Figure 2.7 is a schematic plot illustrating the geometry we are using here, where z is the distance from a point outside of the fiber to the surface of the fiber tip in the axial direction. The dependence of the fluorescence collection efficiency $\phi(z)$ on the radius of the inner cladding (b) and the NA is given by

$$\phi(z)=\begin{cases}\dfrac{1}{2}\left(1-\sqrt{1-(NA/n)^2}\right), \text{ for } z \le \dfrac{bn}{NA}\sqrt{1-(NA/n)^2} \\ \dfrac{1}{2}\left(1-\dfrac{z}{\sqrt{z^2+b^2}}\right), \text{ for } z > \dfrac{bn}{NA}\sqrt{1-(NA/n)^2}\end{cases} \tag{5}$$

where n is the index of refraction of the sample. This represents the fact that the fraction of the fluorescence collected from values of $z \le \frac{bn}{NA}\sqrt{1-(NA/n)^2}$ is determined by the NA of the fiber, while that from the larger values of z is determined by the solid angle subtended from the fiber. By substituting Eq. (5) into Eq. (1) and doing the integral, we obtain the following equation for the TPF power detected with a DCF, in the regime where $b < n\pi a^2/\lambda$,

$$P_f^{DCF}=\kappa\frac{\pi\eta C^2 P_L^2 n}{4R\tau_{out}\lambda}\left[\begin{array}{l}1-\dfrac{\pi n a^2}{\sqrt{n^2\pi^2a^4-\lambda^2b^2}} \\ -\dfrac{2}{\pi}\sqrt{1-(NA/n)^2}\arctan\dfrac{\lambda b\sqrt{1-(NA/n)^2}}{\pi a^2\, NA} \\ +\dfrac{2n a^2}{\sqrt{n^2\pi^2a^4-\lambda^2b^2}}\arctan\dfrac{\lambda bn}{NA\sqrt{n^2\pi^2a^4-\lambda^2b^2}}\end{array}\right] \tag{6}$$

The ratio of the TPF power detected from the dual-clad fiber to that with the conventional single-mode fiber as a function of the inner-cladding NA can be calculated

by using Eqs. (2), (3) and (6), as shown in Figure 2.8. The detection efficiency increases nearly quadratically with the increasing of the inner-cladding NA.

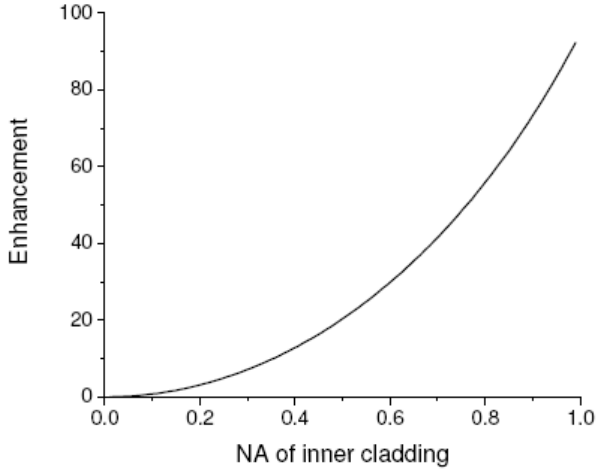

Figure 2.8 Calculated enhancement of the detected TPF with a dual-clad fiber over a single-mode fiber as a function of the NA of the inner cladding of the DCF.

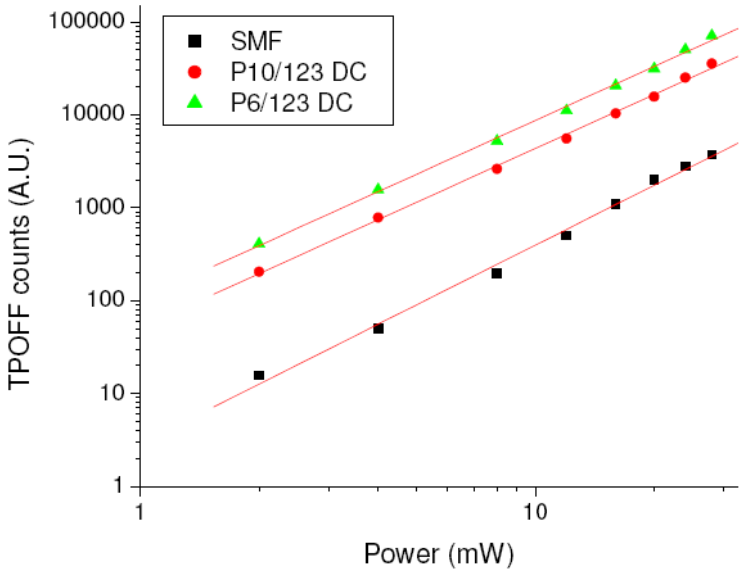

Figure 2.9 The two-photon fluorescence signals measured by single-mode fiber and double-clad fibers. The TPOFF counts were measured by inserting the fiber probe into 100-nM 6Tamra solutions.

The enhanced TPOFF signal using DCF is demonstrated in Figure 2.9. The fibers were put into 6-Tamra solutions directly. The DCFs used have 10-μm core (P10/123DC,

Liekki Corp.) and 6-μm core (P6/123DC), respectively. The inner cladding diameter is 123μm and is identical for the two DCFs. The SMF used in this study has a 4.1-μm mode field diameter (MFD) and a NA of 0.16 with a cladding size of 125 μm. The DCFs achieved more than a order of magnitude enhancement over the SMF.

2.5 Time-correlated single-photon-counting and time-resolved measurements

2.5.1 Time-resolved measurements

A real promise of the TPOFF probe scheme developed here is the potential of adapting fluorescent analysis techniques to *in vivo* use. The bulky optics needed in confocal or multiphoton microscopes limit applications such as fluorescence correlation spectroscopy (FCS) or fluorescence resonance energy transfer (FRET) for use in living organisms or in deep tissue. Therefore, we equipped a time-correlated single-photon counting (TCSPC) system in our detection apparatus. With the TCSPC system, we can measure the fluorescence lifetime of the fluorophores and monitor the dynamic behaviors of disease-specific molecules. The ability to conduct dynamic measurements with a TPOFF probe opens up the possibility to conduct a range of fluorescence analytic techniques *in vivo*, such as FCS and flow cytometry, which will be discussed in Chapter 4 and Chapter 5.

Steady-state fluorescence intensity measurements are relatively simple to implement and have been employed in analyzing many biologically important events, such as drug uptake monitoring [6, 7]. However, in general, intensity measurement may appear to be relatively insensitive to cellular biochemistry because local fluctuation in the fluorophore concentration may conceal some subtle cellular biochemical changes. On the other hand, fluorescence lifetime measurement reflects temporal information of the excited state of a fluorophore, which is known to be very sensitive to the local biochemical environment, and this environment may for example differ between diseased

and normal tissues [20]. In addition, fluorescence lifetime is independent of the concentration of fluorophores, excitation intensity, and optical losses by tissue scattering and absorption. Furthermore, instead of using wavelength-resolved measurements, fluorescence lifetime provides another dimension to separate the fluorescence signal of interest from background noise. Thus, fluorescence lifetime can offer more precise and accurate information of cellular biochemical changes, which is critical to diagnosing diseases in their earlier stages even before morphological alterations can be seen under a microscope [21].

With the fiber-based two-photon fluorescence spectroscopy, we can quantify cancer signatures and monitor anticancer drug-induced cell apoptosis under various situations including *in vitro* assay, *ex vivo* detection, and ultimately real-time *in vivo* monitoring.

2.5.2 Time Correlated Single Photon Counting (TCSPC)

Time Correlated Single Photon Counting (TCSPC) is an ultrafast laser spectroscopy technique which is based on correlating each detected photon to the time it is detected relative to the excitation laser pulse. It exploits the fact that for low-level, high-repetition rate signals the light intensity is usually low enough that the probability of detecting more than one photon in one signal period is negligible. The situation is illustrated in Figure 2.10.

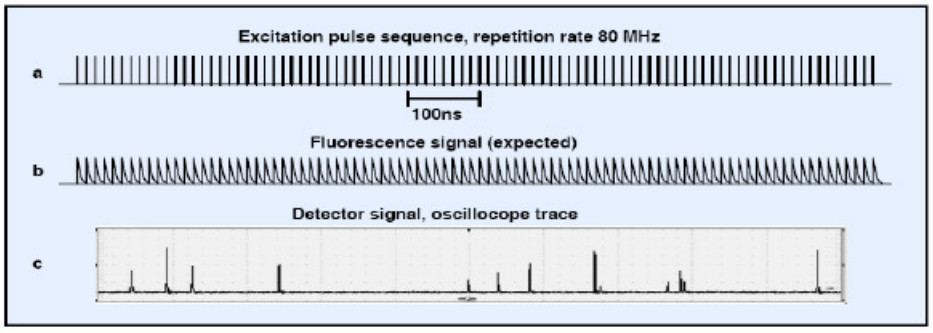

Figure 2.10 Detector signal for fluorescence detection at a pulse repetition rate of 80 MHz. (from BH handbook [22])

After recording enough photons, we can reconstruct the time-resolved waveform of the relaxation process of the energy states and thus the lifetime of the fluorophore, as illustrated in Figure 2.11. As in typical single-photon counting techniques, the signal-to-noise ratio is only limited by the shot noise. Thus, the more photons recorded, the higher the signal-to-noise ratio. Furthermore, it is desirable to have less than one fluorescence photon in one repetition period to avoid a "pile-up" effect in the detection. Therefore, TCSPC is an excellent fit for multiphoton spectroscopy because the excitation rate for the multiphoton process is usually lower than that for one-photon excitation [23, 24].

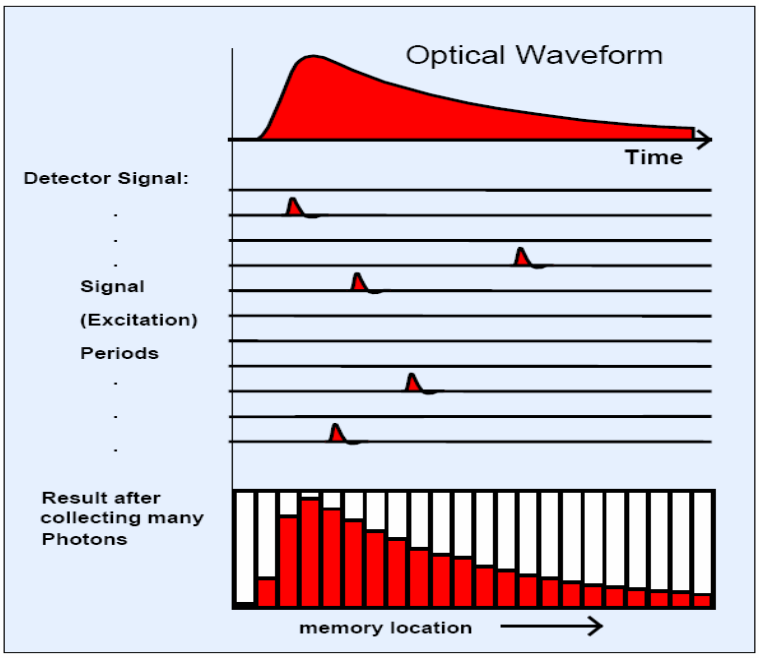

Figure 2.11 Principle of TCSPC (BH handbook).

Figure 2.12 (a) is the instrument response function (IRF) of our detection system. The full-width-at-half-maximum (FWHM) of the IRF is about 330 fs. Figure 2.12(b) shows typical fluorescence lifetime measurements using the TPOFF probe described here.

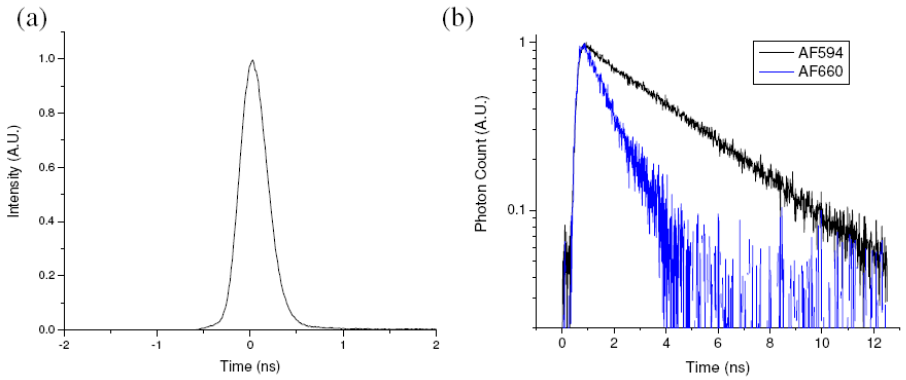

Figure 2.12 (a) Instrument response function (IRF) of our system. **(b)** Fluorescence lifetime measurements on Alexa-Flour 594 and 660, black and blue lines respectively, with the TPOFF probe system.

The instrument response function (IRF) (impulse response) was measured by sending scattered excitation femtosecond laser light into the detection system. Fluorescence lifetime of fluorescent dyes Alexa-Flour 594 and 660 were measured by directly putting the TPOFF probe into 30-nM dye solutions. Distinct fluorescent lifetimes of the two dyes were observed. The ability of conducting time-resolved lifetime measurements provides additional information for TPOFF probe to quantify low concentration fluorescent molecules.

2.6 References

1. F. Helmchen, and W. Denk, "Deep tissue two-photon microscopy," Nature Methods 2, 932-940 (2005).
2. E. E. Graves, J. Ripoll, R. Weissleder, and V. Ntziachristos, "A submillimeter resolution fluorescence molecular imaging system for small animal imaging," Med Phys 30, 901-911 (2003).
3. V. Ntziachristos, A. G. Yodh, M. Schnall, and B. Chance, "Concurrent MRI and diffuse optical tomography of breast after indocyanine green enhancement," Proc Natl Acad Sci U S A 97, 2767-2772 (2000).
4. U. Utzinger, and R. R. Richards-Kortum, "Fiber optic probes for biomedical optical spectroscopy," Journal of Biomedical Optics 8, 121-147 (2003).
5. J. Y. Ye, M. T. Myaing, T. B. Norris, T. Thomas, and J. Baker, "Biosensing based on two-photon fluorescence measurements through optical fibers," Optics Letters 27, 1412-1414 (2002).
6. T. P. Thomas, M. T. Myaing, J. Y. Ye, K. Candido, A. Kotlyar, J. Beals, P. Cao, B. Keszler, A. K. Patri, T. B. Norris, and J. R. Baker, "Detection and analysis of tumor fluorescence using a two-photon optical fiber probe," Biophysical Journal 86, 3959-3965 (2004).
7. T. P. Thomas, A. K. Patri, A. Myc, M. T. Myaing, J. Y. Ye, T. B. Norris, and J. R. Baker, "In vitro targeting of synthesized anti body-conjugated dendrimer nanoparticles," Biomacromolecules 5, 2269-2274 (2004).
8. M. T. Myaing, J. Y. Ye, T. B. Norris, T. Thomas, J. R. Baker, W. J. Wadsworth, G. Bouwmans, J. C. Knight, and P. S. J. Russell, "Enhanced two-photon biosensing with double-clad photonic crystal fibers," Optics Letters 28, 1224-1226 (2003).
9. T. P. Thomas, J. Y. Ye, Y. C. Chang, A. Kotlyar, Z. Cao, I. J. Majoros, T. B. Norris, and J. R. Baker, "Investigation of tumor cell targeting of a dendrimer nanoparticle using a double-clad optical fiber probe," J. Biomed. Opt. 13, 6 (2008).
10. M. T. Myaing, J. Urayama, A. Braun, and T. B. Norris, "Nonlinear propagation of negatively chirped pulses: Maximizing the peak intensity at the output of a fiber probe," Optics Express 7, 210-214 (2000).
11. G. P. Agrawal, Nonlinear Fiber Optics (San Diego : Academic Press, 2001).
12. M. T. Myaing, "Conventional and Photonic Crystal Fiber Based Two-photon Fluorescence Biosensing," in Applied Physics(University of Michigan, Ann Arbor, 2004).

13. A. Lago, A. T. Obeidat, A. E. Kaplan, J. B. Khurgin, P. L. Shkolnikov, and M. D. Stern, "2-PHOTON-INDUCED FLUORESCENCE OF BIOLOGICAL MARKERS BASED ON OPTICAL FIBERS," Optics Letters 20, 2054-2056 (1995).
14. L. Fu, and M. Gu, "Fibre-optic nonlinear optical microscopy and endoscopy," J Microsc 226, 195-206 (2007).
15. T. P. Thomas, M. T. Myaing, J. Y. Ye, K. Candido, A. Kotlyar, J. Beals, P. Cao, B. Keszler, A. K. Patri, T. B. Norris, and J. R. Baker, Jr., "Detection and analysis of tumor fluorescence using a two-photon optical fiber probe," Biophys J 86, 3959-3965 (2004).
16. T. P. Thomas, A. K. Patri, A. Myc, M. T. Myaing, J. Y. Ye, T. B. Norris, and J. R. Baker, Jr., "In vitro targeting of synthesized antibody-conjugated dendrimer nanoparticles," Biomacromolecules 5, 2269-2274 (2004).
17. G. E. Keiser, "A review of WDM technology and applications," Opt Fiber Technol 5, 3-39 (1999).
18. F. Helmchen, D. W. Tank, and W. Denk, "Enhanced two-photon excitation through optical fiber by single-mode propagation in a large core," Appl Optics 41, 2930-2934 (2002).
19. L. Zenteno, "HIGH-POWER DOUBLE-CLAD FIBER LASERS," J. Lightwave Technol. 11, 1435-1446 (1993).
20. J. R. Lakowicz, Principles of fluorescence spectroscopy (Kluwer Academic/Plenum, New York, 1999).
21. M. A. Mycek, K. T. Schomacker, and N. S. Nishioka, "Colonic polyp differentiation using time-resolved autofluorescence spectroscopy," Gastrointest Endosc 48, 390-394 (1998).
22. W. Becker, "The bh TCSPC Handbook."
23. W. Becker, Advanced time-correlated single photon counting techniques (Springer, Berlin ; New York, 2005).
24. D. V. O'Connor, and D. Phillips, Time-correlated single photon counting (Academic Press, London ; Orlando, 1984).

CHAPTER 3
Enhanced Two-photon Fluorescence Biosensing Using a Double-clad Optical Fiber Probe

3.1 Introduction

Noninvasive tissue fluorescence analysis by conventional spectroscopic techniques presents significant challenges because of the absorption and scattering of light in tissues [1]. Visualization of fluorescent probes in tissues, such as the distribution of a fluorescent drug, has been achieved by whole-body imaging [2]; however, this approach requires large amounts of a fluorescent material, and it is difficult to obtain quantitative information at low fluorophore concentrations. Our group has demonstrated a minimally-invasive technique, using a two-photon optical fiber fluorescence (TPOFF)-based detection system for the quantification of tissue fluorescence both *in vitro* and in live animals [3, 4]. When compared to single-photon excitation [5], two-photon excitation has the advantage of having greater penetration into tissue samples [6, 7]. Moreover, analytes with multiple emission wavelengths can be simultaneously quantified using a single-excitation laser [8]. As the two-photon excitation and emission wavelengths are widely separated and can be easily filtered, the sensitivity of detection is enhanced, especially for multi-wavelength analytes. Previous works have demonstrated that by using a single-mode fiber (SMF) to deliver femtosecond laser pulses into cell and tissue samples and to collect the emitted fluorescence back through the same fiber, this

allowed the detection and quantification of targeted fluorescent antibodies and nanoparticles [3, 4, 9].

One of the limitations of a SMF is that its small numerical aperture (NA, ~ 0.1) results in inefficient signal collection. In order to quantify low levels of localized florescence such as that occur with tissue-specific targeting of a nanoparticle, a more sensitive *in situ* fluorescence quantification technique is required. Although the application of a multimode fiber (MMF) would enable efficient fluorescence collection through its large NA, the sensitivity for two-photon fluorescence is compromised because of its inefficient excitation and lower resolution. In order to solve these 'trade-off' problems between the SMF and the MMF, we use a double-clad fiber in the single fiber detection scheme. The ultrafast pulses are delivered through the single-mode core to maintain the high excitation efficiency, and the fluorescence signal can be collected back through both the core and the high-NA inner cladding. A double-clad photonic crystal fiber (DCPCF) which has a NA of 0.8 at 1μm was used in initial studies by Myaing *et al*. The collection efficiency was found to be more than an order of magnitude higher when using the DCPCF as compared to the SMF [10]. By attaching a gradient index lens to the DCPCF, a scanning microscope based on the DCPCF for visualizing fluorescent images of individual cells was demonstrated [11]. However, the use of a DCPCF for *in situ* fluorescence quantification is limited because of the entry of fluids into its air holes by capillary action. In this chapter, the biological application of a solid double-clad optical fiber (DCF) will be demonstrated. Because of the absence of air holes in the fiber, the DCF can be applied to aqueous environments and enables *in vivo* measurements with high sensitivity. A significant improvement over conventional single-clad, single-mode fibers has been achieved. Our studies show for the first time that the improved sensitivity of a double-clad fiber as compared to that of a single-clad fiber allows sensitive quantification of targeted nanoparticles in tumor cells.

3.2 Methods and materials

3.2.1 The TPOFF system and the fibers

The two-photon optical fiber fluorescence (TPOFF) detection system used was similar to that described in Chapter 2. The SMF used in this study had a mode field diameter of 4.1 μm with an NA of 0.16 (F-SBA, Newport). The DCF had a 10-μm diameter inner core with an NA of 0.07 and a 123-μm inner cladding with an NA of 0.46 (P-10/123DC, Thorlab). Femtosecond laser pulses generated from a Ti:sapphire oscillator (Coherent, Mira 900) with a pulse duration of 50 fs and center wavelength of 800 nm were used as the excitation source. Fibers were directly inserted into dye solutions, cell pellets, or into tumor samples through a 30-gauge needle. The fluorescence emission was collected through the same fiber and then separated from the excitation beam by a dichroic mirror. The fluorescence was then sent through a short-pass filter and counted using a photon-counting photomultiplier tube [4].

3.2.2 Biocompatible dendrimer nanoparticles and conjugates

The Generation 5 (G5) poly(amidoamine) (PAMAM) dendrimer was synthesized and characterized at the Michigan Nanotechnology Institute for Medicine and Biological Sciences, University of Michigan. Methanol (MeOH, HPLC grade), acetic anhydride (99%), triethylamine (99.5%), dimethyl sulfoxide (DMSO, 99.9%), dimethylformamide (DMF, 99.8%), 1-[3-(dimethylamino)propyl]-3-ethylcarbodiimide HCl (EDC, 98%), citric acid (99.5%), sodium azide (99.99%), D_2O, NaCl, and volumetric solutions (0.1 M HCl and 0.1 M NaOH) for potentiometric titration were purchased from Aldrich Co. and used as received. The Spectra/Por dialysis membrane (MWCO 3500) and Millipor Centricon ultrafiltration membrane (YM-10) was from Fisher. The 6-Carboxytetramethyl rhodamine, succinimidyl ester (6-TAMRA-SE, 6T-SE, Properties: MW=528, soluble in DMF and DMSO, Abs = 546, Em = 576 measured in MeOH, $\varepsilon = 9.5 \times 10^4$) was

purchased from Invitrogen (Carlsbad, California). Folic acid (FA, 98%) and all other reagents were from Sigma (St. Louis, MO).

Our group have previously established the G5-PAMAM (G5) dendrimer nanoparticle as a suitable platform for conjugating multiple molecules for specific targeting of drugs and imaging agents into cells [12]. The G5 dendrimer has several attractive properties as a molecular delivery platform, including uniformity, biocompatibility, defined branched chain structure, and the capability for chemically coupling multiple molecular entities to its surface amino groups. The three-dimensional architecture of the PAMAM dendrimers resembles globular proteins, and the G5 has the size of hemoglobin (~ 5 nm). PAMAM dendrimers are commercially available and are synthesized from an ethylene diamine (EDA) initiator core, with exhaustive Michael addition of methyl acrylate followed by condensation (amidation) reactions of the resulting ester with large excesses of EDA [12]. PAMAM dendrimers have recently been shown to be highly suitable for drug delivery, detection of biochemical functions such as apoptosis, and for tumor imaging [12]. The structure and molecular weight of dendrimer up to generation 3 is shown in Figure 3.1.

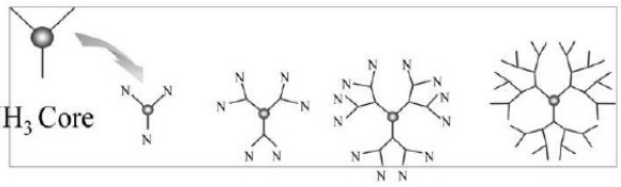

Generation	G0	G1	G2	G3
Surface Amine Groups	3	6	12	24
Molecular Weight	359	1,044	2,414	5,154

Figure 3.1 Synthesis and structure of PAMAM dendrimer nanoparticles up to generation 3.

For the FA receptor (FAR)-specific targeting *in vitro* and *in vivo,* we synthesized the targeted and non-targeted conjugates G5-6T-FA and G5-6T respectively, using procedures similar to those we have described previously [13]. After the synthesis of each intermediary conjugate, the product obtained was purified by intensive dialysis or by repeated ultrafiltration, using a 10 kDa membrane filter and using PBS followed by water. The purified compound was lyophilized before undergoing the subsequent reaction step.

1. G5 Carrier: The G5 dendrimer platform used in this study had a number average molecular weight of 26530 g/mol, as determined by gel permeation chromatography (GPC) equipped with multi-angle laser light scattering and refractive index detectors. The average number of primary amino groups was 110, as determined by potentiometric titration.

2. G5 with 70 amino groups acetylated [G5-Ac(70)]: Initially the primary amino groups on the G5 were partially acetylated. Acetylation of the primary amino groups was used to neutralize the positively charged primary amines on the dendrimer surface from further reaction or intermolecular interaction within biological systems. The quantity 1.51859 g (5.724×10^{-3} mol) of G5 in 100 mL of absolute MeOH was reacted with 378.1 µL (4.007×10^{-3} mol) of acetic anhydride in the presence of 698.1 µL (5.009×10^{-3} mol, 25% molar excess) of triethylamine at room temperature and stirring overnight. The yield of the purified product was 1.51208 g (89.64%), with an average of 70 acetyl groups as determined by proton nuclear magnetic resonance (^{1}H NMR) [14]. Leaving 40 surface amines allows for the efficient attachment of multiple functionalities, such as receptor ligands, fluorescent dyes, and drugs [13].

3. G5 with 70 acetyl groups and 4 covalently conjugated 6TAMRA [G5-Ac(70)-6T(4)]: To 46.4 mg (1.574×10^{-6} mol) of G5-Ac(70) in 17 mL DI water and 1.7 mL 1M $NaHCO_3$ solution was added dropwise 2.8 mL of 5 mg (9.478×10^{-6} mol) 6-TAMRA in

DMSO solution at a reduced temperature. This was then stirred for 24 hours. The yield of the purified product was 40 mg (68 %).

4. Fully acetylated G5-6TAMRA [G5-Ac(fully)-6T(4)] ["**G5-6T**", control conjugate for biological testing]: As a standard procedure after conjugation of multiple functionalities, any free amine groups remaining are neutralized by acetylation to obtain a fully neutralized final product. A mixture of 12.24 mg (3.876 X 10^{-7} mol) G5-Ac(70)-6T(4) dendrimer conjugate, 1.65 µL (1.755 X 10^{-5} mol) acetic anhydride, and 3.04 µL (2.18 X 10^{-5} mol) triethylamine in 0.5 mL of absolute MeOH was allowed to react at room temperature by stirring overnight. The purified product obtained (G5-6T) had a molecular weight of 33090 g/mol, as determined by GPC.

5. G5 containing 5 covalently conjugated folic acid molecules [G5-Ac(70)-FA(5)]: Conjugation of FA to the partially acetylated dendrimer was carried out via condensation between the µ-carboxyl group of FA and the primary amino groups of the dendrimer. Because of the higher reactivity of the µ-carboxylic group of FA as compared to its α-carboxyl, under the conditions used, conjugation takes place primarily through the µ-carboxyl. Leaving the α-carboxyl of FA free is a prerequisite for its full affinity toward the FA-receptor. The FA was initially activated by reacting 65.37 mg FA (1.48 X 10^{-4} mol) with a 14-fold excess of EDC (399.24 mg, 2.08 X 10^{-3} mol) in a solvent mixture of 48 mL of DMF and 16 mL of DMSO at room temperature. After 3 hours, the FA-active ester solution obtained was added dropwise to an aqueous solution of the partially acetylated product G5-Ac(70) (0.79055 g, 2.683 X 10^{-5} mol) in 180 mL of water. The reaction was allowed to proceed at room temperature with intensive stirring for 3 days. The yield of the purified product obtained was 0.8543 g (99.8%), with 5 FA per dendrimer as determined by ^{1}H-NMR analysis [13]. In the ^{1}H-NMR of the purified G5-6T-FA, the absence of any sharp peaks and the observed broadening of the aromatic proton peaks were indicative of the lack of presence of any free FA and the presence of covalently conjugated FA. Additional characterization by gel permeation column

chromatography (equipped with a UV detector) and HPLC analysis also failed to show any presence of free FA.

6. G5-Ac(70)-FA(5)-6T(4): To 100.07 mg (3.147 X 10^{-6} mol) G5-Ac(70)-FA(5) in 35 mL DI water and 3.5 mL 1M $NaHCO_3$ solution was added dropwise 4.6 mL of 10 mg (1.896 X 10^{-5} mol) 6-TAMRA in a DMSO solution at reduced temperature, and it was stirred for 24 hours. The yield of the purified product was 0.09612 g (90.1 %).

7. G5-Ac(fully)-FA (5)-6T(4) ["**G5-6T-FA**", targeted conjugate for biological testing]: A combination of 21.74 mg (6.41 X 10^{-7} mol) G5-Ac(70)-FA(5)-6T(4) dendrimer conjugate, 2.34 μL (2.484 X10^{-5} mol) acetic anhydride, and 4.33 μL (3.105 X 10^{-5} mol) triethylamine in 0.5 mL of absolute MeOH was allowed to react at room temperature overnight. GPC analysis of the product obtained (G5-6T-FA) gave a molecular weight of 35200 g/mol. On the basis of the integration values of the methyl protons in the acetamide groups and the aromatic protons by ^{1}H NMR analysis, the numbers of attached FA and 6TAMRA molecules were calculated to be 5 and 4, respectively.

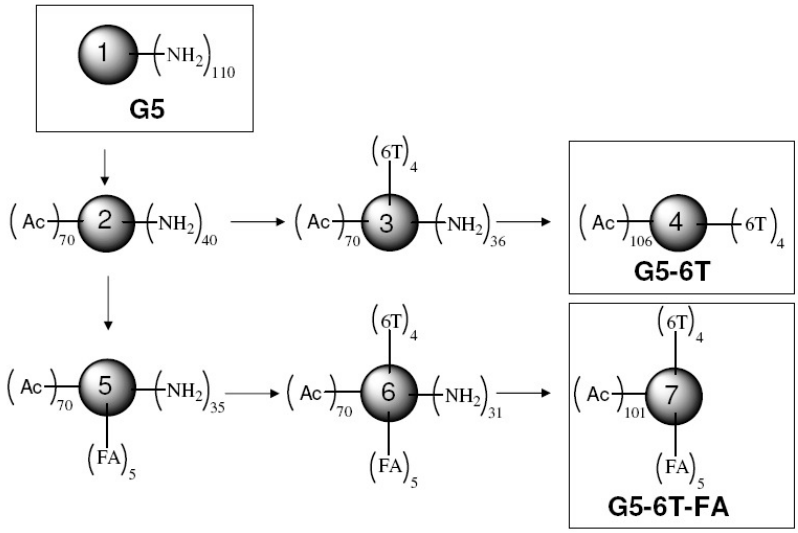

Figure 3.2 Synthetic scheme of a generation 5 PAMAM dendrimer (G5)-based nanoparticle containing folic acid (FA) as the targeting molecule and 6-TAMRA as the sensing fluorophore for targeting FA-receptor-expressing KB cells and tumors.

3.2.3 Cell culture and in vitro studies:

KB cells were obtained from ATCC (Rockville, MD). RPMI cell culture medium, trypsin-EDTA, penicillin/streptomycin, and Dulbecco's phosphate buffered saline (PBS, pH 7.4) were from Gibco/BRL (Gaithersburg, MD). The KB cell line which expresses high levels of FAR on its membrane was used for the receptor-specific targeting of the G5-6T-FA conjugate. Cells were maintained in folate-free RPMI medium containing 10% serum to provide extracellular FA similar to that found in human serum. For the *in vitro* studies, cells plated in 75 cc flasks were trypsinized, rinsed, and re-suspended in phosphate buffered saline containing 0.1% bovine serum albumin (PBSB). The cells in suspension were treated with different concentrations of the conjugates for 1 hour at 37ºC, rinsed, and centrifuged to collect the cell pellets [15]. The optical fiber was then inserted into different regions of the cell pellet and TPOFF counts were then collected [16].

3.2.4 Animal model and *in vivo* studies:

Female, severe combined immunodeficiency (SCID) mice were purchased from Charles River Laboratories (Wilmington, MA). Folate-deficient diet was from TestDiet (Richmond, IN). For the *in vivo* studies, KB cell tumors were developed in 7-week-old SCID mice as described in reference [17]. The mice were housed in a specific pathogen-free animal facility at the University of Michigan Medical Center in accordance with the regulations of the University's Committee on the Use and Care of Animals as well as with federal guidelines, including the Principles of Laboratory Animal Care. The animals were fed *ad libitum* with Laboratory Autoclavable Rodent Diet 5010 (PMI Nutrition International, St. Louis, MO). Two weeks before tumor cell injection, the food was changed to a folate-deficient diet. KB cell tumors were developed by subcutaneous inoculation of $1x10^6$ cells each in the left and right flank areas. The cells were trypsinized, rinsed, and injected as a 0.1-ml suspension using sterile PBS. The tumors

were allowed to reach 0.7–0.8 cm in diameter before analysis. Fifteen nmols of the conjugates in 0.1 mL of PBS or PBS alone as a control were administered through the tail vein. Fifteen hours later, at the end of the study, the mice were anesthetized with isoflurane and the tumors were excised and frozen. The optical fibers were inserted into the tumor through a 30-guage needle, with the tip of the fiber placed at the proximal end of the needle hole. The needle with the fiber was sonicated in a bath sonicator between tumor sample measurements. The fluorescence of multiple internal regions of the tumors was quantified using the two-fiber probes under identical conditions.

The statistical significance of differences among the groups was analyzed by the Student-Newman-Keuls test, with significance calculated at $p < 0.05$.

3.3 Results and discussions

3.3.1 Enhanced sensitivity by double-clad fiber

The fluorescence emissions of the standard solutions of G5-6T-FA and G5-6T were initially quantified using DCF and SMF probes, as shown in Figure 3.4. The DCF fiber showed lower background fluorescence when measured in PBS buffer and a 5-fold higher conjugate fluorescence as compared to the SMF. The background fluorescence obtained in PBS was 1175 ± 42 and 258 ± 4.6, respectively, when the SMF and DCF probes were used. This detection background was mainly from the autofluorescence of the fiber core. The fact that the SMF has a higher background was attributed to the doping material in the SMF core. Special treatments might have been applied to the core of this sensor-grade SMF to achieve its relative higher NA of 0.16. The low detection background of the DCF probe ensures the accurate measurements of samples with an extremely low concentration of fluorophores. Other independent measurements using the two fibers similar to what is presented in Figure 3.3 have shown that the standard TPOFF

counts were linear at least in up to 1-µM concentrations of the conjugates. This is consistent with the linearity in TPOFF counts in up to 100-µM concentrations of the "G5-Fluorescein" conjugates previously demonstrated using the SMF [16].

The background-subtracted counts (mean ± SE) obtained for 5, 10, 30, 100 and 300 nM of G5-6T-FA conjugate were respectively -13 ± 6, 65 ± 11, 127 ± 6, 679 ± 32 and 2079 ± 11 using the DCF, and -6 ± 5, 32 ± 19, 3 ± 2, 110 ± 8 and 501 ± 24 for the SMF (Figure 3.3(b)). This shows that the lower detection limit for the conjugate is less than 10 nM for the DCF and >100 nM for the SMF. The increased sensitivity of the DCF versus the SMF is due to the unique fiber structure, which allows the laser beam to propagate in single mode through the inner core for a high excitation rate while having an efficient collection of fluorescence through its inner cladding (outer core), and is also due to the lower background fluorescence of the former.

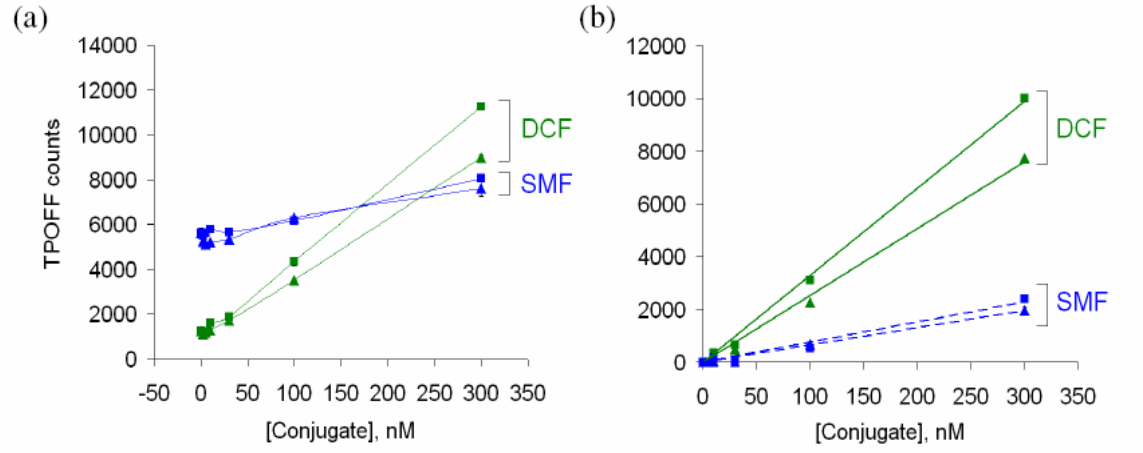

Figure 3.3 (a) TPOFF measurements of standard solutions of GF-6T-FA (triangles) and G5-6T (squares) using SMF and DCF probes. The TPOFF photon counts are measured by putting the fibers in the solutions directly. The data shown are the mean ± SE of four to five measurements for each concentration. **(b)** Data corrected for the detection background.

3.3.2 In vitro cell measurements

Confocal images of the KB cells treated with 100-nM of targeted conjugate G5-6T-FA and non-targeted G5-6T, respectively, are shown in Figure 3.4. The cells were incubated with the conjugate solutions for 1 hour, followed by staining with the nuclei dye DAPI. In the cells treated with G5-6T-FA, the 6-TAMRA can be seen both in the cytoplasm and the plasma membrane, which indicates the uptake of the targeted conjugate G5-6T-FA and the internalization of the dendrimer conjugates. On the other hand, for cells treated with G5-6T, only DAPI-stained nuclei can been seen under the fluorescence microscope.

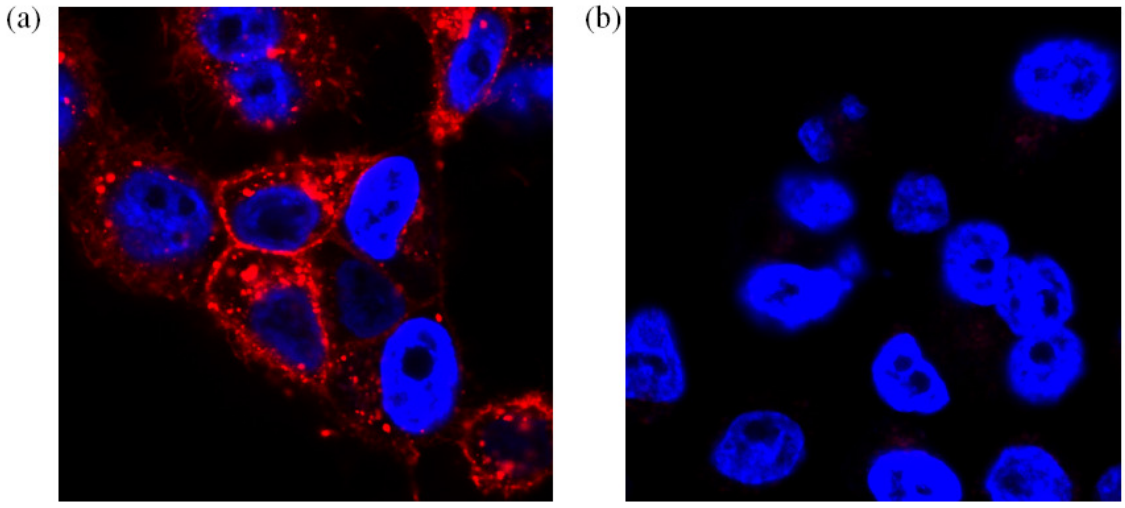

Figure 3.4 *In vitro* study of FA receptor-expressing KB cells targeted with fluorescent nanoparticles of (a) G5-6T-FA in comparison with non-targeted (b) G5-6T measured with confocal fluorescence microscopy. The blue color indicates DAPI-stained nuclei, and the red dots represent 6-TAMRA on the dendrimer conjugates, which shows localization of G5-6T-FA primarily in the cytosolic compartment.

The DCF fiber was then utilized to quantify the *in vitro* targeting of the dendrimer conjugates in FA receptor-expressing KB cells. In untreated control cell pellets, the mean background fluorescence taken by the SMF and the DCF were 1313 ± 52 and 2089 ± 165 counts per second, respectively. This observation is in contrast to the increased

background fluorescence of the SMF in PBSB. The increased DCF counts observed in the control cell pellet could be because of the autofluorescence of endogenous fluorophores. Several cellular components such as collagen, tryptophan, and porphyrins are known to be fluorescent, and low levels of these agents are apparently being detected by the more sensitive DCF fiber.

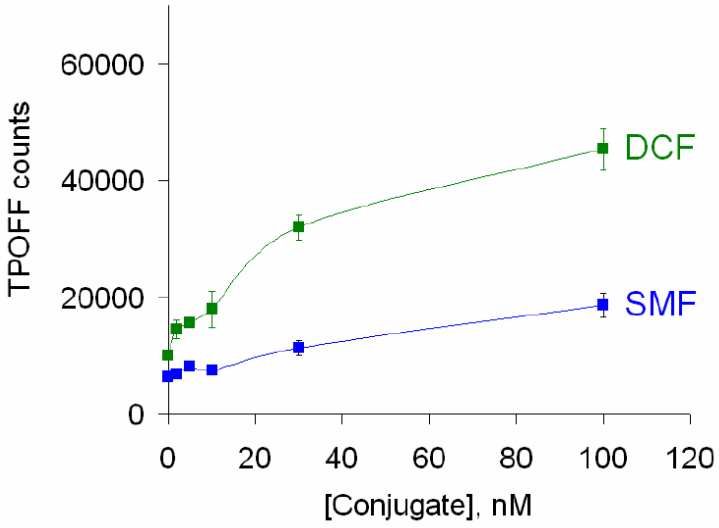

Figure 3.5 Comparison of the targeting of G5-6T-FA in KB cells determined by SMF and DCF probes. The KB cells were incubated with different concentrations of the conjugates for 1 hour. The cells were then rinsed and collected as cell pellets. The TPOFF counts were taken by inserting the fiber probes into multiple locations of the cell pellets. $p<0.05$ for all DCF points versus SMF, except for at zero concentration.

As shown in Figure 3.5, the fluorescence of the cell pellet was significantly higher for the DCF fiber at all concentrations of the G5-6T-FA conjugate tested, consistent with results from the standard solutions. The increased sensitivity of the DCF fiber is further evident from the marked difference in the slopes of the two curves at lower doses of the conjugate. Low levels of non-specific binding of the control conjugate G5-6T were detected only by the DCF fiber. The binding curves observed by the DCF fiber are indicative of the FA receptor-specific interaction, as was reported previously [15]. The

receptor-specific binding of the G5-6T-FA was further confirmed by the reversal of the binding of 300 nM G5-6T-FA by pre-incubating the cells with a 50-fold excess of free FA. The DCF-TPOFF counts in cells incubated with 300 nM G5-6T-FA in the absence and presence of 15 μM free FA were 15411 ± 247 and 2903 ± 546, respectively. The standard error for the measurement of different regions of the cell pellets varied from 2%-20% for the different concentrations of the conjugate investigated. As the TPOFF measurement quantifies the fluorescence of only a few microns surrounding the fiber, this variability could result from the differences in the fluorescence intensities for the 4-5 cell regions tested in the cell pellets at each concentration. A broad population distribution for binding of the conjugate has been observed by flow cytometry by measurement of the individual fluorescence of 10,000 cells [3]. The saturation behavior of the binding was also observed in the flow cytometry data as shown in Figure 3.6.

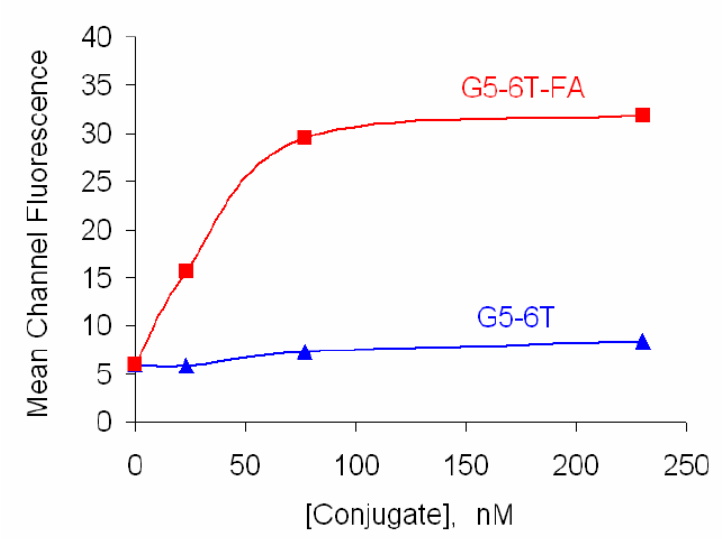

Figure 3.6 Flow cytometry measurements of the uptake of targeted (G5-6T-FA) and non-targeted (G5-6T) dendrimer conjugate nanoparticles in KB cells. The cells were maintained in FA-free medium and incubated in different concentrations of the respective conjugates for 1 hour.

3.3.3 In vivo targeted folic acid receptor-expressing tumor cells

The DCF probe was then used to confirm the findings in references [3, 4] that the G5-6T-FA conjugate could target FAR-expressing tumors *in vivo* in mice. The KB tumors were developed in SCID mice and were intravenously injected with 15 nmols each of the targeted conjugate G5-6T-FA, the non-targeting conjugate G5-6T or their vehicle PBS (control). After 15 hours, the tumors were isolated and the TPOFF counts were taken in different internal regions of the tumor using the DCF or SMF-TPOFF probes. The data shown are mean ± SE of counts taken in four or five different regions of four tumors for each condition.

As shown in Figure 3.7, there were approximately 3-fold higher background-subtracted counts for the targeted conjugate as detected by the DCF probe in comparison to the counts obtained by the SMF probe. There was a 3-4-fold increase in the uptake of the targeted conjugate (G5-6T-FA) in comparison to the control conjugate G5-6T, which again is consistent with our previous findings [3, 4]. Using the slope of the standard curve generated for the G5-6T-FA (Figure 3), the concentration of the targeted conjugate in the tumor was 1016 ± 174 nM and 1251 ± 117 nM measured by the DCF and SMF, respectively. In consistent with these results, our previous studies using the SMF have shown the accumulation of 1 to 5 µM G5-6T-FA in KB tumors [3, 4].

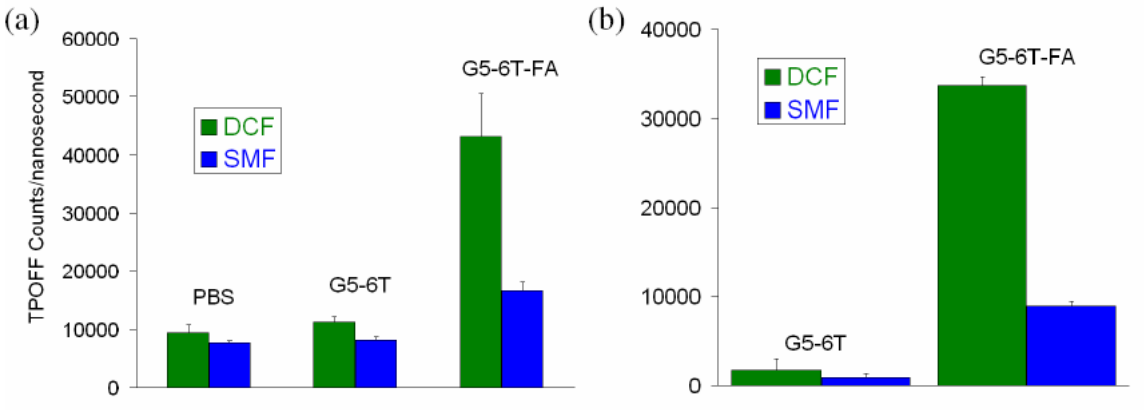

Figure 3.7 (a) *In vivo* KB tumor targeting of G5-6T-FA, determined by DCF (green bars) and SMF (blue bars) TPOFF probes. The KB tumors were developed in SCID mice and were intravenously injected with 15

nmols each of the targeted conjugate G5-6T-FA, the non-targeting conjugate G5-6T or their vehicle PBS (control). After 15 hours, the tumors were isolated and the TPOFF counts were taken in different internal regions of the tumor using the DCF or SMF-TPOFF probes. The data shown are mean ± SE of counts taken in four or five different regions of four tumors for each condition. **(b)** The counts corrected for the background fluorescence of the PBS tumor (control).

3.3.4 *In situ* quantification of fluorophores with different emission wavelength

With the ability to excite multiple dyes by 2PE, we can quantify different cancer signatures simultaneously. For example, some breast cancer cells overexpress human epidermal growth factor receptor 2 (HER2) , and some overexpress HER1 (or EGFR) [18]. It is important to quantify the ratio between the different receptors on the tumor cell, so the doctors can most efficient treatment for the patients. For example, the FDA-approved humanized antibody Herceptin (Trastuzumab, developed by Genentech, CA) is currently used for targeted therapy for breast cancer [19, 20]. It is important to use this drug only in the patients who are most likely to respond, because only tumors with HER2 amplification will respond to this drug [21, 22]. The accurate quantification of the HER2 expression prior to treatment with Herceptin is therefore crucial. However, current technique can only be semi-quantitative on determine the ratio of different disease signatures. We can use the TPOFF probe to simultaneously quantify multiple fluorophores with different emission wavelength to achieve the goal of simultaneous quantification of multiple disease signatures.

For proof of principle, we conjugated Herceptin (HN) with two different dyes, Alex Fluor(AF)-594 and AF-600 (Invitrogen) to produce HN-AF594 and HN-AF660. Xenograft tumors were developed in mice using either Control (C) or HER2-expressing (H) MCA-207 Cells. Two nanomolars of HN-AF594, HN-AF660, or their 1:1 mixture were injected into the mice. After 18 hours, the tumors were isolated and measured by the DCF-TPOFF probe. The measured uptake of the Herceptin conjugates in the tumors are

illustrated in Figure 3.8. Specific-binding of Herceptin conjugates on HER2 expressing tumors were observed in both wavelength channels. The left panel shows the uptake of the conjugates when the two different conjugates were administered respectively into different mice. The right panel shows the uptake of the conjugates when they were administered together in a mixture. In the right panel, the fluorescence signals from different conjugates were measured in the same tumor simultaneously. The ability to quantify multiple fluorescent species with different emission wavelength in the same tumor was demonstrated. Because of the equal competition between the two conjugates for receptor binding, the concentration of each conjugates in tumor when administered together (right panel) is only half the values of that obtained when individually administered (left panel).

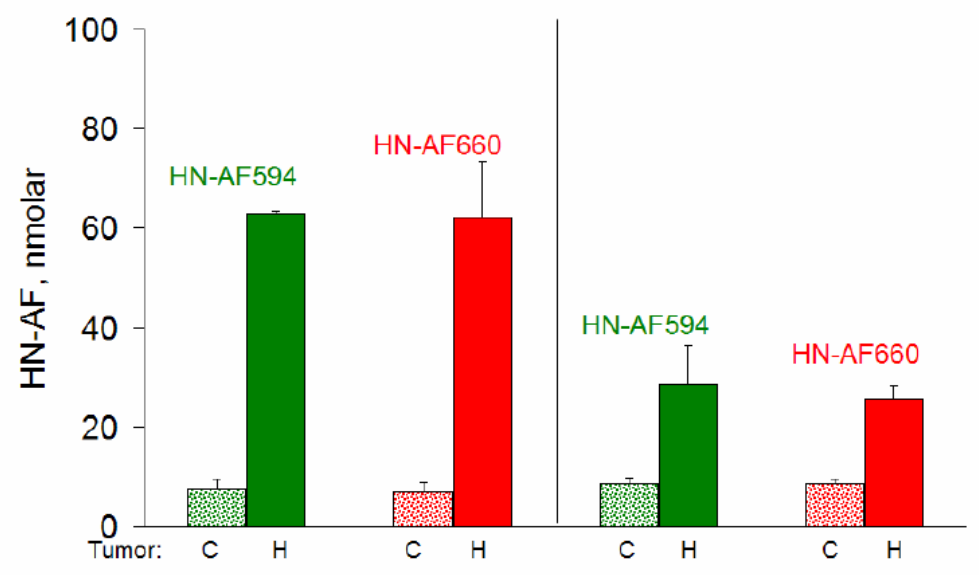

Figure 3.8 *In situ* quantification of HER2. Xenograft tumors were developed in mice using either Control (C) or HER2-expressing (H) MCA-207 Cells. The mice were injected with HN-AF594, HN-AF660, or their mixture. After 18 h, the tumor fluorescence were measured using the DCF-TPOFF probe. The concentration of each conjugates in tumor when administered together (right panel) is only half the values of that obtained when individually administered (left panel) due to the equal competition between the two conjugates for receptor binding.

3.4 Conclusion

The results in this study demonstrate that the DCF-TPOFF probe has at least a 3-fold improved tissue detection limit compared to the similar-in-diameter SMF used under similar conditions. Although the tissue background fluorescence due to endogenous fluorescent cell components is increased because of the improved sensitivity of the DCF probe, selection of appropriate fluorophores with emission wavelengths separated from endogenous emissions (e.g., red-shifted fluorophores such as Deep Red) for analysis is expected to further increase the resolution and sensitivity of the DCF. On the other hand, an understanding of the ratio of the sensitive endogenous fluorescence to that of the exogenously administered component may facilitate the more accurate determination of time-dependent changes with variables such as the power or coupling of the laser over time. The core of the DCF fiber used in this study is twice as large as that of the SMF, causing lower peak intensity at the excitation end of the DCF fiber, and the usage of fibers with a comparable core size would further enhance the sensitivity of the DCF probe. The improved sensitivity of the DCF versus the SMF and the application of a small 30-guage needle make this a superior optical fiber probe technique in quantifying fluorescent signals in deep tissues. Nanomolar quantities of multiple fluorophores with different emission wavelengths or lifetimes could be discerned and quantified using this technique. We envision that the TPOFF probe will serve as a minimally-invasive diagnostic tool for screening tumor markers, such as the EGF-receptor 2 (HER2) in women with breast cancer, when used in conjunction with a fluorescent marker such as the fluorescently tagged antibody Herceptin.

3.5 References

1. S. Svanberg, "Tissue diagnostics using lasers," in *Lasers in Medicine*, R. W. Wayanant, ed. (CRC Press, Boca Raton, FL, 2002), pp. 135-169.
2. R. Weissleder, and V. Ntziachristos, "Shedding light onto live molecular targets," Nature Medicine **9**, 123-128 (2003).
3. T. P. Thomas, J. Y. Ye, C.-S. Yang, M. T. Myaing, I. J. Majoros, A. Kotlyar, Z. Cao, T. B. Norris, and J. Baker, J. R., "Tissue distribution and real-time fluorescence measurement of a tumor-targeted nanodevice by a two photon optical fiber fluorescence probe," Proceedings of the SPIE **6095** (2006).
4. T. P. Thomas, M. T. Myaing, J. Y. Ye, K. Candido, A. Kotlyar, J. Beals, P. Cao, B. Keszler, A. K. Patri, T. B. Norris, and J. R. Baker, Jr., "Detection and analysis of tumor fluorescence using a two-photon optical fiber probe," Biophysical Journal **86**, 3959-3965 (2004).
5. B. M. Cullum, G. D. Griffin, G. H. Miller, and T. Vo-Dinh, "Intracellular measurements in mammary carcinoma cells using fiber-optic nanosensors," Analytical Biochemistry **277**, 25-32 (2000).
6. J. C. Jung, and M. J. Schnitzer, "Multiphoton endoscopy," Optics Letters **28**, 902-904 (2003).
7. A. Periasamy, *Methods in Cellular Imaging* (Oxford University Press, NY, 2001).
8. C. Xu, W. Zipfel, J. B. Shear, R. M. Williams, and W. W. Webb, "Multiphoton fluorescence excitation: new spectral windows for biological nonlinear microscopy," Proc Natl Acad Sci U S A **93**, 10763-10768 (1996).
9. T. P. Thomas, A. K. Patri, A. Myc, M. T. Myaing, J. Y. Ye, T. B. Norris, and J. R. Baker, Jr., "In vitro targeting of synthesized antibody-conjugated dendrimer nanoparticles," Biomacromolecules **5**, 2269-2274 (2004).
10. M. T. Myaing, J. Y. Ye, T. B. Norris, T. Thomas, J. R. Baker, W. J. Wadsworth, G. Bouwmans, J. C. Knight, and P. S. J. Russell, "Enhanced two-photon biosensing with double-clad photonic crystal fibers," Optics Letters **28**, 1224-1226 (2003).
11. J. Y. Ye, M. T. Myaing, T. P. Thomas, I. Majoros, A. Koltyar, J. R. Baker, W. J. Wadsworth, G. Bouwmans, J. C. Knight, P. S. J. Russell, and T. B. Norris, "Development of a double-clad photonic-crystal-fiber based scanning microscope," in *Conference on Multiphoton Microscopy in the Biomedical Sciences V*, A. S. P. T. C. Periasamy, ed. (Spie-Int Soc Optical Engineering, San Jose, CA, 2005), pp. 23-27.
12. T. P. Thomas, Shukla, R., Majoros, I. J., Myc, A., Baker Jr J. R., "Poly (amidoamine) Dendrimer-based Multifunctional Nanoparticles," in

Nanobiotechnology: Concepts, Methods and Perspectives, Mirkin, ed. (Wiley-VCH, 2007).

13. I. J. Majoros, T. P. Thomas, C. B. Mehta, and J. R. Baker, Jr., "Poly(amidoamine) dendrimer-based multifunctional engineered nanodevice for cancer therapy," Journal of Medicinal Chemistry **48**, 5892-5899 (2005).
14. I. J. Majoros, Keszler, B., Woehler, S., Bull, T., Baker Jr., J. R., "Acetylation of Poly (amidoamine) Dendrimers," Macromolecules **36**, 5526-5529 (2003).
15. T. P. Thomas, I. J. Majoros, A. Kotlyar, J. F. Kukowska-Latallo, A. Bielinska, A. Myc, and J. R. Baker, Jr., "Targeting and inhibition of cell growth by an engineered dendritic nanodevice," Journal of Medicinal Chemistry **48**, 3729-3735 (2005).
16. J. Y. Ye, T. P. Thomas, M. T. Myaing, J. R. Baker Jr., and T. B. Norris, "Biosensing based on two-photon fluorescence measurements through optical fibers," Optics letters **27**, 1412 -1414 (2002).
17. J. F. Kukowska-Latallo, K. A. Candido, Z. Cao, S. S. Nigavekar, I. J. Majoros, T. P. Thomas, L. P. Balogh, M. K. Khan, and J. R. Baker, Jr., "Nanoparticle targeting of anticancer drug improves therapeutic response in animal model of human epithelial cancer," Cancer Research **65**, 5317-5324 (2005).
18. R. Nahta, G. N. Hortobagyi, and F. J. Esteva, "Growth factor receptors in breast cancer: potential for therapeutic intervention," Oncologist **8**, 5-17 (2003).
19. J. Baselga, E. A. Perez, T. Pienkowski, and R. Bell, "Adjuvant trastuzumab: a milestone in the treatment of HER-2-positive early breast cancer," Oncologist **11 Suppl 1**, 4-12 (2006).
20. M. J. Piccart-Gebhart, M. Procter, B. Leyland-Jones, A. Goldhirsch, M. Untch, I. Smith, L. Gianni, J. Baselga, R. Bell, C. Jackisch, D. Cameron, M. Dowsett, C. H. Barrios, G. Steger, C. S. Huang, M. Andersson, M. Inbar, M. Lichinitser, I. Lang, U. Nitz, H. Iwata, C. Thomssen, C. Lohrisch, T. M. Suter, J. Ruschoff, T. Suto, V. Greatorex, C. Ward, C. Straehle, E. McFadden, M. S. Dolci, and R. D. Gelber, "Trastuzumab after adjuvant chemotherapy in HER2-positive breast cancer," N Engl J Med **353**, 1659-1672 (2005).
21. R. L. Jones, and I. E. Smith, "Efficacy and safety of trastuzumab," Expert Opin Drug Saf **3**, 317-327 (2004).
22. M. Marty, F. Cognetti, D. Maraninchi, R. Snyder, L. Mauriac, M. Tubiana-Hulin, S. Chan, D. Grimes, A. Anton, A. Lluch, J. Kennedy, K. O'Byrne, P. Conte, M. Green, C. Ward, K. Mayne, and J. M. Extra, "Randomized phase II trial of the efficacy and safety of trastuzumab combined with docetaxel in patients with human epidermal growth factor receptor 2-positive metastatic breast cancer administered as first-line treatment: the M77001 study group," J Clin Oncol **23**, 4265-4274 (2005).

CHAPTER 4
Fiber-optic Two-photon Fluorescence Correlation Spectroscopy

4.1 Introduction

Fluorescence correlation spectroscopy (FCS) is a highly sensitive technique to extract dynamical information on small particles or even single molecules from the intrinsic intensity fluctuations of the fluorescence signal in a dilute solution under thermal equilibrium. It was first introduced in 1972 by Magde *et al.*[1]. Beginning in the 1990s with the application of confocal and multiphoton techniques in FCS, the range of application of FCS in biophysical and biochemical research has grown rapidly [2-5]. Because of the capability of quantifying biomolecular interaction and associated kinetics, FCS has become an invaluable tool. The information accessible by FCS includes concentration and diffusion coefficients of molecules in solution, aggregation formation, transport rates, chemical reaction rates, and the photophysical properties of the molecules [6-8].

In a traditional FCS setup, a confocal or multiphoton microscope is employed. The use of bulky optical instrumentation limits the use of FCS *in situ* or *in vivo* deep inside the body. Use of a fiber-optic probe as a miniaturized microscope for simultaneous excitation and detection of fluorescence molecules provides a promising approach for those applications [9]. Various applications of fiber-optic sensors have been reported [10]. However, most of the applications only measure the fluorescence intensity. Use of a

fiber probe in conducting FCS can provide dynamic information for analyzing quantities such as mobility, binding dynamics, and flow velocity of the fluorescent species at a remote site. Recently, Garai *et al.* reported the use of a single-mode fiber (SMF) with a mode field diameter (MFD) of 3.3um to conduct one-photon excited (1PE) fiber-optic-based FCS and used this probe to detect aggregation of the amyloid-β peptide *in vitro*. However, the high background, as is often the case in the 1PE scheme, limits the possibility from extending the technique to single-molecular level applications [11, 12].

The problem with the high background might be solved by applying two-photon excitation (2PE) as an alternative approach to conducting fiber-optic based FCS. One of the most important advantages of 2PE is the remarkably low background noise level because of the large separation in wavelength between the laser and the fluorescence signal. In addition, due to the quadratic dependence of the excitation efficiency on laser intensity, the excitation volume is limited to only a small region close to the fiber tip [13, 14]. The probe volume is thus reduced, compared to the 1PE case under the same geometry of the fiber probe, which is desirable for FCS. A better signal-to-noise ratio can be expected due to the combination of the reduced background and the probe volume. Other potential advantages of 2PE include the ability to excite multiple fluophores with a single laser line, and decreased concentration depletion because of reduced out-of-focus photobleaching, thus allowing for a longer acquisition time without affecting the experimental result [5, 15].

In previous chapters we have described the development of a two-photon optical fiber fluorescence (TPOFF) probe as a minimally invasive technique for quantifying fluorescence in solid tumors in live mice in a real-time basis as reported previously [14, 16]. This technique exploits both the advantages of fiber optics and of two-photon excitation. The enhanced detection efficiency by using double-clad fibers (DCF) in biological applications has also been reported recently. The ability to quantify nanomolar

concentrations has been demonstrated [17-19]. In this chapter, we further investigate the capability of conducting FCS measurement with this novel double-clad fiber probe.

4.2 Theory of two-photon excited fluorescence correlation spectroscopy

In a typical FCS setup, a laser beam is focused into a solution under thermal equilibrium. The focused laser beam and the detection optics define the probe volume of the system. As fluorescent particles move in and out of this minute open region, the total fluorescence *F(t)* detected will fluctuate due to the change of the total number of molecules *N(t)* present in the probe volume. The temporal autocorrelation function of *F(t)* contains information about the average duration and amplitude of the fluctuations. The decay rate and the shape of the autocorrelation function *G(τ)* reveal the mechanism of the process and the dwell time of the particles in the probe volume. The magnitude of *G(τ)* provides information about the number density of the fluorescent molecules or particles in the probe volume. The total detected fluorescence *F(t)* is proportional to the number of particles in the focal volume, *N(t)*. The normalized autocorrelation function is defined as

$$G(\tau) = \frac{\langle \delta F(t) \delta F(t+\tau) \rangle}{\langle F(t) \rangle^2} \tag{1}$$

where $\delta F(t) = F(t) - \langle F(t) \rangle$ is the fluctuation of the fluorescence signal *F(t)* at about its average value and $\langle\ \rangle$ denotes an ensemble average, which for a stationary random process can be taken as a long-time average [20].

For two-photon excitation, the total detected fluorescence can be expressed as

$$\delta F(t) = \alpha \cdot I_0^2 \int S^2(\vec{r}) \delta C(\vec{r}, t) dV \tag{2}$$

where α is a constant proportional to the detection efficiency, the two-photon cross section, and the quantum yield of the fluophore; I_0 is the average laser intensity at the geometric center of the focus; $S(\vec{r})$ is the dimensionless spatial profile of the laser

beam; and $\delta C(\vec{r},t)$ is the fluctuation of the concentration at different points inside the probe volume.

Although in our 2PE daul-clad fiber configuration, the probe volume is determined only by the excitation profile of the laser beam propagating in the central core. The excitation profile can be calculated by taking the square of the laser beam spatial profile $S(\vec{r})$. The spatial profile of the laser beam emitted from the fiber core can be well approximated by one half of a Gaussian beam. With a Gaussian approximation for the spatial profile, the analysis of the diffusion for FCS data is the same as conventional 2PE FCS. The autocorrelation function takes the following form:

$$G(\tau) = \frac{1}{\langle N \rangle} \cdot \frac{1}{\left(1+\frac{\tau}{\tau_d}\right)} \cdot \frac{1}{\sqrt{1+k^2\frac{\tau}{\tau_d}}} \tag{3}$$

where $\langle N \rangle$ is the average number of particles in the probe volume and $k = w_0/Z_R$ is the ratio of the radius of the beam waist w_0 to the Rayleigh range Z_R.

The beam waist and the diffusion time τ_d are related by

$$w_0^{\,2} = 8D\tau_d \tag{4}$$

where D is the diffusion coefficient. The relation between the diffusion coefficient and the hydrodynamic radius of the particle R can be expressed by the Stokes-Einstein equation:

$$D = \frac{k_B T}{6\pi\eta R} \tag{5}$$

where k_B is the Boltzmann constant, T is the temperature, and η is the viscosity of the solution. With the measured diffusion time τ_d, the size of the particle R can be calculated through

$$R = \frac{4k_B T}{3\pi\eta \cdot w_0^{\,2}}\tau_D \tag{5a}$$

The probe volume V can be calculated from the laser spatial profile $S(\vec{r})$ through the relation,

$$V = \gamma^{-1} \int S^2(\vec{r}) d\vec{r}^3 \tag{6}$$

where $\gamma = \int S^4(\vec{r}) d\vec{r}^3 \Big/ \int S^2(\vec{r}) d\vec{r}^3$ represents the volume contrast defined by the geometric shape of the beam. For a radially Gaussian, axially Lorentzian profile, as is the case here, γ=3/16 [13].

From Eq. (3), one can calculate the average number of particles in the probe volume by taking the inverse of *G(0)*. However, in the presence of high background, the relation between *G(0)* and *N* has to be modified accordingly. The total measured fluorescence is $F_{tot}(t) = F(t) + B(t)$, where *B(t)* is the background count rate. However, only the fluctuation of the fluorescence signal *F(t)* from the particles contributes to *G(τ)*. Therefore, the autocorrelation function at time zero has to be modified to

$$G(0) = \frac{1}{\langle N \rangle} \cdot \frac{F^2}{F_{tot}^2} = \frac{N}{(N + N_B)^2} \tag{7}$$

where N is the average number of particles in the probe volume and N_B is the equivalent number of particles due to background fluorescence [11].

4.3 Methods and materials

4.3.1 Two-photon fiber FCS apparatus

The experimental setup was similar to that described in Chapter 2. However, in order to increase the single-to-noise ratio of FCS measurements, the monochromator in the detection system was removed. The fluorescence signal was detected by the PMT directly after the filters, as shown in Figure 1(a). The Ti:sapphire laser (Coherent Inc., Mira 900) generated 50-fs pulses at 800 nm with a 76-MHz repetition rate. The pulse was first double-passed through a 2000 line/mm transmission grating to pre-compensate the

fiber dispersion and thus optimized the peak intensity of the output pulse at the distal fiber end. The beam was coupled into the inner core of the fiber with a 40X microscope objective (NA=0.65). The size of the beam at the back aperture of the objective was adjusted to match the mode field diameter of the fiber core. The fluorescence signal was collected back through the same fiber and was separated from the excitation beam by a dichroic mirror. The fluorescence signal was filtered by two short pass filters (E750SP and E735SP, Chroma) to block the scattered laser light and a set of band-pass filters (Melles Griot D525/250, HQ510/50) for fluorescence wavelength selection. The signal is detected by a photomultiplier tube (PMT, Hamamatsu, H7422-40) and recorded by a time-correlated single photon counting (TCSPC) module (SPC-630, Becker and Hickl, GmbH) installed in a computer.

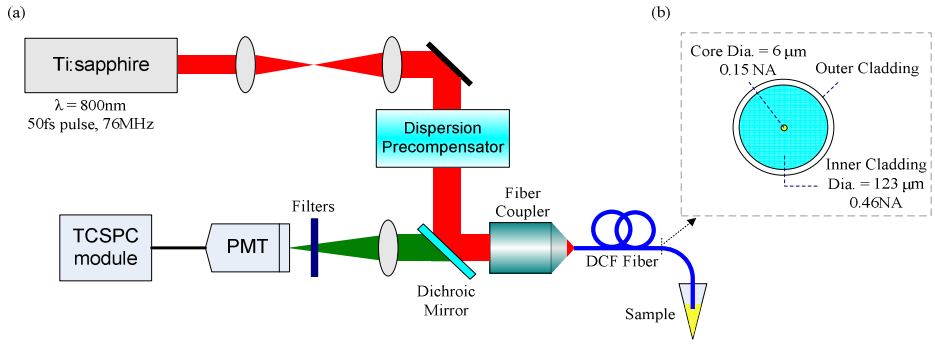

Figure 4.1 (a)Experimental setup for the fiber-optic fluorescence correlation spectroscopy. (b) Cross-section geometry of the double-clad fiber used in this study.

4.3.2 Enhanced FCS sensitivity by the double-clad fiber

The DCF used in this study has an inner core diameter of 6 µm with an NA of 0.15 and an inner cladding diameter of 123 µm with an NA of 0.46. The schematic of the DCF cross-section is illustrated in Figure 1(b). The total coupling efficiency was 69% with 49% of the output power in the core.

The unique feature of the DCF enables simultaneous optimization of the excitation and collection efficiencies. The 2PE efficiency is maintained by propagating ultrafast pulses through the inner single-mode core of the DCF, while the collection efficiency is improved by the high numerical aperture (NA) multimode inner cladding (outer core), which is confined with a second cladding. A significantly improved detection sensitivity of the DCF was obtained. The DCF has a 17-fold increase in the two-photon fluorescence signal compared to the SMF. In FCS, the sensitivity is quadratically proportional to the brightness of the fluorescent particles. A 17-fold increase in the signal translates to about 290-fold increase in the signal to noise ratio in FCS measurements. In the experiments, we found that the SMF does not have enough sensitivity for two-photon fiber FCS (2P-FFCS) to detect fluorescence particles smaller than 100 nm. The adoption of a DCF is crucial for ultrasensitive detection of 2P-FFCS.

4.3.3 Sample preparation

Fluorescent nanospheres were purchased from Invitrogen (FluoSpheres, Molecular Probe). The spectral absorption and emission maxima of the nanospheres were 505 nm and 515 nm, respectively, for one-photon excitation. Quantum dots (QDs) were also purchased from Invitrogen (Q21331MP, Molecular Probe). The emission maximum of the quantum dots is 565 nm.

Because of the high sensitivity of FCS in dilute solutions, any agglomerates or fluorescent impurities in the solutions can make up an appreciable fraction of the signal, obscuring correlations due to the species of interest. Therefore, the size distributions of all nanosphere samples were checked by dynamic light scattering (DLS, DynaPro, Protein-Solutions Inc.) before FCS measurements. All the samples were dissolved in MilliQ water (Millpore) unless stated otherwise. Spheres were diluted to appropriate concentrations and then sonicated for 15 minutes. After sonication, the 12 nm and 18 nm radius nanospheres and QDs were first filtered with a 0.1um syringe filter (GE water &

process technology) and then with a 0.05um membrane filter (Millipore). Filtering is a critical step for accurate measurements, especially for nanospheres smaller than 50 nm [4]. All samples were confirmed to have a narrow size distribution by dynamic light scattering measurements. The measured sizes are summarized in Table 1.

4.4 Diffusion measurements

4.4.1 Two-photon fiber FCS measurements

The 2P-FFCS system was used to measure the diffusion (due to Brownian motion) of fluorescence nanospheres in water solutions by directly dipping the fiber tip into the solution. Figure 4.2 shows the raw data of the intensity fluctuation of the fluorescence signal detected by the detector. For 100-nm fluorescence nanoparticle (blue trace), the fluctuation can be clearly seen when the particle move around the probe volume. However, for smaller particles, it is impossible to tell the size of the particle by only looking at the time trace. FCS is the technique to extract information from noise looking signal.

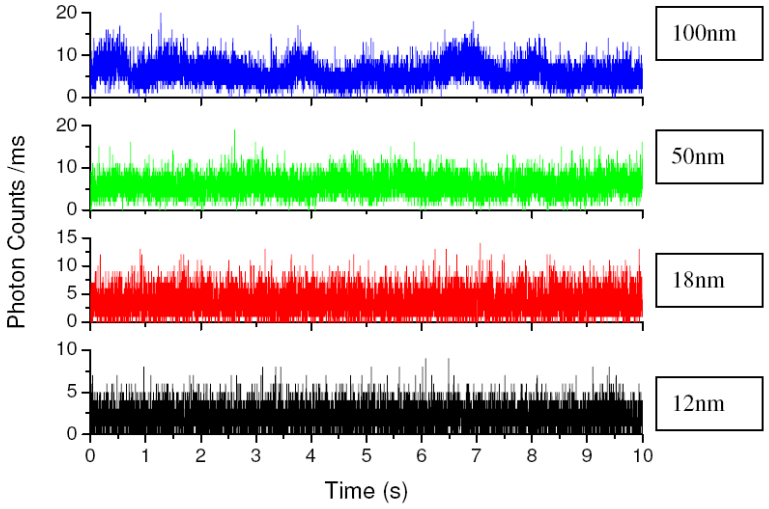

Figure 4.2 Fluorescence intensity fluctuation time trace of different size beads. Each point shown is the number of photons detected in 1 ms. The average count rates are 7.2, 5.7, 3.5, 2.2 kcps for 100 nm, 50 nm, 18 nm, 12 nm beads respectively.

After doing an autocorrelation of the time traces, we obtain the FCS curves as shown in Figure 4.3. The results of QDs measurements were added to the figure. The nominal radii of the QDs and the nanospheres provided by the manufacturer are 7 nm, 12 nm, 18 nm, 50 nm and 105 nm, respectively, which are measured by transmission electron microscopy (TEM). The FCS curves for the diffusion of these nanoparticles are shown in Figure 4.3(a). The curves are normalized to better illustrate the more rapid diffusion time of smaller particles. The solid curves are the fits of the data using Eq. (3). The total output power from the fiber for all the measurements was 20 mW, except for 105-nm radius beads. The excitation power for 105-nm beads was lowered to 10 mW to avoid occasional overflow of the detection unit. The acquisition time for each set of data was ~3 minutes. The data were acquired by the FIFO (first in first out) mode (also called time-tagged time-resolved mode) in the TCSPC module, and the correlation curves were calculated afterward by software (SPCM) provided by the manufacturer. The correlation curves were calculated directly from the single photon counting trace recorded, and the resolution is limited only by the dead time of the TCSPC module, which is ~100 ns. Higher signal-to-noise ratio (SNR) can be obtained with longer acquisition time, providing the solution is well prepared and impurity free. However, even when all the samples were filtered and sonicated before measurements, the longer the experimental time, the higher the probability to observe agglomerates, especially for small nanospheres, which can affect the accuracy of the measurement significantly. Therefore, the acquisition time was kept shorter than 5 minutes, but for 12- and 18-nm radius beads, the curves were averaged four times to obtain a better SNR. The average mean diffusion times obtained from the FCS curves were 41, 54, 89, 247, and 544 ms, respectively. The relation between the particle sizes and the measured diffusion times is plotted in Figure 4.3(b). The solid line is the theoretical prediction from the Stokes-Einstein equation. The measured diffusion times for all the beads are consistent with the theory. The calculated

MFD of the core of the DCF from the experimental data was determined to be 5.9±0.2 µm, which is close to the value given in the specification of 6 µm.

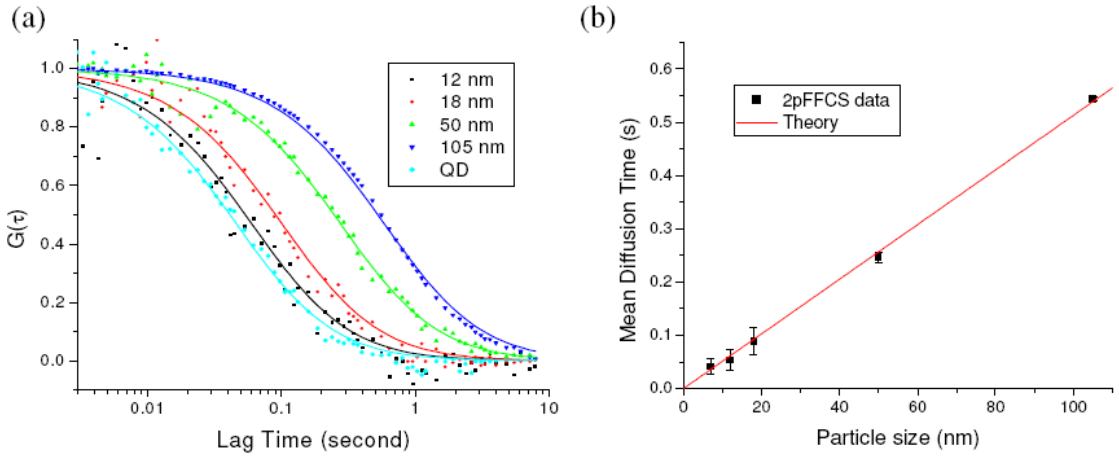

Figure 4.3 (a) Fluorescence correlation curves of quantum dots (cyan diamond) and fluorescent nanospheres of radii 12 nm (black square), 18 nm (red circle), 50 nm (green upward triangle), and 105 nm (blue downward triangle). The solid curves are the corresponding fits. **(b)** The measured mean diffusion times versus nominal particle sizes as measured with TEM. The solid line is the theoretical prediction from the Stokes-Einstein relation.

4.4.2 Accuracy of the measurements

The sizes measured by DLS and 2P-FFCS are compared to the nominal sizes given by the manufacturer and are summarized in Table 1. Since both DLS and FCS measure the hydrodynamic radius of the particles, the comparison gives a good indication of the accuracy of the technique [7]. The manufacturer-provided nominal sizes are measured by TEM, which measures the radius of the spheres on a dry surface. From the diffusion time measured by FCS, the size of the particles can be calculated using Eq. (5a), with w_0 = 3 µm, T =300 K and η= 1.002 X 10^{-3} N s/m. The measured sizes show excellent agreement between these two methods.

TEM[a]	12±2nm	18±2nm	50±3nm	105±5nm
DLS	13.1±2.5	19.6±3.2	52.1 ± 2.1	103.1±1.4
FCS[b]	10.5±3.9	17.3±4.9	48.1±2.0	106.0±0.6

[a]Manufacturer-provided nominal sphere radii measure by TEM.
[b]The sizes are calculated by Eq. (5a) using the diffusion time measured by FCS.

Table 4.1 Comparison of the sphere radii determined by DLS and FCS

The magnitude of *G(0)* provides additional information on the accuracy of the technique. From Eq.(3), we know that $G(0)^{-1}$ is proportional to the average number of molecules $\langle N \rangle$ in the probe volume. However, when the signal and background are comparable, one needs to consider the effect of background on *G(0)* to obtain correct measurements of sample concentrations.

The measured *G(0)* for 6-pM and 60-pM solutions of 50-nm beads were 0.010 and 0.0085, respectively. The reason comparable *G(0)* were obtained despite the 10-fold difference in the concentrations is because of the background. The background photon count rate was 1.6 kHz. The signal count rates were 440 Hz and 4.1 kHz for 6-pM and 60-pM solutions, respectively. According to Eq. (7), the deduced average numbers of particles in the probe volume were 5.5 and 51.9, respectively, which is in agreement with the concentrations used. In addition, from the knowledge of the concentration and average number of particles in the probe volume, the estimated probe volume is ~ 1.49×10^3 μm^3, which matches the calculated probe volume from Eq.(6) of 1.57×10^3 μm^3. Both the recovered concentrations and the probe volume correspond to the theoretical prediction.

4.4.3 Sensitivity of the technique

One of the main motivations to conduct two-photon excited FCS is lower background noise because of easy separation of the excitation laser light from the fluorescence signal. This is especially important when using a fiber probe to do FCS because the light has to travel in a longer medium, the fiber, to reach the probe end. The

longer the interaction length of the light with the medium, the more the scattered light is generated, which increases the background.

Initially, we used a low NA, 10-μm core diameter DCF (P10/123DC, NA =0.07, Thorlab) to implement 2P-FFCS; the background count rate was as low as ~60 counts per second (cps) (including a dark count rate of 19 cps). The background level was about the same as a conventional objective-based FCS system. However, due to the larger probe volume and lower excitation efficiency, that fiber did not have enough sensitivity to measure fluorescent nanospheres with a radius smaller than 50 nm. Therefore, we adopted the 6-μm core DCF to conduct 2P-FFCS measurements of nanospheres here. This fiber showed sensitivity adequate enough to measure fluorescent nanospheres as small as 12 nm in radius. Nevertheless, this fiber had a higher background count rate of ~1.6 kHz, possibly due to higher doping in the core to achieve higher NA. We investigated the power dependence of the background by putting the fiber tip into pure water in the same experimental configuration. The background photon counts versus total fiber output power is shown in Figure 4.4. The slope on the log-log plot is 1.7, which indicates the majority of the background is caused by 2PE fluorescence of impurities or dopants inside the fiber. Garai *et al.* also observed the high background due to autofluorescence from single-mode fibers. The existence of the high background from the intrinsic fluorescence of the fiber complicated the application of a fiber-optics based FCS system to single-molecule-level measurements [11].

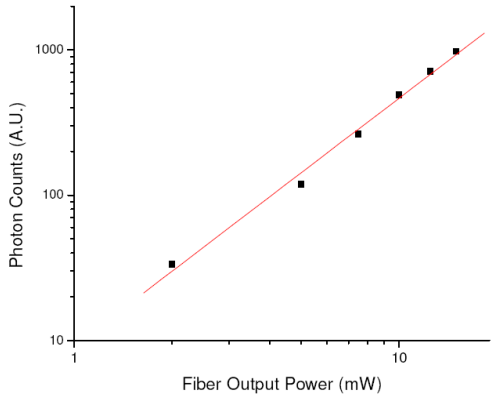

Figure 4.4 The power dependence of the background photon counts when the fiber tip was put into pure MilliQ water. The abscissa represents the total output power at the probe end of the DCF, and the ordinate represents the detected photon counts per second. The solid line is the linear fit on the log-log plot, and the slope was found to be 1.7.

4.4.4 Reducing the background from the fiber

Fortunately, the use of ultrafast pulses for 2PE FCS enables additional background reduction through time-gated detection [3, 21]. As shown in Figure 4.5, the background from the scattering and autofluorescence from the fiber can be separated from the fluorescence signal in a time-resolved measurement. A software time-gated analysis can be applied when using TCSPC for FCS measurements. We find that the background can be reduced for as high as 5-fold without losing a significant amount of the 2PE fluorescence signal because of the long delay time provided by the fiber.

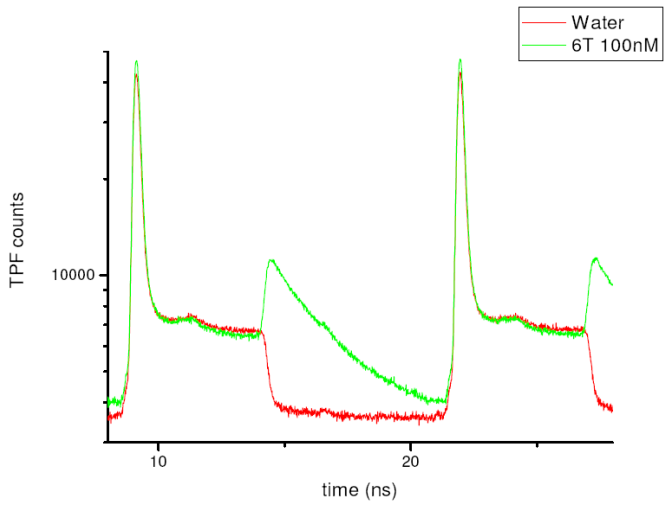

Figure 4.5 Time-resolved fluorescence lifetime measurements. The red trace is the background signal when putting the fiber tip into pure de-ionized water. The green trace is the fluorescence lifetime measurement when putting the TPOFF probe into 100-nM 6-TAMRA solution. The fiber length was 60 cm. The bandpass filter in front of the PMT was removed to illustrate the effect of the background of the fiber. The laser repetition rate was 76 MHz, therefore the time duration in each period was 13 ns.

4.4.5 Reduce the excitation volume by a micro-lens

We have demonstrated that our technique can measure fluorescent nanospheres as small as 12 nm in radius. We also demonstrated the ability to measure QDs with 7-nm radius. The SNR of the QD measurement is comparable to the 50-nm fluorescent nanosphere, which is about 40-fold brighter than the 12-nm nanosphere. No averaging was required to resolve the QDs from other size particles, which shows the potential to use QDs as fluorescent probes for *in vivo* fiber FCS. QD's are known for their exceptional 2PE cross-section and photostability. There have been various applications using QD for *in vivo* multiphoton FCS studies [22, 23].

The main limitation to conducting two-photon FCS through a fiber is the excitation efficiency at the probe end. The 2PE efficiency, which is determined by the geometry of the fiber, is more than one order of magnitude lower than a setup with a high

numerical aperture objective lens. However, in contrast to the one-photon scheme, the size of the probe volume in the 2P-FFCS is determined by the two-photon fluorescence excitation volume rather than by the collection geometry. Thus, we can further engineer the fiber tip to simultaneously reduce the probe volume and increase the excitation efficiency. Fabrication of a micro-lens at the fiber tip may be a promising way to enable the implementation of *in vivo* FCS measurement deeper inside the body.

4.5 FCS in a flow system

4.5.1 Flow velocity measurement

In a system where the samples are flowing or have translational movements, FCS can be used to measure the flow velocity. If the speed of the translational flow is V, assuming the particle is much smaller than the beam waist w_0, the average transition time $\tau_t = \frac{w_0}{V}$, the autocorrelation function G(τ) becomes

$$G(\tau) = \frac{1}{\langle N \rangle} \cdot \frac{1}{\left(1 + \frac{\tau}{\tau_{diff}}\right)} \cdot \exp\left[-\left(\frac{\tau}{\tau_t}\right)^2 \cdot \frac{1}{\left(1 + \frac{\tau}{\tau_{diff}}\right)} \right] \tag{7}$$

In the case where the movement due to translational flow is much faster than the diffusion, or $\tau_{diff} >> \tau_t$, the equation can be simplified to

$$G(\tau) = \frac{1}{\langle N \rangle} \cdot \exp\left[-\left(\frac{\tau}{\tau_t}\right)^2 \right] \tag{8}$$

By fitting the autocorrelation curve to this equation, we can obtain the speed of the flowing particles.

Figure 4.6 shows FCS measurements on flowing 500-nm diameter fluorescence microspheres in a 1500-μm inner diameter plastic micro tube. The flow rate was

controlled by a syringe pump. As shown in Figure 4.6 (b), the mean dwell time, which is the mid-point in the FCS curve, is inversely proportional to the flow rate as predicted by the theory.

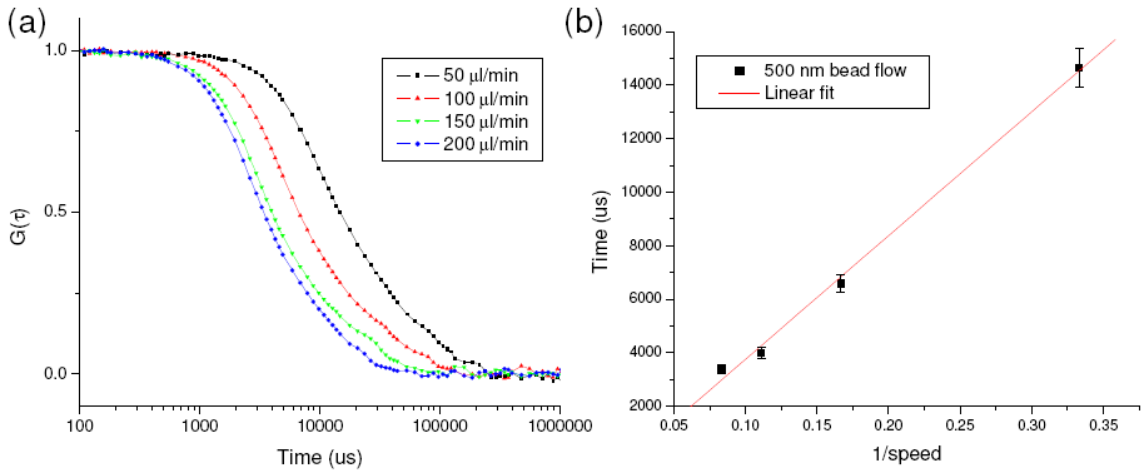

Figure 4.6 (a) FCS measurements on 500 nm microspheres with different flow rates. The flow velocity was controlled by a syringe pump. **(b)** The mean dwell time of the particles in the probe volume at different flow velocity.

4.5.2 Cell size measurement with FCS

The size of cells are in the order of 10-20um, R_{cell}, which is much larger than the focus of the objective. The relationship between the transition time of small particles, such as quantum dots (R_{Qdot}=15~20nm), and cells is:

$$\frac{w_0}{\tau_{Qdot}} = flow \quad velocity = \frac{Cell \quad size}{\tau_{cell}}$$

Therefore, we can use nanometer scale particles such as quantum dot or simple fluorescence dye to calibrate the speed of flow. Then flow the cells through the capillary with the same flow rate. By fitting the autocorrelation curve, we can derive the size of the cell [24].

4.5.3 Use FCS to distinguish cells

The FCS curves of different molecule or particles are different. The information obtained from FCS measurements can provide additional dynamic information of the fluorescent species. For larger paticle with size larger than the focal spot size, the shape or fluorescent molecule distribution of the particle can affect the shape of the FCS curve due to non-even excitation when the particle pass through the probe volume. Therefore, it is possible to use FCS curves to distinguish different fluorescent species even though they have comparable size.

Figure 4.7 shows the FCS curves of two differently labeled cells. Untransfected MCA-207 cells with DiD labeled on the membrane and stably GFP-transfected MCA-207 cells were measured. The cells were flowed in a 500-μm inner diameter plastic micro tube. The two kinds of cells showed different transient decay behavior. The GFP-expressing cells showed a faster decay curve because the GFPs are inside the whole cell while the DiD is only on the membrane.

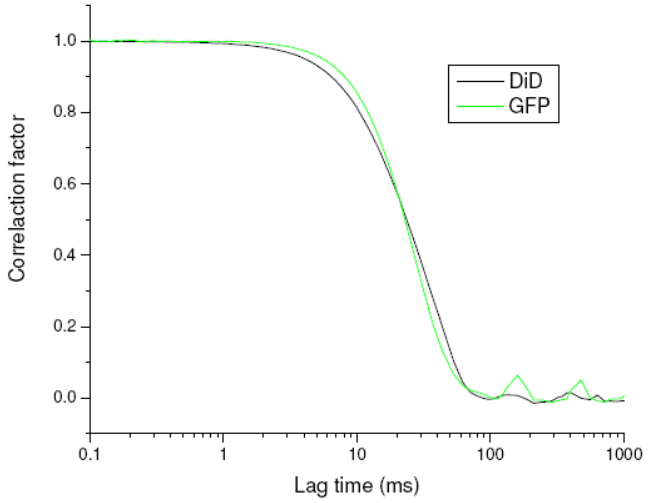

Figure 4.7 FCS measurements of differently labeled cells. The black line is normal MCA-207 cell with DiD labeled on the membrane. The green line is GFP-expressing MCA-207 cell with GFPs inside the cell. The flow velocity was ~ 4.2 mm/s.

4.6 Conclusion

To summarize, a two-photon-excitation fiber-optic-based fluorescence correlation spectroscopy system based on a double-clad fiber probe has been developed. This technique exploits both the advantages of 2PE and of fiber optics. The ability to detect fluorescent nanospheres as small as 12 nm in radius has been demonstrated. We have also shown that a smaller detection size limit is achievable when quantum dots are employed as the fluorescent probe. Because of the two-photon excitation scheme, the background noise from the coherent scattering and autofluorescence of the fiber is reduced, as compared to the one-photon scheme. Our study showed that it is critical to employ a double-clad fiber for a fiber-based two-photon FCS measurement to achieve adequate sensitivity for the measurements of fluorescent nanoparticles. Because of the pulsed 2PE scheme, multiple fluophores with different excitation maxima can be excited simultaneously and fluophores with different lifetimes can also be discerned. Thus, we envision this novel fiber sensor technique can have multidimensional detection capability and serve as a minimally-invasive diagnostic tool to detect and identify sparse amounts of disease-specific molecules in body fluids or on neoplastic cells *in vivo* for early screening and treatments.

4.7 References

1. D. Magde, W. W. Webb, and E. Elson, "Thermodynamic Fluctuations in a Reacting System - Measurement by Fluorescence Correlation Spectroscopy," Physical Review Letters **29**, 705-& (1972).
2. M. Eigen, and R. Rigler, "Sorting Single Molecules - Application to Diagnostics and Evolutionary Biotechnology," Proceedings of the National Academy of Sciences of the United States of America **91**, 5740-5747 (1994).
3. M. Bohmer, M. Wahl, H. J. Rahn, R. Erdmann, and J. Enderlein, "Time-resolved fluorescence correlation spectroscopy," Chemical Physics Letters **353**, 439-445 (2002).
4. K. M. Berland, P. T. C. So, and E. Gratton, "2-Photon Fluorescence Correlation Spectroscopy - Method and Application to the Intracellular Environment," Biophysical Journal **68**, 694-701 (1995).
5. P. Schwille, U. Haupts, S. Maiti, and W. W. Webb, "Molecular dynamics in living cells observed by fluorescence correlation spectroscopy with one- and two-photon excitation," Biophysical Journal **77**, 2251-2265 (1999).
6. E. L. Elson, and D. Magde, "Fluorescence Correlation Spectroscopy .1. Conceptual Basis and Theory," Biopolymers **13**, 1-27 (1974).
7. R. Rigler, and E. Elson, *Fluorescence correlation spectroscopy : theory and applications* (Springer, Berlin ; New York, 2001).
8. E. L. Elson, "Quick tour of fluorescence correlation spectroscopy from its inception," Journal of Biomedical Optics **9**, 857-864 (2004).
9. F. Helmchen, "Miniaturization of fluorescence microscopes using fibre optics," Exp Physiol **87**, 737-745 (2002).
10. O. S. Wolfbeis, "Fiber-optic chemical sensors and biosensors," Analytical Chemistry **78**, 3859-3873 (2006).
11. K. Garai, M. Muralidhar, and S. Maiti, "Fiber-optic fluorescence correlation spectrometer," Applied Optics **45**, 7538-7542 (2006).
12. K. Garai, R. Sureka, and S. Maiti, "Detecting amyloid-beta aggregation with fiber-based fluorescence correlation spectroscopy," Biophysical Journal **92**, L55-L57 (2007).
13. J. Mertz, C. Xu, and W. W. Webb, "Single-molecule detection by two-photon-excited fluorescence," Optics Letters **20**, 2532-2534 (1995).

14. J. Y. Ye, M. T. Myaing, T. B. Norris, T. Thomas, and J. Baker, "Biosensing based on two-photon fluorescence measurements through optical fibers," Optics Letters **27**, 1412-1414 (2002).

15. S. A. Kim, K. G. Heinze, and P. Schwille, "Fluorescence correlation spectroscopy in living cells," Nature Methods **4**, 963-973 (2007).

16. T. P. Thomas, M. T. Myaing, J. Y. Ye, K. Candido, A. Kotlyar, J. Beals, P. Cao, B. Keszler, A. K. Patri, T. B. Norris, and J. R. Baker, "Detection and analysis of tumor fluorescence using a two-photon optical fiber probe," Biophysical Journal **86**, 3959-3965 (2004).

17. M. T. Myaing, J. Y. Ye, T. B. Norris, T. Thomas, J. R. Baker, W. J. Wadsworth, G. Bouwmans, J. C. Knight, and P. S. J. Russell, "Enhanced two-photon biosensing with double-clad photonic crystal fibers," Optics Letters **28**, 1224-1226 (2003).

18. T. P. Thomas, J. Y. Ye, Y. C. Chang, A. Kotlyar, Z. Cao, I. J. Majoros, T. B. Norris, and J. R. Baker, "Investigation of tumor cell targeting of a dendrimer nanoparticle using a double-clad optical fiber probe," J Biomed Opt **13**, 014024 (2008).

19. M. T. M. J.Y. Ye, T.P. Thomas, I.J. Majoros, A. Kotlyar, J.R. Baker, Jr., W.J. Wadsworth, G. Bouwmans, J.C. Knight, P.J. Russell, T.B. Norris, "Development of a double-clad photonic-crystal-fiber based scanning Microscope," in *Proceedings of the SPIE*(2005), pp. 23-27.

20. N. L. Thompson, "Fluorescence correlation spectroscopy," in *Topics in Fluorescnce Spectroscopy*, J. R. Lakowicz, ed. (Plenum Press, New York, 1991).

21. D. C. Lamb, A. Schenk, C. Rocker, C. Scalfi-Happ, and G. U. Nienhaus, "Sensitivity enhancement in fluorescence correlation spectroscopy of multiple species using time-gated detection," Biophysical Journal **79**, 1129-1138 (2000).

22. D. R. Larson, W. R. Zipfel, R. M. Williams, S. W. Clark, M. P. Bruchez, W. F. W., and W. W. Webb, "Water-Soluble Quantum Dots for Multiphoton Fluorescence Imaging in vivo," Science **300**, 1434-1436 (2003).

23. H. Kobayashi, Y. Hama, Y. Koyama, T. Barrett, C. A. Regino, Y. Urano, and P. L. Choyke, "Simultaneous multicolor imaging of five different lymphatic basins using quantum dots," Nano Lett **7**, 1711-1716 (2007).

24. P. S. Dittrich, M. Jahnz, and P. Schwille, "A new embedded process for compartmentalized cell-free protein expression and on-line detection in microfluidic devices," Chembiochem **6**, 811-+ (2005).

CHAPTER 5
Fiber-optic Intravital Two-photon Flow Cytometry

5.1 Introduction

Current research on cancer metastasis emphasizes the detection and quantification of various types of disseminating tumor cells (DTCs) or circulating tumor cells (CTCs) [1, 2]. It has been reported that the presence of CTCs in the blood stream correlates strongly with cancer metastasis and progression [3]. Therefore, there is great interest in developing techniques to detect the presence of cancer cells in the blood stream. Quantitative detection of CTCs can help clinicians to assess patients' responses to therapy and can aid in prognosis diagnosis [2, 4, 5]. Conventional flow cytometry is the standard technique to rapidly obtain quantitative information on a large number of cells. However, because of the stable hydrodynamic flow stream required to achieve quantitative measurements of cell information, it can only be performed *in vitro* or *ex vivo*. Blood samples need to be extracted from patients or animals, followed by *ex vivo* labeling and detection. The removal of cells from their native environment and the additional processing before the measurements can introduce potential artifacts. In addition, the extracted blood samples contain different cell populations each time, which cannot reflect the real situation in the living body. Consequently, it is desirable to enumerate the cells *in vivo* in real time to monitor the progress of the disease [5, 6].

To noninvasively detect circulating cells *in vivo*, several efforts have been made using microscope-based one-photon or multiphoton excitation schemes [5-8]. However,

because of the scattering and absorption of biological tissue, only the peripheral blood vasculature can be accessed by these free-space detection techniques. The blood volume sampled by these techniques is always less than 0.5 μL/min (consider a blood vessel of ~ 50 μm in diameter with an average flow velocity of 5 mm/s) [9]. The concentration of CTCs in the blood stream is less than 1 cell per milliliter at the early stage of metastasis. In order to sample a large volume of blood, long-term monitoring is necessary. However, for free-space monitoring techniques, in order to keep the focus of the laser beam on the blood vessel, the subject has to be immobilized or anesthetized, which limits the acquisition time. The sampled blood volume is thus too small to practically identify the rare CTCs in clinical applications. A fiber-optic probe can be applied as a minimally invasive technique to access large blood vessels deep inside the body to increase the sampled blood volume.

The novel double-clad fiber-based two-photon optical fiber fluorescence (DCF-TPOFF) probe developed here can serve as an alternative way to conduct long-term real-time *in vivo* flow cytometry as a minimally invasive technique. The fiber probe can be inserted into a larger vein deeper inside the body as in an intravenous drip. We have demonstrated that we can thread the fiber through a 30-gauge needle and use the fiber probe to implement *in vivo* fluorescence measurements on solid tumors [10, 11]. The ability to measure multiple biomarkers with different excitation and emission spectra have also been demonstrated previously [12]. The ability to use this probe to conduct dual-wavelength-channel *in vivo* monitoring of cell circulation will be demonstrated in this chapter.

In addition to the advantage that the fiber probe can access larger blood vessels to sample more blood volume, the scattering and absorption problems due to turbid blood and tissue are circumvented. Because of the two-photon excitation scheme, the excitation region is only 5 μm in diameter in the lateral direction and 25 μm in the axial direction along the fiber. Hence, we have single-cell resolution. The excitation and detection

happen right at the fiber tip, Scattering from blood cells and plasma would have minimal effects on the collection of fluorescent photons. Enhanced detection efficiency on GFP-expressing cells compared to the free-space detection scheme is confirmed. Although *in vivo* detection of GFP-expressing cells in the blood stream has been demonstrated recently by Boutrus *et al.*[8], the detection efficiency was still low compared to that of longer wavelength near infrared florescent dye. The ability to efficiently detect GFP-expressing cells will further assist the study of cancer metastasis on mouse models.

5.2 Flow cytometry

5.2.1 Conventional flow cytometry [13]

In conventional flow cytometry, the laser beam is focused into a stream of flowing cells to examine microscopic properties of cells as they move through the focus. This technology allows measurement of multiple parameters on individual live cells, identification of extremely rare cells, and the sorting of cells at high speeds while maintaining cell viability.

A typical flow cytometer consists of three functional units: (1) a fluidics system, which controls the passage of cells through the sensing system; (2) an optical system, which comprises a light source together with some light-collecting optics and detectors; (3) a data analysis system, which collects data and performs analysis on the electrical signals collected from the detectors (Figure 5.1) [13].

The fluidics system serves to deliver cells in suspension to a probing point, where a laser beam is focused. Most instruments utilize a lamina/sheath flow technique to confine cells to the center of the flow stream. Cells enter the chamber under pressure through a small aperture surrounded by the sheath fluid (usually physiological saline). The pressure-driven sheath used in most flow cytometers operates at a flow rate of 1~10

m/s. Up to 100,000 particles can be analyzed less than a minute [14]. The sheath fluid in the sample chamber not only prevents clogging, but also creates a hydrodynamic focusing effect and aligns the cells into a stream. Accurate and precise positioning of the sample fluid within the sheath fluid is critical to efficient operation of the flow cytometer. Adjustment of the relative sheath and sample pressure ensures that cells pass through the probing area one after another [15].

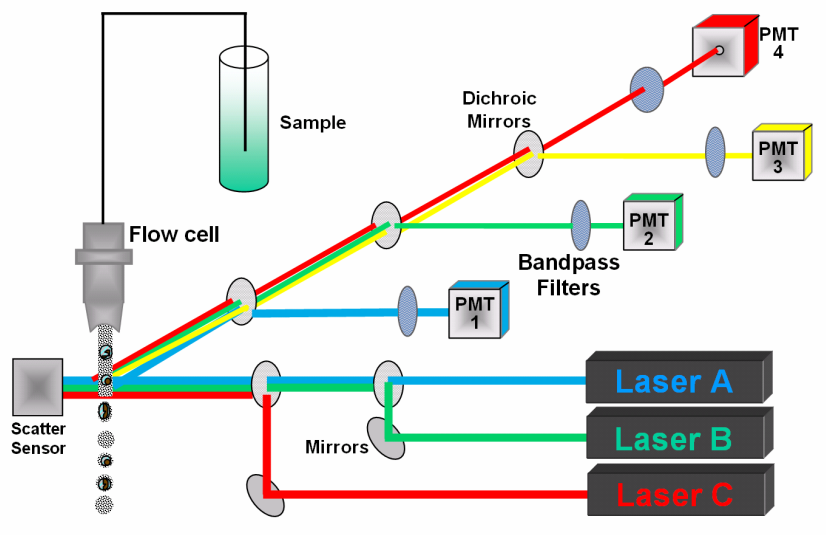

Figure 5.1 Schematic layout of a conventional flow cytometer (from Purdue University Cytometry Laboratories)

The optical system focuses a laser beam on the stream and collects scattered and fluorescent light from cells as they pass through. Scattered and emitted fluorescent signals from individual particles are captured by a large numerical aperture (N.A.) lens and sent to an array of detectors through a series of beam splitters and optical filters. The light scattering behavior of objects of dimensions near the wavelength of light is dependent on the refractive index difference between the particle and the medium and on the particle size.

5.2.2 two-photon flow cytometry

A two-photon flow cytometry system was developed in our group [13]. The schematic of the setup is shown in Figure 5.2. The excitation source was a Ti:Sapphire laser (Mira-900 Coherent Inc. Santa Clara, CA) which generates 50-fs pulses at 800nm with 76-MHz repetition rate (typically with 10mW average power at focus). The femtosecond laser pulses were focused by a long working distance Olympus 40X 0.55NA infinity corrected microscope objective (Olympus America Inc. Melville, NY) into the square capillary tube. The average power used for cell measurements was between 10 and 20mW at the excitation region. The laser excited fluorescent tags in the cells via two-photon transitions. A telescope was used to expand and collimate the laser beam to overfill the back lens of the objective, which produced a 2μm spot in the focal plane. The fluorescence photons were collected by PMTs and analyzed.

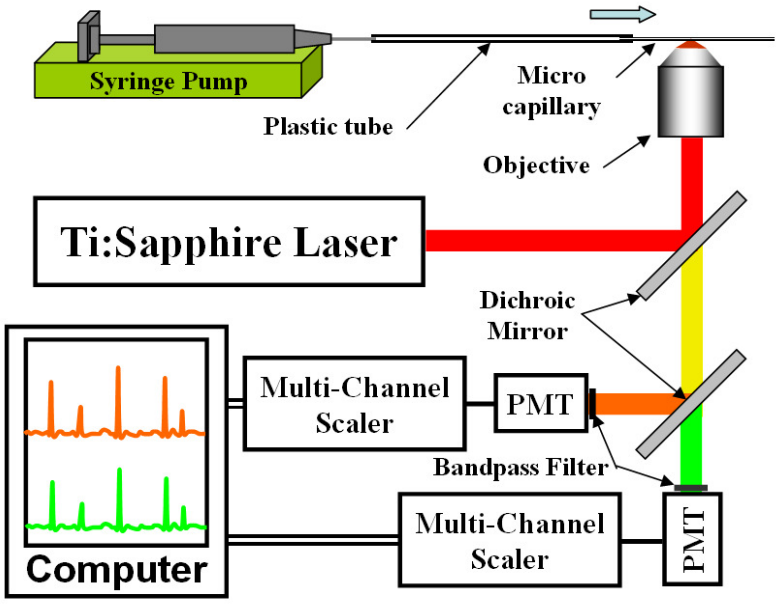

Figure 5.2 Schematic diagram of the free space two-channel two-photon flow cytometry setup for ratiometric measurement demonstration.

5.2.3 Two-photon free-space *in vivo* flow cytometry

By focusing femtosecond laser pulses from a mode-locked Ti:Sapphire oscillator into a blood vessel beneath the skin as illustrated in Figure 5.3, fluorescent tagged circulating cells in the blood stream can be excited via two-photon excitation. The nonlinear excitation defines a localized excitation volume within the blood vessel to allow only one cell to be excited at a time. This technique is able to detect and monitor circulating fluorescent microspheres or fluorescently labeled cells injected through the tail vein of a live mouse. Compared with *ex vivo* flow cytometry measurement, this method is more sensitive and accurate to reveal the dynamics of circulating cells. The advantage of simultaneous excitation of multiple dyes has made it possible to use the two-photon flow cytometer to monitor the dynamics of two cell populations in the same mice, allowing metastatic breast cancer to be analyzed in the complex physiology of an intact animal model [13].

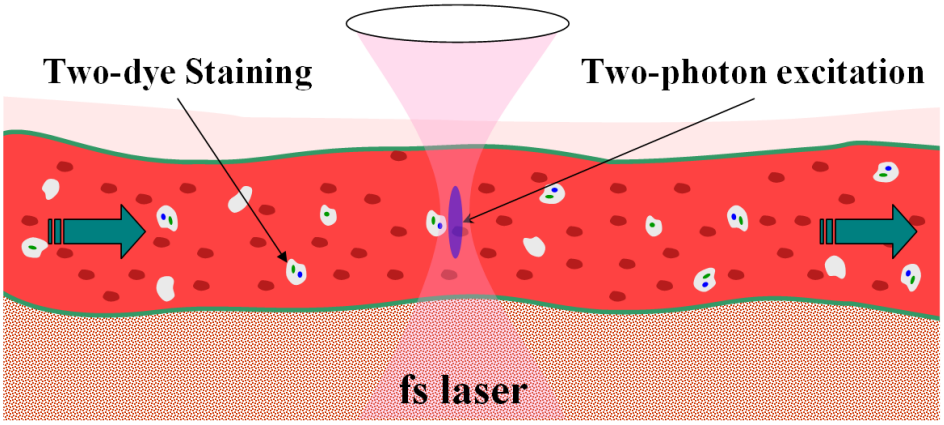

Figure 5.3 Schematic diagram of *in vivo* flow cytometry, from [13].

5.3 *In vitro* Study

5.3.1 Fiber-optic flow cytometry with single-cell resolution

Before applying the DCF-TPOFF probe for *in vivo* studies, several dyes and fluorescent proteins has been tested by our system *in vitro* to determine the suitable fluophores for *in vivo* study. Membrane-binding lipophilic dyes DiD (Ex/Em:648/669 nm) (Vybrant cell labeling solution V22887, Invitrogen) and DiI (Ex/Em:550/568 nm) (Vybrant V-22885, Invitrogen) were selected for the study because of their different spectral characteristics, as shown in Figure 5.4. The whole-blood autofluorescence and absorption spectra are shown in Figure 5.2. Because of the lower autofluorescence and absorption for wavelengths higher than 600 nm, DiD was expected to be a better candidate for *in vivo* measurements.

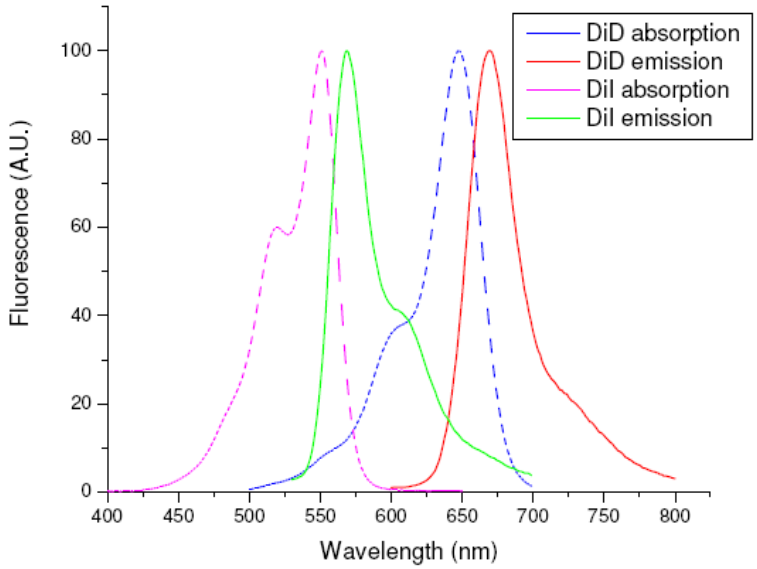

Figure 5.4 Absorption and emission spectra of DiD and DiI. (Data downloaded from Invitrogen.com)

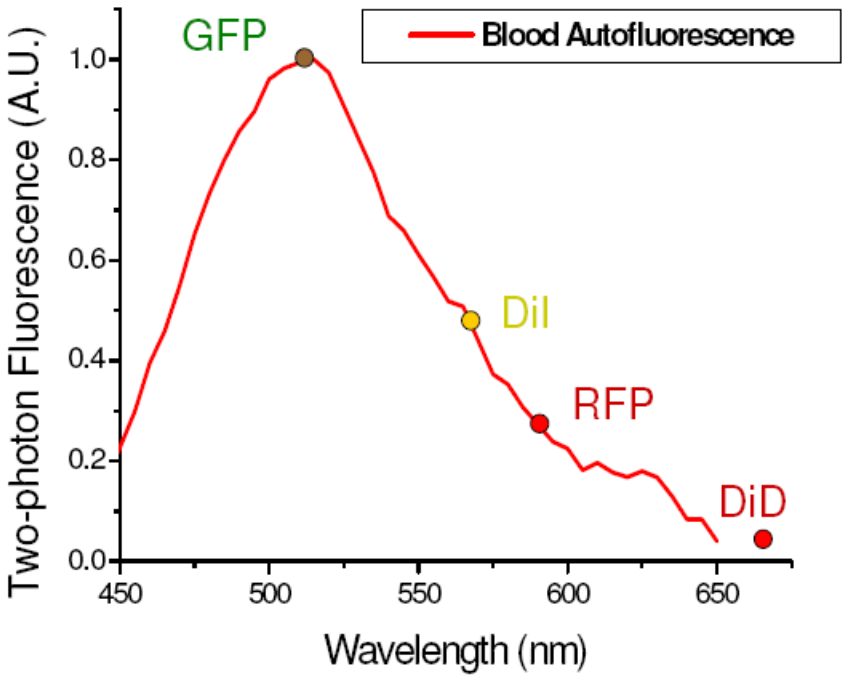

Figure 5.5 Two-photon autofluorescence of human whole blood with the emission wavelength of tested fluorophores marked on it.

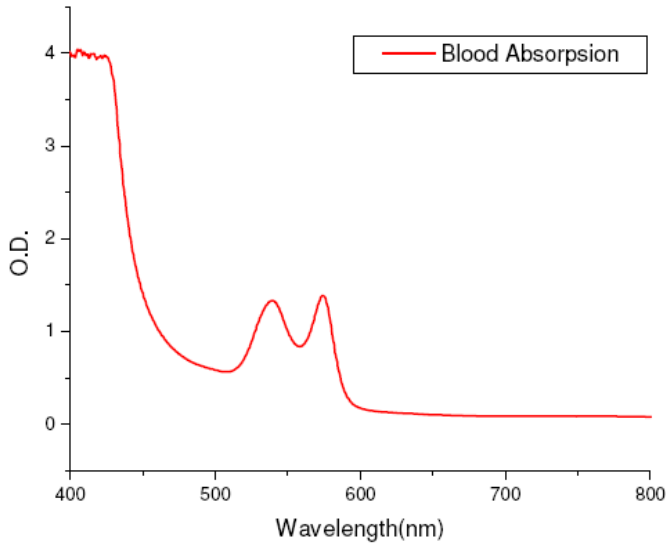

Figure 5.6 Absorption spectrum of whole blood measured by a spectrometer.

MCA-207 cells were labeled by DiD and DiI, respectively according to the manufacturer's protocol. Five μL of DiD or DiI solutions were added to 1 x 10^6 cells

suspended in 1 mL serum-free cell culture medium. The cells were incubated for 20 minutes at 37°C. The cells were then washed by PBS and re-suspended in PBS at a concentration of 1 x 10^6 cells per milliliter. The cells were then diluted into PBS or 50% bovine whole blood and 50% PBS mixture to reach a final concentration of 0.5 million cells per milliliter. The cells were flowed in 250-μm inner diameter plastic tubes (Tygon, K-06418-01). Representative measured fluorescent traces are shown in Figure 5.4. The thresholds were adjusted so that no cell was detected for the control (unstained) cell suspension in PBS. The flow rate was set at 100 μL/minute. The laser power at the output of the fiber was 20 mW.

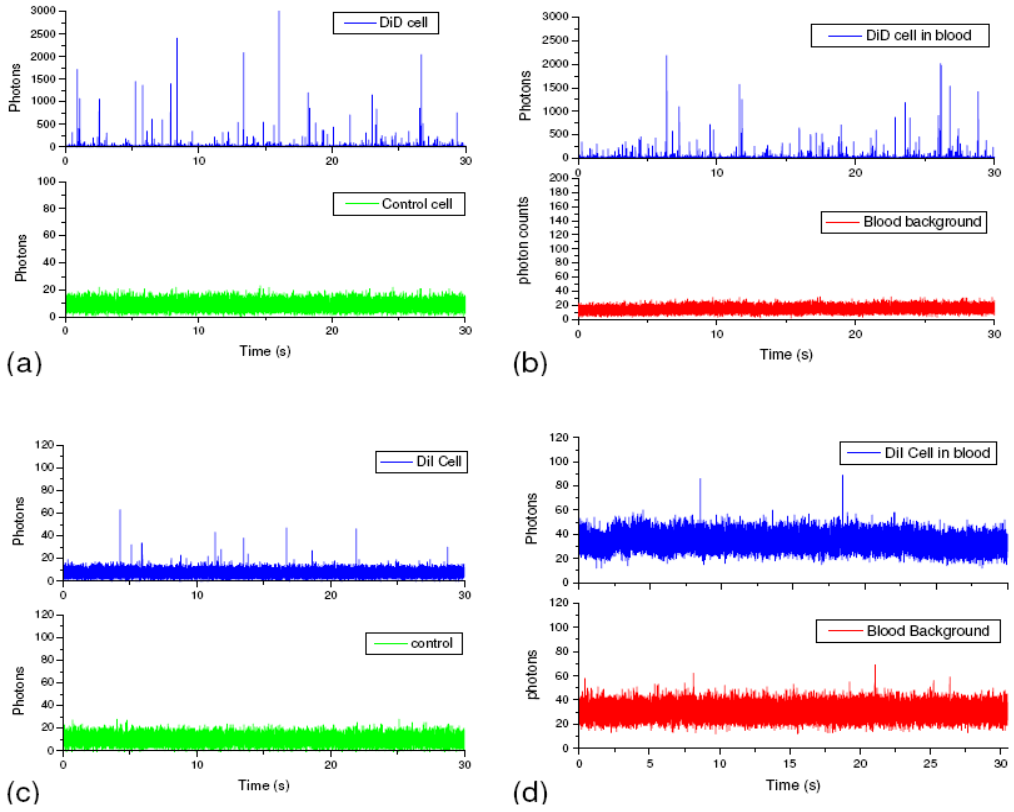

Figure 5.7 Representative raw data of fluorescent dye labeled cells flowing in a vessel monitored by TPOFF probe. **(a)** Fluorescence photon counting time trace of DiD-labeled (upper panel, blue) and unstained (lower panel, green) MCA-207 cells suspended in PBS flowing in a 250μL inner diameter tube. The flow rate was 100μL/minute. Each time point represents the number of photons detected by the photon counting module in 1 ms. **(b)** DiD cell suspension in a mixture of 50% bovine whole blood and 50% PBS. **(c)** Fluorescence photon counting

time trace of DiI-labeled (upper panel, blue) and unstained (lower panel, green) MCA-207 cells suspended in PBS flowing in a 250μL inner diameter tube. **(d)** DiI cell suspension in a mixture of 50% bovine whole blood and 50% PBS.

The numbers of detected cells per minute for DiI-labeled or DiD-labeled cells in PBS or in blood are shown in Figure 5.8 (a). The number of detected cells for DiD cells in PBS was 595 ± 50.6 per minute, which was about 16.5 times more than the number for DiI cells of 36 ± 8.1 per minute. The average numbers of detected cells in whole blood were 735 and 3 for DiD and for DiI cells, respectively. The reason that many fewer DiI-labeled cells were detected was because of the lower two-photon fluorescence signal for the DiI cells relative to the DiD-labeled cells, as shown in Figure 5.8(b). The maximum photon counts per millisecond never exceed 120 counts for DiI cells. In addition to the lower two-photon fluorescence (TPF) signal strength of DiI, the absorption and autofluorescence of blood are both higher at the emission wavelength of DiI (emission maximum: 568 nm), which makes the detection of DiI more difficult in whole blood. However, the main reason for the much lower detection rate and fluorescence photons was because of the low two-photon cross-section of DiI at 800 nm of excitation [16]. As shown in Figure 5.9, there is a dramatic drop in the two-photon cross-section for DiI around 800 nm. The two-photon cross-section dropped about three orders of magnitude from 700 nm to 800 nm. The two-photon cross-section is an important factor that needs to be taken into consideration when choosing the fluophores.

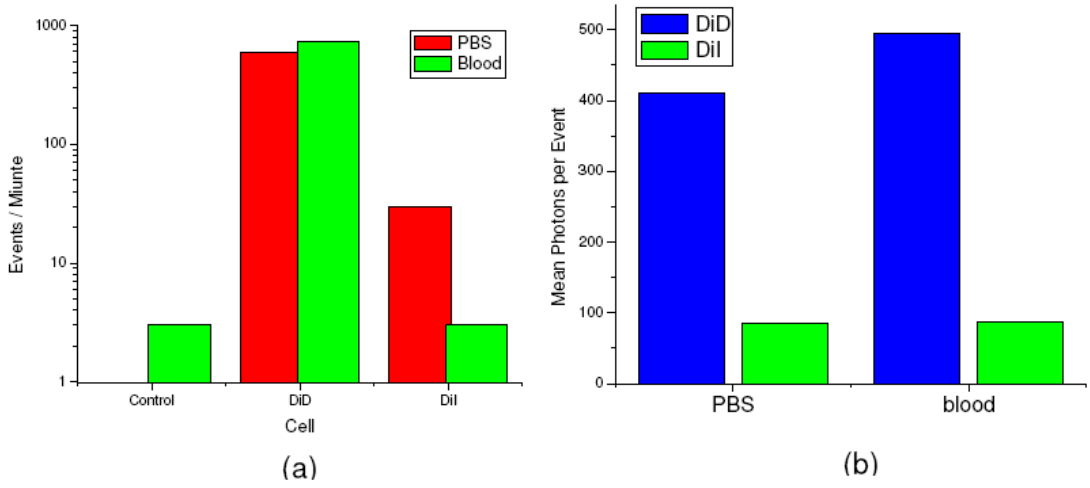

Figure 5.8 Detection rate and event brightness of DiD-labeled cells and DiI-labeled cells. (a) Detected events per minute for control cells, DiD cells and DiI cells in PBS and in 50% bovine whole blood, respectively. (b) Mean photons per detected cell for DiD-labeled (blue bar) and DiI-labeled (green bar) cell suspensions in PBS and in blood, respectively.

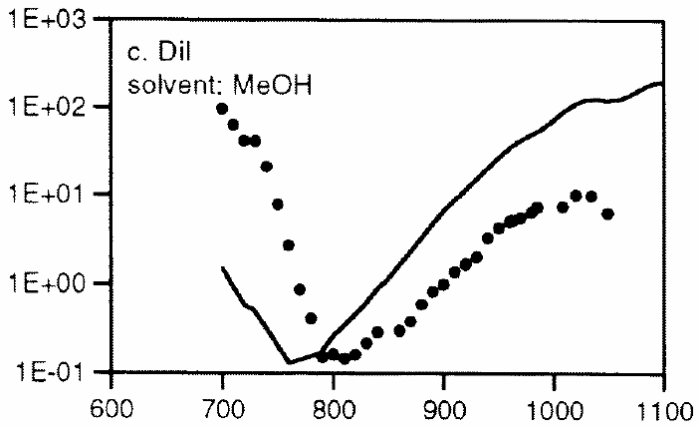

Figure 5.9 Two-photon cross-section of DiI. Black dots are two-photon cross-section. (Reproduced from reference [16])

From previous studies, DiD was found to be a better dye for two-photon excitation fluorescence flow cytometry studies not only because of the lower autofluorescence and absorption of the whole blood at the emission wavelength of DiD, but also because of its superior TPF brightness. From the data, we observed that the

whole blood has almost no effect on the detected photon counts for the events of DiD-labeled cells. As shown in Figure 5.8(b), the mean photon counts for cells flowing in blood were even higher than the counts for the cell suspension in the PBS. The higher counts in blood might be due to its higher viscosity, which made the cells linger longer around the probe volume of the fiber probe. Figure 5.10 and Figure 5.11 are the peak energy (total photons in the peak) and the peak maximum (height) distributions of the DiD cell events, respectively. The mean numbers of photons per peak (mean fluorescence) are 820.8 and 989.5 for the PBS and blood cell suspensions, respectively. The average peak maxima are 181 and 269 for PBS and blood, respectively. Both the peak energy and the peak maximum distributions are not affected by the blood, which is very different from the free space detection scheme using a high numerical aperture objective as described in section 5.2.3. In free space measurement, we observed on average about one order of magnitude lower photon counts when monitoring flowing cells in whole blood due to the scattering and absorption by the components in the blood (Figure 5.12). Representative data of the photon counting trace of DiD-labeled cells flowing in PBS and in blood are shown in Figure 5.12 (a). Using a fiber probe to do TPF flow cytometry in the blood, the problems of absorption and scattering are eliminated. By combining two-photon excitation and fiber-optic detection, the cells being detected are right at the probe volume determined by the excitation beam profile at the fiber tip, and the emitted TPF photons are collected by the fiber directly, before going through multiple scattering as in the free space detection scheme.

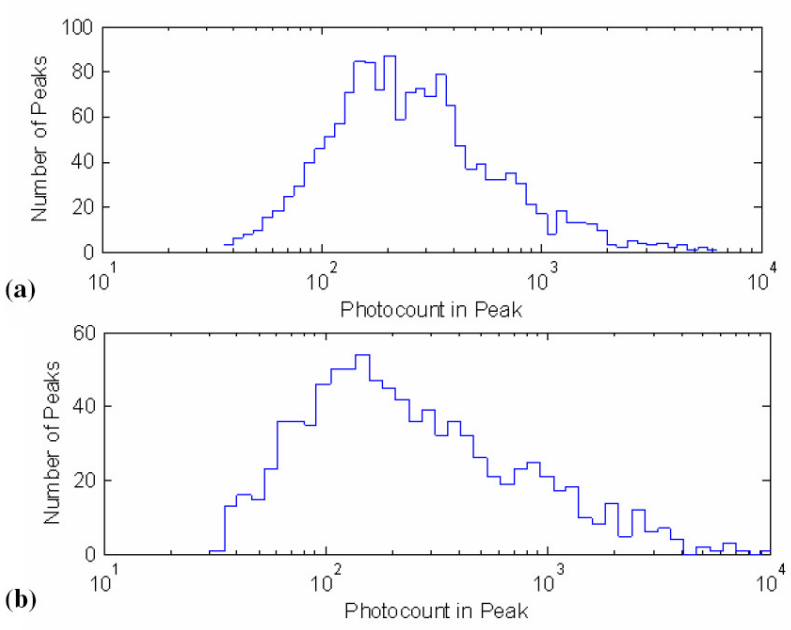

Figure 5.10 Distribution of total photons in each peak detected in DiD cell events. (a) Cells flow in PBS. (b) Cells flow in 50% whole blood.

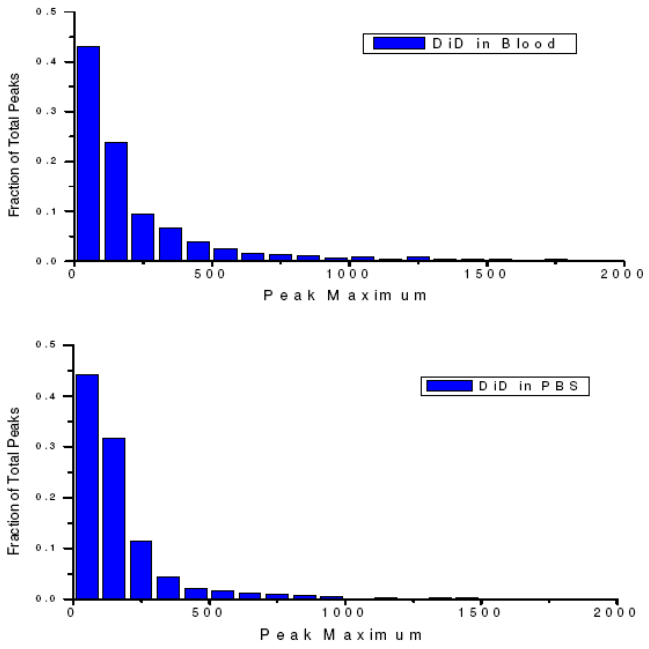

Figure 5.11 Peak maximum distribution of DiD labeled cells flowing in PBS (bottom) and whole blood (top).

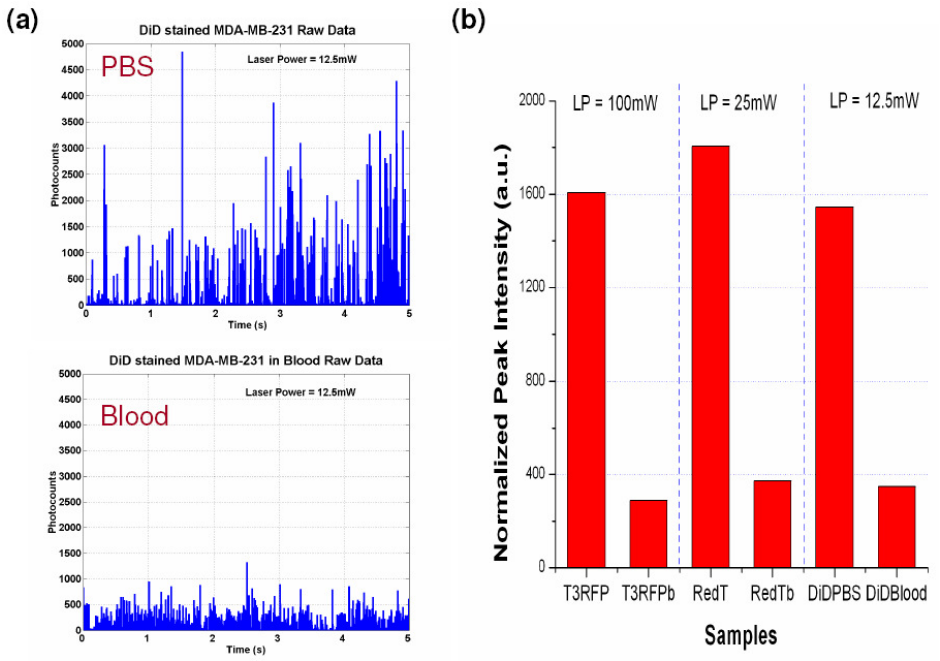

Figure 5.12 Reduced signal strength in blood using free-space detection. (a) Free space detection photon counting trace for DiD-labeled cells flowing in PBS (upper panel) and in blood (lower panel). (b) Comparison of the detected peak intensity (total photon counts) for cell suspensions in PBS and in blood [13].

5.3.2 Detecting GFP-expressing cells in whole blood

The use of green fluorescent protein (GFP) is ubiquitous in life science research. The Nobel Prize in Chemistry this year was given to the people who discovered and engineered GFP [17]. It is of great interest to monitor GFP-expressing cancer cells circulating *in vivo* to study cancer biology in GFP-transfected animal models. However, because of the high scattering and absorbing nature of the blood and tissue around the emission wavelength of GFP, it has been difficult to detect GFP-expressing cells *in vivo* [18, 19]. We have seen in the previous section that using the two-photon fiber probe to investigate flowing cells has circumvented the scattering and absorption problem of the whole blood. Here we further investigate the feasibility of using the TPOFF probe for GFP-expressing cells in whole blood. The eventual goal would be to use the probe for *in*

vivo monitoring of circulating GFP-expressing cancer cells in real time to investigate cancer metastasis in mouse tumor models.

To investigate the feasibility of using a fiber probe for flow cytometry to detect GFP-expressing cells in whole blood, we flowed DiD-labeled normal MCA-207 cells and GFP-transfected cells through a 250-μm inner diameter tube with the same concentration of 1 x 10^6 per milliliter. One end of the tube was fixed, and the fiber probe was inserted into the fixed end. The fiber probe end was fixed and controlled by a translation stage, so the position of the fiber inside the tube would not change when changing the sample. The cells were injected into the other end of the tube through a 30-gauge syringe needle. The flow rate was controlled by a syringe pump (KDS-100, KDS scientific). The flow rate was 100 μL/min. Assuming a cell diameter of 10 μm and the lateral diameter of the two-photon excitation region of 5μm, together with the information of the flow rate and cell concentration, we found the expected number of cells detected per minute was about 1000 ([25/250]^2 x 0.1 x 1 x 10^6).

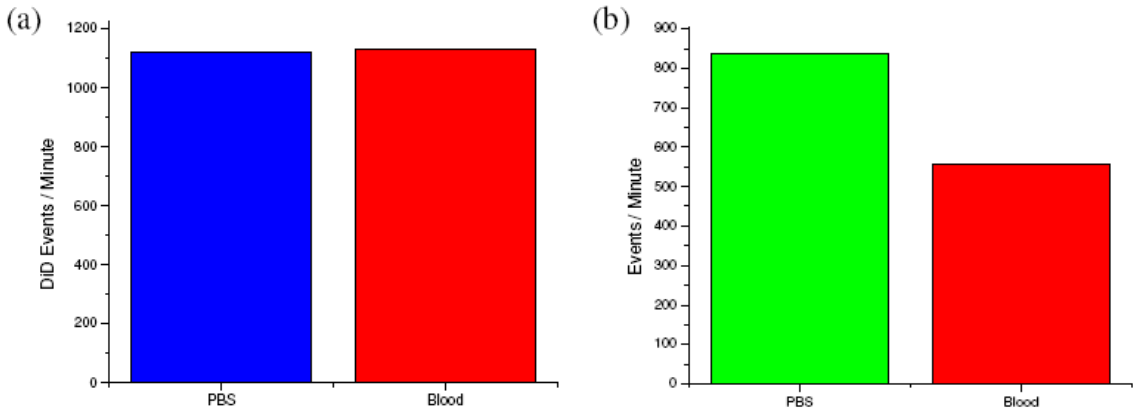

Figure 5.13 (a) Average numbers of detected DiD-labeled cell in PBS (blue bar) and in whole blood (red bar). **(b)** Average numbers of detected GFP-expressing cells in PBS (green bar) and in whole blood (red bar).

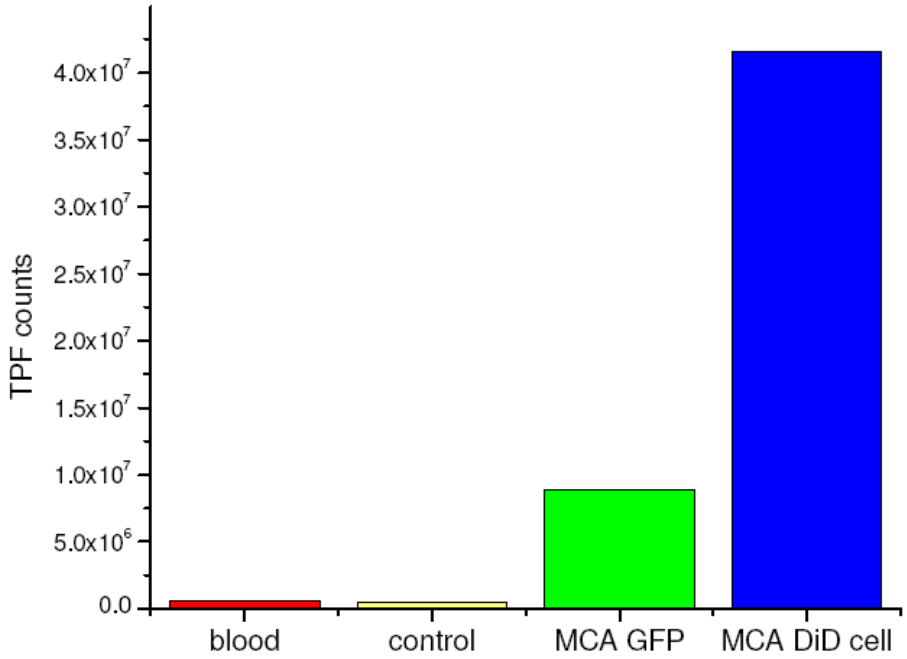

Figure 5.14 Two-photon fluorescence brightness of 100% whole blood (red bar) and cell pellets of unstained MCA-207 cells (control, light yellow bar), GFP- expressing MCA-207 cells (green bar), and DiD-stained MCA-207 cells (blue bar). The measurements were taken by putting the TPOFF probe into the cell pellets or the whole blood with 20mW output power from the fiber.

DiD-labeled cells were flowed first in PBS and in 50% whole blood to test the system. Figure 5.13(a) shows the average detected DiD-labeled cells. The numbers of detected DiD-labeled cells in PBS and in blood are 1119 and 1134, respectively. The numbers are about the same as the expected numbers from calculation. The result is also consistent with the detection rate of DiD-labeled cells in the previous section. Therefore, it is reasonable for us to assume that the number of DiD-labeled cells detected accurately represents the total number of interrogated cells under the experimental conditions. The numbers of detected GFP-expressing cells in PBS and in blood are 820 and 558 per minute, respectively, as shown in Figure 5.13(b). The number of GFP cells detected is fewer than the number of DiD cells in PBS although they have the same concentration. This is because the TPF brightness of DiD cells is much greater than that of GFP cells.

Figure 5.14 shows the measured TPF brightness for MCA-207 GFP expressing cells, MCA-207 normal cells labeled with DiD on the membrane, control MCA-207 cells, and 100% bovine whole blood. The measurements were taken by inserting the fiber probe directly into cell pellets rather than through the mean photon counts of the detected peak events. The former method can better represent the average brightness of different samples, as the photon counts in the detected peaks when the cells are flowing could vary greatly when they travel though the laser beam at different locations. The average brightness of the DiD-labeled cells is about 5-fold higher. However, because the DiD was only labeled on the membrane, if we consider the average brightness of the fluophores, DiD has a much higher molecular brightness than the GFP because when the cells flow through the probe volume of the fiber probe, most of the time only part of the cells flow through the probe volume, and the membrane will always be there first. If the membrane dye is bright enough so that we won't miss it when it is there, the longer-wavelength membrane dye can serve as a reporter to tell us a cell is within the probe region. The lesser number of GFP-expressing cells detected in PBS was simply because the GFPs are dimmer. However, the question arose as to why the number of GFP cells detected in 50% whole blood was only about two-thirds of the events in PBS. The reason was the raised background photon counts from the autofluorescence of the whole blood. Figure 5.15 shows the energy distribution of the detected GFP cell peaks in PBS and in blood, respectively. The median fluorescence energies in each peak for cells flowing in PBS and in blood are 91 and 93 photons, respectively. The average numbers of photons in each peak are 227.5 and 232.2, respectively. The blood did not seem to have an influence on the collected photons of the events.

If we look at the peak maximum distribution in Figure 5.16 (a), the fraction of total peaks with a peak maximum of less than 20 photons is zero for cells flowing in the blood and the fraction for a peak maximum of 20-30 is only half of that for a peak maximum of 30-40 photons. The reason is because the background threshold in blood is

about 25 photon counts, so every peak with a maximum photon count lower than 25 photons would not be counted as an event. The fraction of the peaks with a peak maximum lower than 25 photons for cells flowing in PBS was about 30% as shown in Figure 5.16(b), which can neatly account for the reduced detectable events when cells are flowing in whole blood.

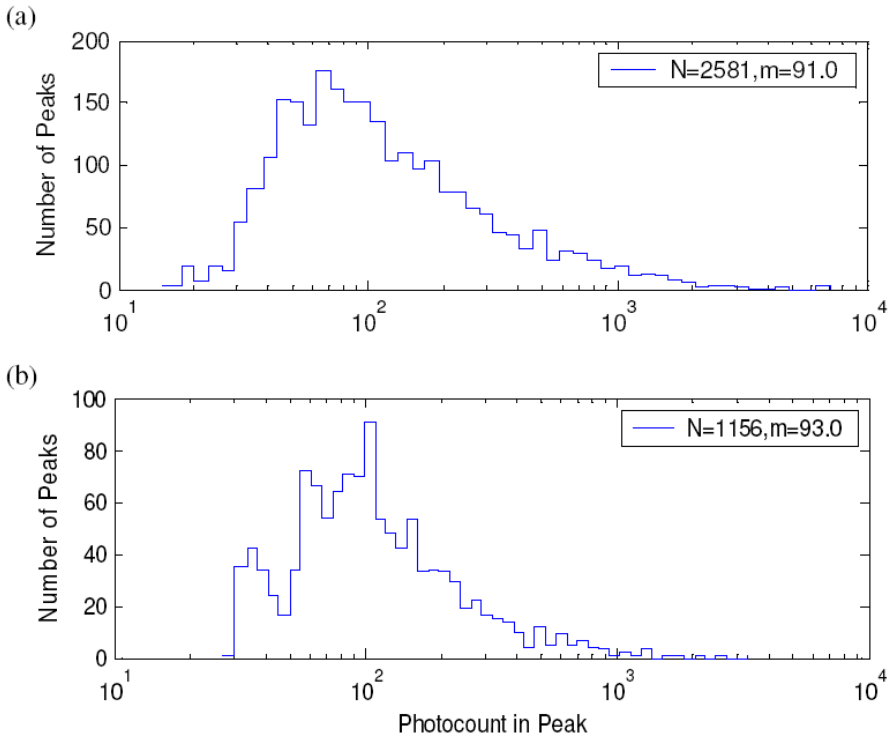

Figure 5.15 (a) Peak energy distribution of the detected GFP-expressing cells in PBS. (b) Peak energy distribution of the detected GFP-expressing cells in blood.

If we assume the detected number of DiD-labeled cells correctly represents the total number of cells interrogated, we can use the ratio between the number of DiD-labeled cells detected and the number of GFP-expressing cells detected during the same time period to calculate the detection efficiency of GFP-expressing cells. When flowing GFP-expressing cells in PBS, the fraction of detected GFP cells was 74.8%. When flowing GFP cells in 50% whole blood, the fraction of detected GFP cells was 49.2%.

Although the higher background of blood caused the detection of GFP cells in whole blood to be more difficult, compared to less than 5% of the detection rate when using comparable laser intensity at the focus for the free space detection scheme (using high NA objective) in either PBS or blood [5, 13, 20], we have achieved detection sensitivity that is one order of magnitude higher than the free space technique. The problem for free space detection was basically due to the corpuscular nature of whole blood, which caused scattering of the photons. Because of using the fiber-optics based technique, scattering or absorption of the blood or tissue are no longer problems, which make this technique a promising method for *in vivo* long-term monitoring of fluorescent protein-expressing cells circulating in the blood stream.

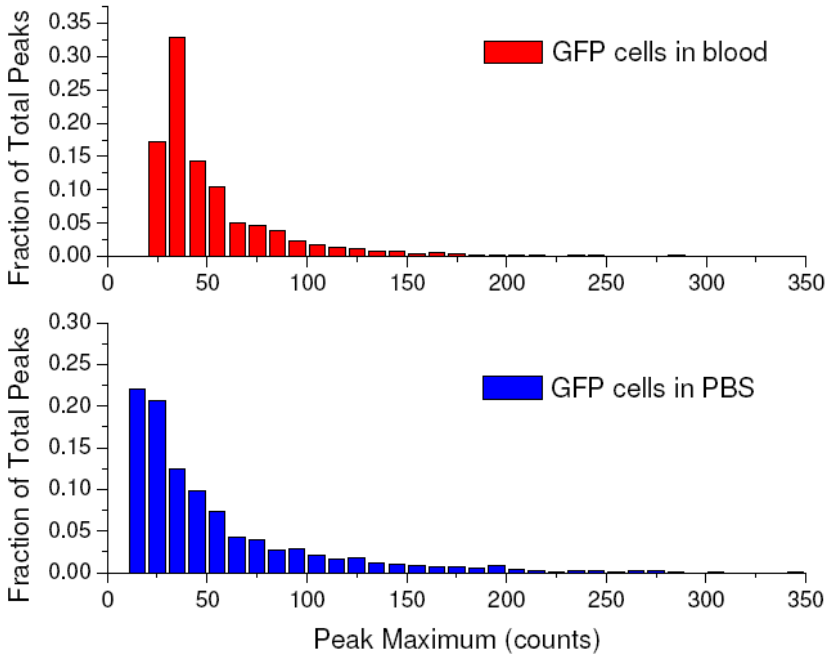

Figure 5.16 Peak maximum distribution of the events for GFP-expressing cells flowing in **(a)** blood and **(b)** PBS. The mean photon counts for the background for the blood was 14 photons with a standard deviation of about 4 counts. The peak detection threshold for the peaks in the blood was 26 photons. The mean photon count of the background for PBS was 2.5 photons, with a standard deviation of 1.6 photons. The peak detection threshold for the cell suspension in PBS was 9 photons.

5.3.3 Dual- labeled fluorescent cells

The problems of scattering and absorption because of blood cells can be circumvented by combining two-photon excitation and fiber-optic detection, as shown in the previous section. The fiber probe achieved one order of magnitude higher sensitivity, compared to free space detection when detecting GFP-expressing cells in the whole blood. However, because we had to conduct the measurements on different samples separately, the result can only be quasi-quantitative. There are many factors which could affect the obtained ratio of detection, such as fluctuation of the cell concentration, the clog of blood around the fiber probe which causes background fluctuation, etc. To quantitatively measure the ratio of GFP cells detected, we conducted dual-channel detection on dual-labeled cells— GFP-expressing and DiD-labeled—on the membrane. The fluophores are excited simultaneously, and the emitted TPF photons are separated into two wavelength channels: short-wavelength channel (510/50 nm, "short"), for GFP, and long-wavelength channel (680/30 nm, "long") for DiD. Before conducting the two-channel detection, the dual-labeled cells were investigated by the original single-channel setup by changing the filters to select the desired wavelength range. Similar numbers of DiD events were observed; however, fewer GFP events were obtained on the dual-labeled cells. As shown in Figure 5.17, the average numbers of detected cells in the GFP wavelength channel in PBS and in blood were 608 and 280, respectively. The detection ratios correspond to 54.3% and 24.7%, respectively.

The detection efficiency is lower, compared to cells that express GFP only, as shown in the previous section. Conventional flow cytometry analysis of the dual-labeled GFP-DiD MCA-207 cells is shown in Figure 5.18. Almost all cells appear to be dual-labeled. Therefore, the reduced detection efficiency of the dual-labeled cells in the GFP channel is not due to the uneven labeling of the cells. In addition, because all the cells express GFP and DiD fluorescence simultaneously, our assumption of using the ratio

between the events detected in the two channels to calculate the detection rate of GFP-expressing cells is reasonable.

The reduced detection rate is believed to be due to the lower green fluorescence signal emitted from the dual-labeled cells, as shown in Figure 5.19. The underlying mechanism remains unclear. It could be quenching between the GFP and the DiD fluophores or simply the absorption of the emitted green fluorescence by the fluophores on the membrane. The lower GFP fluorescent signal from the GFP-DiD dual-labeled cells was observed previously in our group as well [20], which increased the difficulty of detection. However, because of the complex *in vivo* environment and the fact that there are all kinds of species which have an autofluorescence wavelength peak of around 510-530 nm, the use of dual-labeled cells and dual channels is an important advance for the optical investigation of circulating tumor cells *in vivo*.

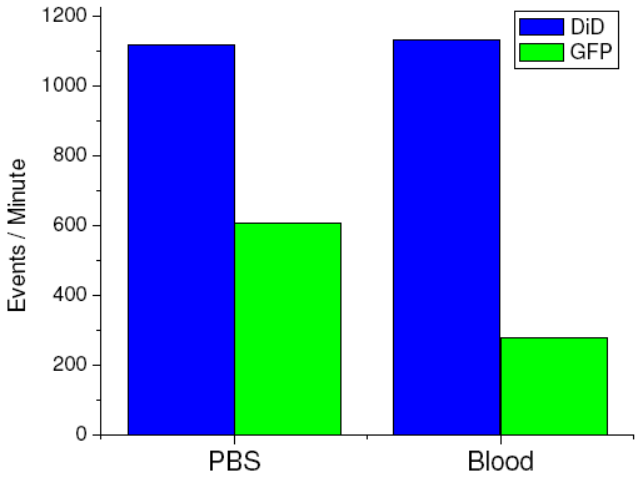

Figure 5.17 Detected number of events for the DiD emission wavelength range (680/30 nm) (blue bars) and the GFP emission wavelength (510/50 nm) for the dual-labeled cell suspension in PBS and in blood.

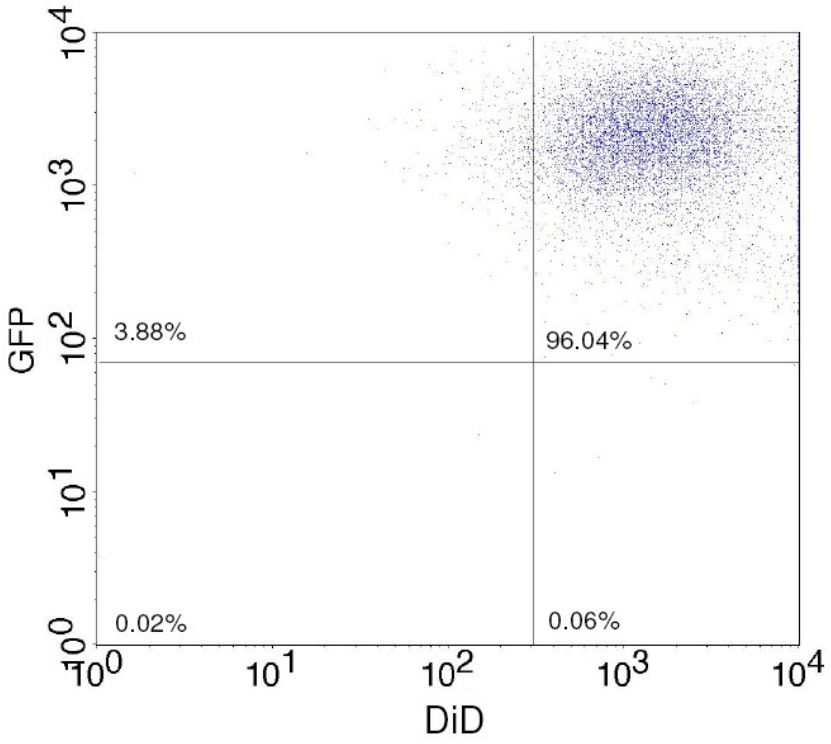

Figure 5.18 Conventional flow cytometry measurements of DiD labeled GFP-expressing MCA-207 cells.

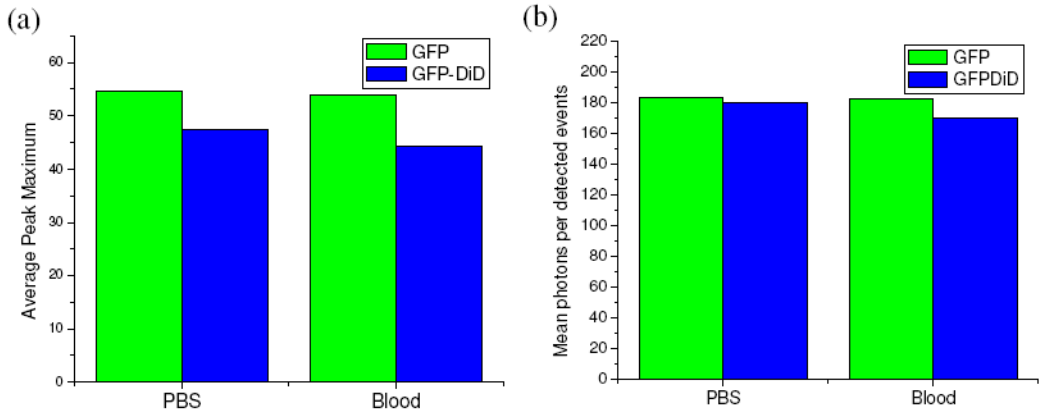

Figure 5.19 (a) Comparison of the average peak maximum of GFP-pressing only (green bars) cell suspension and GFP/DiD-dual-labeled (blue bars) cell suspension in PBS and in blood. **(b)** Comparison of the average total photons in each detected peak for GFP-expressing cells (green bars) and dual-labeled GFP/DiD cells (blue bars) in PBS and in blood.

5.3.4 Dual-channel detection of dual labeled cells

The experimental setup for dual-channel detection is shown in Figure 5.20. Pulses generated by a Ti:sapphire oscillator (Coherent Inc., Mira 900) were dispersion pre-compensated to optimize the intensity at output of the fiber. The fluorescence signal was collected back by the same fiber and the objective, and separated from the excitation beam by a dichroic mirror. The fluorescence signal was further separated into two wavelength channels by another dichroic mirror (cutoff 610 nm). The fluorescence signals were filtered by band-pass filters (channel 1: 510/50 nm, channel 2: 680/30 nm) before detection by photomultiplier tubes (PMT, Hamamatsu, H7422-40). The outputs from PMTs were labeled in a router and then processed in a time correlated single photon counting (TCSPC) module (SPC630, Becker and Hickl, GmbH). The DCF used in this study had an inner core diameter of 6 um with an NA of 0.15 and a 123-um inner cladding diameter with an NA of 0.46. The length of the fiber was about 1 m. The output power from the fiber was 20 mW

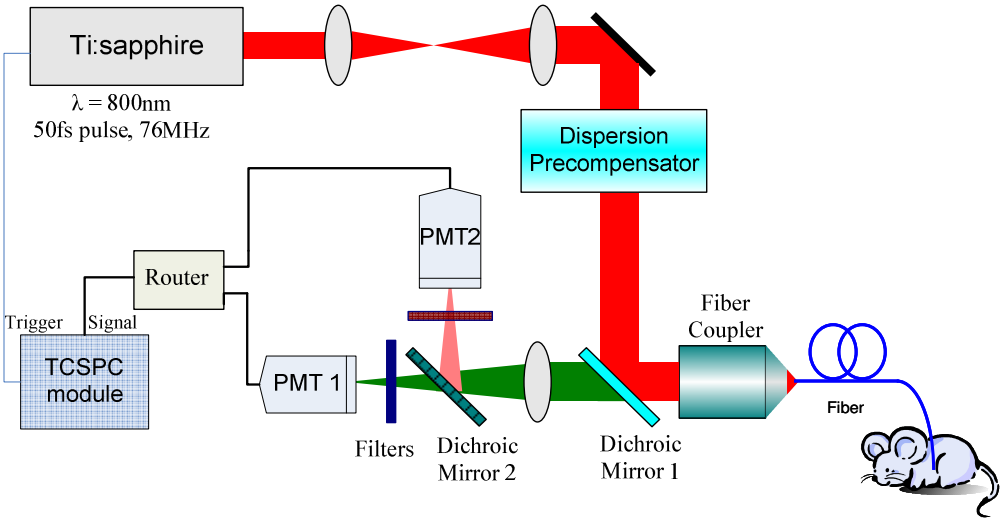

Figure 5.20 Experimental setup for the dual-channel detection.

Representative photon-counting traces of dual-channel detection are shown in Figure 5.21. In Figure 5.21(b), the peaks in two channels nicely line up. The ability to count thousands of cells per minute as in single-channel detection has been confirmed. Besides, the ability to resolve cells in a single-cell level is demonstrated, as shown in Figure 5.21(b). For this particular measurement, the cells were flowed through a 250-µm inner diameter plastic tube, and the flow rate was 100uL/minute. The estimated average flow speed in the tube is 8.4 mm/s. The event time courses for DiD and GFP events are similar, as expected, for simultaneous two-channel detection, as shown in Figure 5.22.

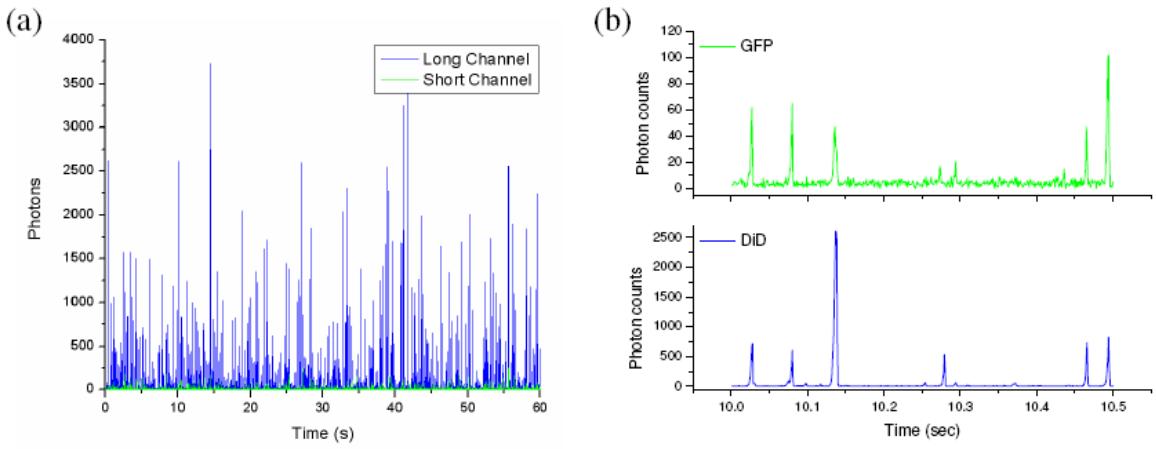

Figure 5.21 (a) Representative two channel detection photon counting traces of dual-labeled GFP/DiD cells flowing in a 250-µm tube. The blue line represents photons collected in the long channel (680/30 nm, DiD) and the green line represents photons collected in the short channel (510/50 nm, GFP). **(b)** Magnified view of the dual-channel detection raw data. Upper panel show the peaks detected in the short channel (GFP), and the lower panel shows the peaks detected in the long channel.

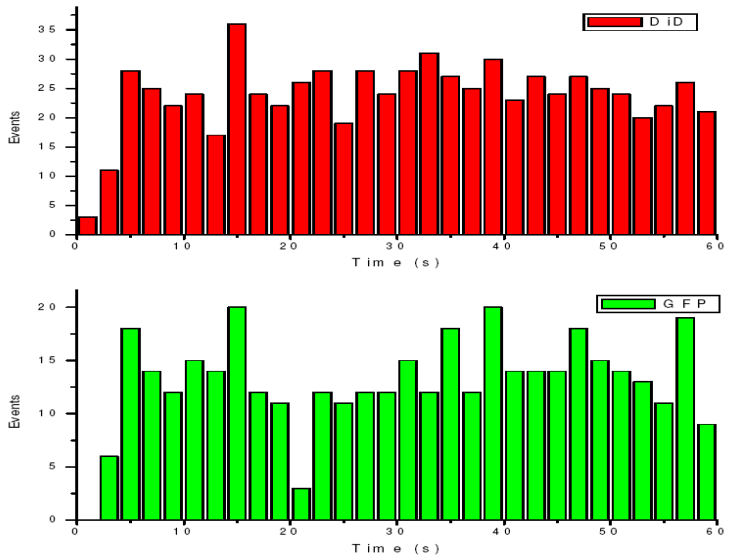

Figure 5.22 Event time courses in long channel (red bars) and short channel (Green bars)

Figures 5.23 and 5.24 are the peak energy distribution and peak maximum distribution for the two channels. For the mean value of both the peak energy and the peak maximum, DiD events are about one order of magnitude higher than for GFP events. Figure 5.25 shows the scatter plot of the TPF energy for correlated events in the short and long channels. We find that the measured peak energy distribution has a wider distribution than the conventional flow cytometry, as shown in Figure 5.18. This is because when the cells flow through the core of the fiber, the distance between the cell and the fiber tip can vary in a wild range. As long as the number of collected photons is higher than the detection threshold when then the cell passes though the excitation volume, the cell is "detected" as an event. Therefore, because DiD has relatively higher TPF brightness, the effective probe volume for DiD is larger, which also results in the wider energy distribution and wider peak width in the DiD channel.

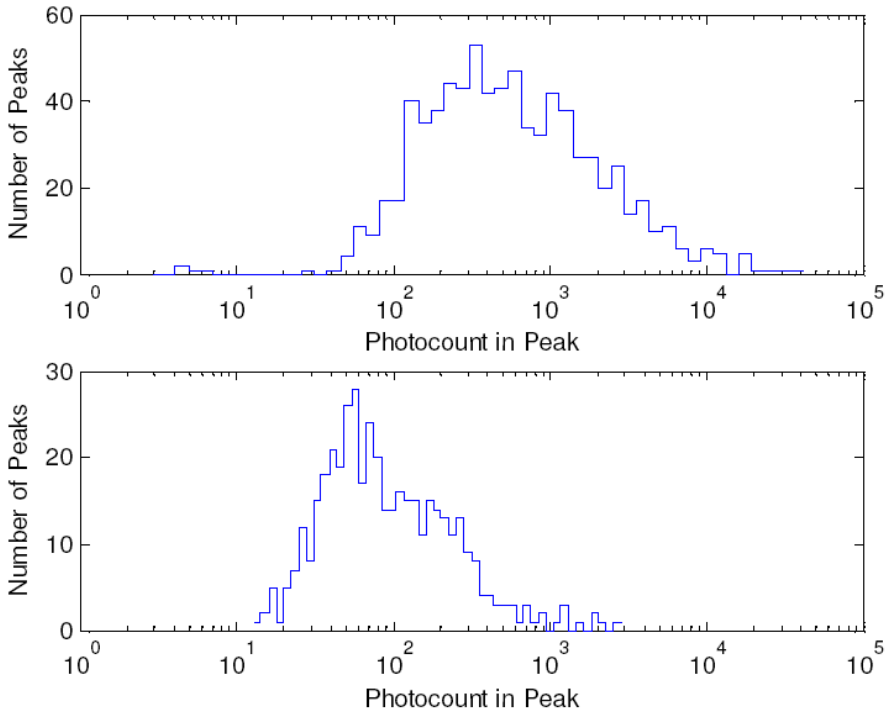

Figure 5.23 (a) Peak energy distribution of the peaks counted in the long Channel (DiD). (b) Peak energy distribution of the peaks counted in the short Channel (GFP).

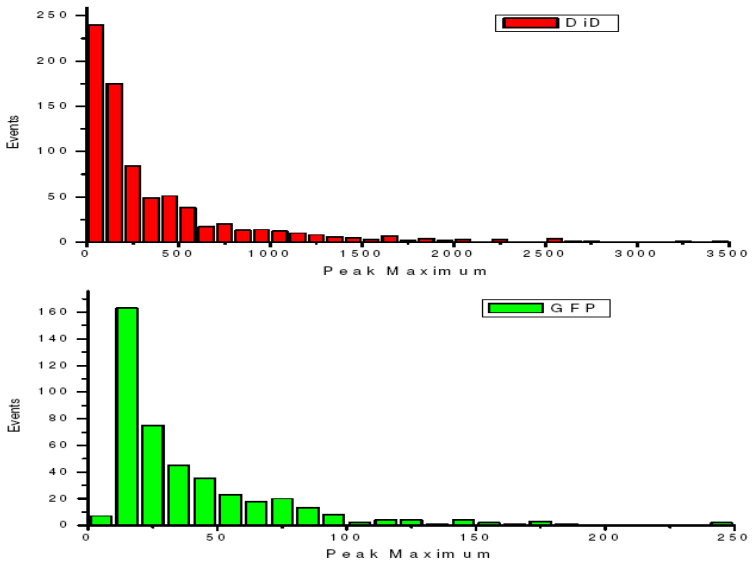

Figure 5.24 Peak maximum distribution of the **(a)** Long channel (DiD) and **(b)** Short channel (GFP). The detecting background threshold for the long channel and short channel was 25 and 12 photons, respectively.

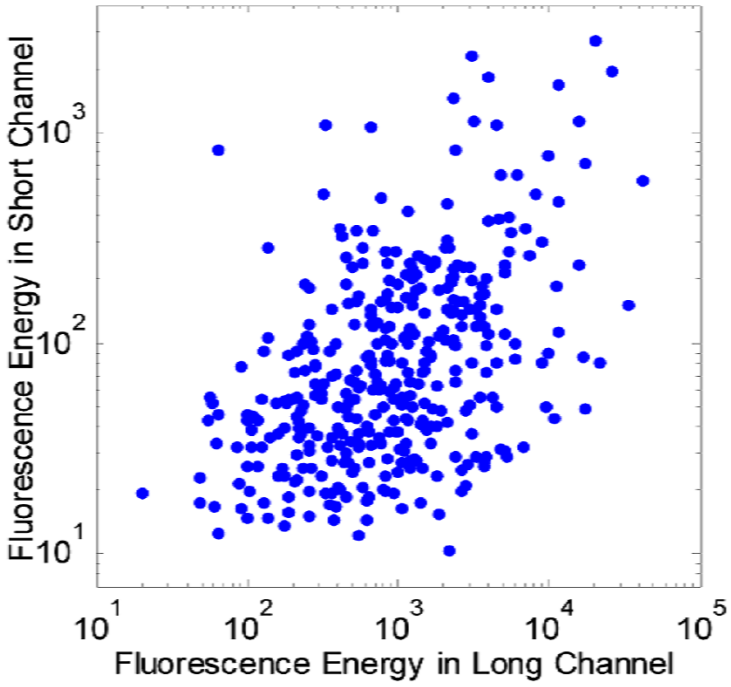

Figure 5.25 Scatter plot of the peak energy of correlated events in the short and long channels.

The peak width distributions of DiD events and GFP events are shown in Figure 5.26. The peak width shown here is the full peak width, which is defined as the time difference between the two crossing points of the peak and the background threshold (background mean + standard deviation of the background). The full peak width can represent more clearly the relationship between the detected peaks of the two channels. The peaks detected in both channels have similar peak-width distribution. However, the peaks detected in the short (GFP) channel have shorter peak widths. This is partly because of the different distribution of these two fluophores and partly because of the higher brightness of the DiD.

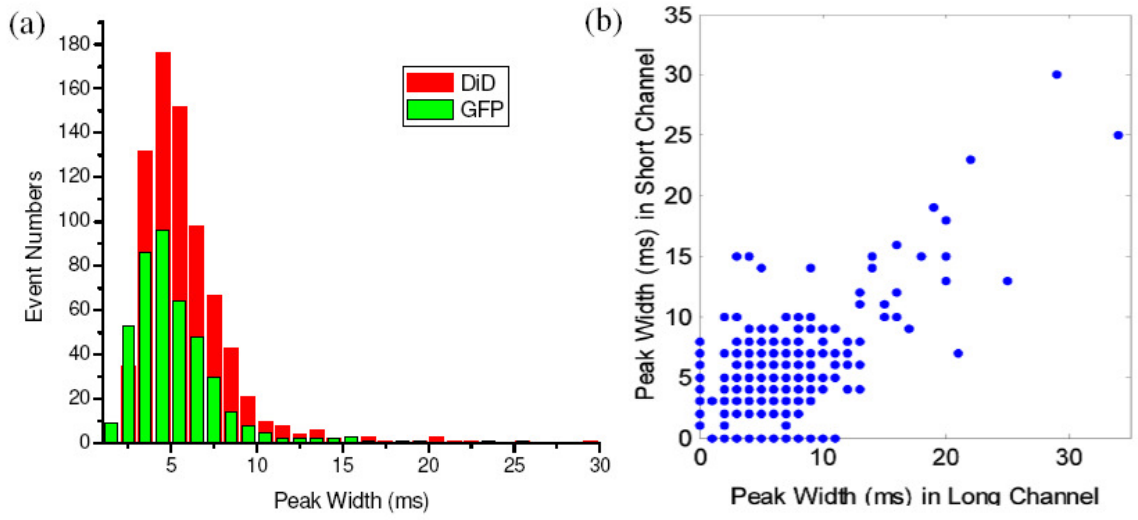

Figure 5.26 (a) Peak width distribution of the peaks detected in the long channel (DiD) and the short channel (GFP). **(b)** Scatter plot on the correlation of the peak widths between the long and short channels.

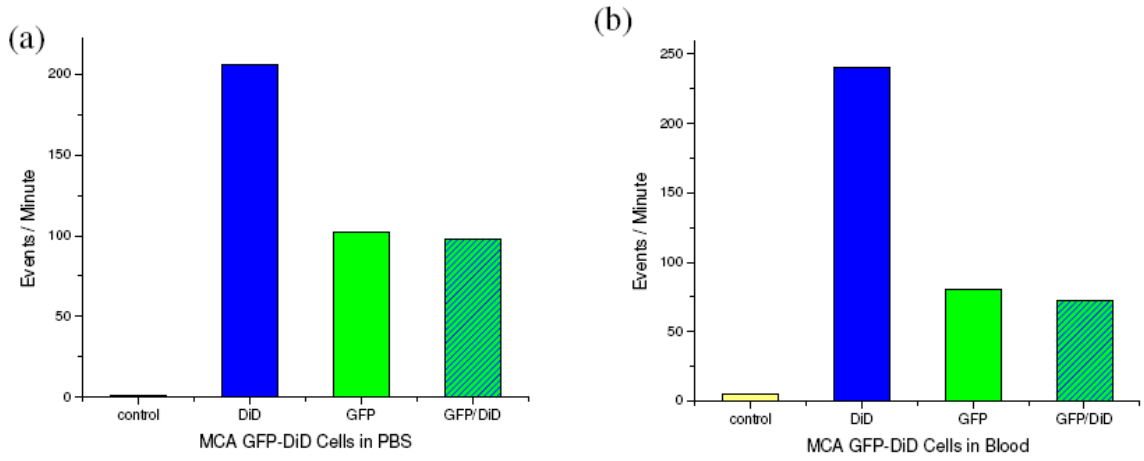

Figure 5.27 Number of cells detected per minute when flowing MCA-207 dual-labeled cells in a 500-μm tube under dual-channel detection to evaluate the detection efficiency of GFP cells in **(a)** PBS and in **(b)** blood. The detected GFP transfected cells in PBS is 49.5% while 96.2% of the detected GFP cells are correlated with a DiD event within a 10-ms interval. When flowing in 50% whole blood, the detected GFP cells are 33.3% of the DiD cells while 90.0% of the events in the GFP channel correlated with a DiD event in the long channel.

Figure 5.27 shows the average number of events detected when flowing DiD-labeled GFP cells in PBS and in 50% whole blood. The cells were flowed in a 500-μm inner diameter plastic tube. The larger inner diameter tube was used to diminish the chance of clogging of the blood. When the blood clogs around the fiber tip and the surrounding tube, the background in the short channel rises several times. For example, when the blood is flowing smoothly in the tube, the background in the short channel is about 14 photons /ms. However, when the blood cells jam around the fiber as is the case when using a smaller tube, the background can rise to as high as 150 photons/ms, which would complicate the data analysis or render the data unusable. The number of detected GFP events in the PBS suspension is 49.5% of the total detected DiD events. For every detected GFP event in the short channel, 96.2% of them are correlated with a DiD event in the long channel within a 10-ms interval. For the cell suspension in 50% whole blood, the detected number of GFP events is 33.3% of the total DiD events, while 90.0% of the GFP events in the short channel are correlated with DiD events in the long channel. The detection rate is similar compared to what we found previously when using single-channel detection. However, the ratio of the detected GFP events in dual-channel detection accurately corresponds to the actual detection sensitivity of GFP-expressing cells relative to DiD-labeled cells because, for every detected GFP event, the TPF signals of GFP and DiD are from the same cells. The ability to conduct two-color dual-channel detection with two-photon excitation greatly enhanced our ability to detect fluorescent protein cells *in vivo*. There are many intrinsic fluophores in the body that fluoresce at the wavelength range of 500-530 nm. The use of a long wavelength dye as a reporter to indicate the existence of a cell at the probe volume makes it easier to identify the cells we are interested in.

5.3.5 Detection efficiency on different fluorescent protein cells

In addition to GFP-expressing MCA-207 cells, we also evaluated GFP-expressing and RFP (red fluorescent protein) -expressing KB cells. The ratio of fluorescent protein-expressing cells detected in the short channel relative to cells detected in the long (DiD) channel is shown in Figure 5.28. The detection rates in PBS are 54.7 %± 8.7 %, 47.3 %± 5.7 %, and 39.5% ± 2.0 % for MCA-207 GFP/DiD, KB GFP/DiD, and KB RFP/DiD cells, respectively. The detection rates in 50% bovine whole blood are 31.5 %± 5.7%, 21.9 % ± 4.7 %, for MCA-207 GFP/DiD and KB GFP/DiD cells, respectively. KB RFP/DiD cell suspension in blood was not measured due to low TPF brightness of the RFP cells. The low TPF brightness of RFP cells is believed to be due to the low two-photon cross-section of RFP compared to GFP, as shown in Figure 5.29 [21].

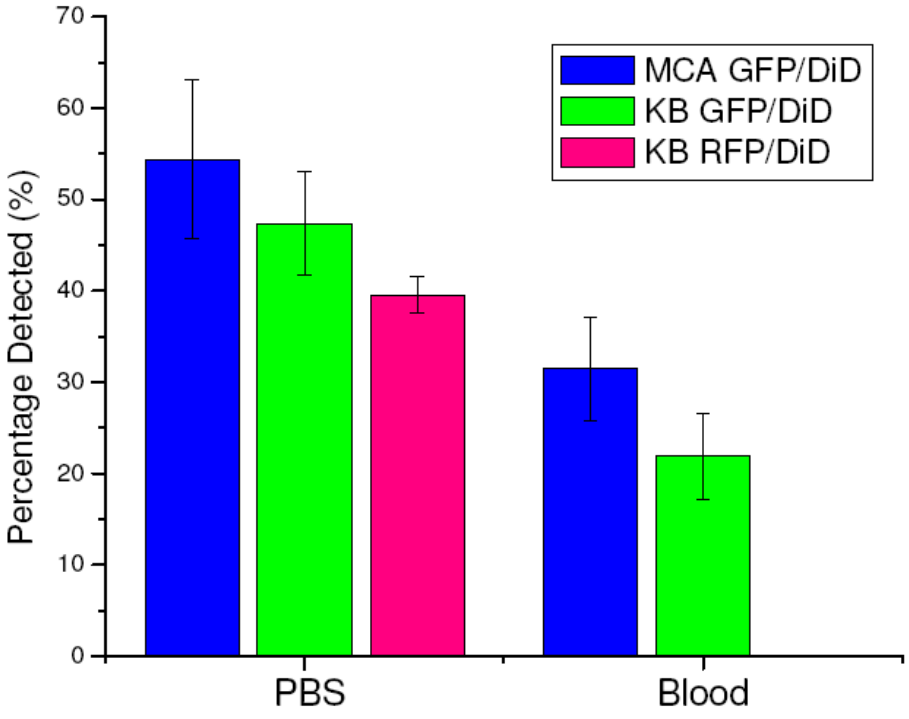

Figure 5.28 Detection rate for different fluorescent protein cell lines. The error bar shown is the standard deviation of the measurements.

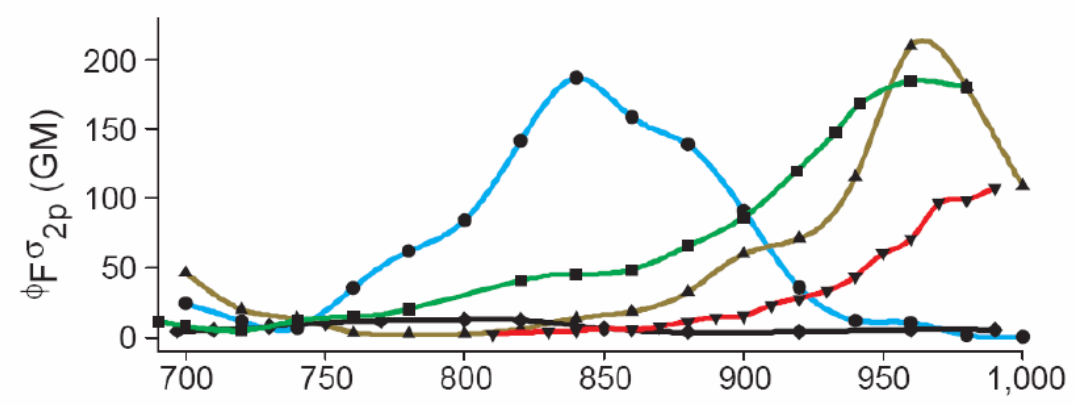

Figure 5.29 Two-photon cross-section of five common fluorescent proteins: enhanced GFP (green, square), RFP (red, downward triangle), CFP (cyan, circle), YFP (yellow, upward triangle), and wild type GFP (black, diamond). (Reprinted with permission [21].)

It is complicated to use the mean fluorescence of the detected events to determine the two-photon fluorescence brightness among cells lines. The effective detectable range for various fluorescent protein cells with different two-photon brightness might vary due to the minimal photon requirements for event thresholds. Therefore, the best way to determine the relative brightness of different fluorescent cells is to measure the cell pellet with the same detector setup. Because of the nature of two-photon excitation, the excitation area in the lateral direction parallel to the fiber facet is around 5 μm in diameter, smaller than the size of a single cell. In the longitudinal direction along the fiber axial axis, the Rayleigh range is about 25μm. Two to three cells might be excited within the range. In the cell pellet, the cells are stacked together, and the fiber tip is put directly on the cells. There is nothing between the cell and the fiber, so the fluorescence photons measured can well represent the two-photon brightness of the cell sample. Figure 5.30 is the two-photon fluorescence measured by putting the fiber tip directly into the cell pellets and 100% bovine whole blood. The fluorescence was measured by the short channel of the system with the same filter set for all of the samples. All of the samples were measured using the same output laser power from the fiber of 20 mW. The TPF signal from GFP-transfected KB cells are only 43.43 % of that from GFP-transfected

MCA-207 cells. The TPF brightness of RFP-transfected KB cells is only 18.93% of that of GFP-transfected MCA-207 cells. The dual-labeled cells are all dimmer than cells that express fluorescent proteins only, as we have seen in section 5.3.3. The lower brightness of KB GFP and RFP cells explained the lower detection rate shown in Figure 5.28.

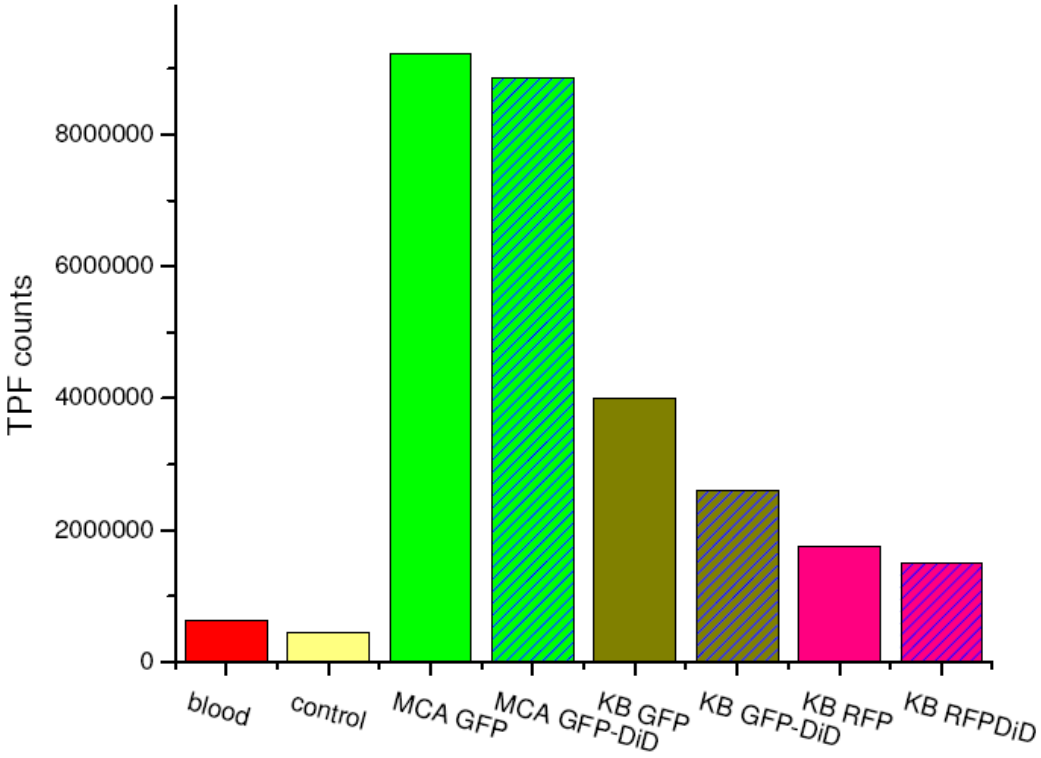

Figure 5.30 Two-photon fluorescence in the short channel measured on undiluted bovine whole blood and cell pellets of unstained MCA-207 cells (control), DiD-stained and unstained GFP-transfected MCA-207 cells, DiD-stained and unstained GFP- transfected KB cells, and DiD-stained and unstained RFP-transfected KB cells.

5.3.6 Effect of flow velocity on the detection rate

The number of cells interrogated is proportional to the amount of fluid that was flowed through the fiber tip. Therefore, it is expected that if the flow rate is increased, the detected cell will increase linearly with the flow rate. For fiber-optics intravital flow cytometry, we propose to put the fiber in a larger vein to monitor the circulating cells.

The reason to put the fiber in a larger vein is not only because of the increased blood volume, but also because of the faster flow speed in a larger blood vessel. Actually, the higher flow speed might be more important. Because of the nature of two-photon excitation, the probe volume is limited. In order to measure more blood, it is important to have more blood flow through the probe region in a limited time period. The solution is to have a higher flow rate.

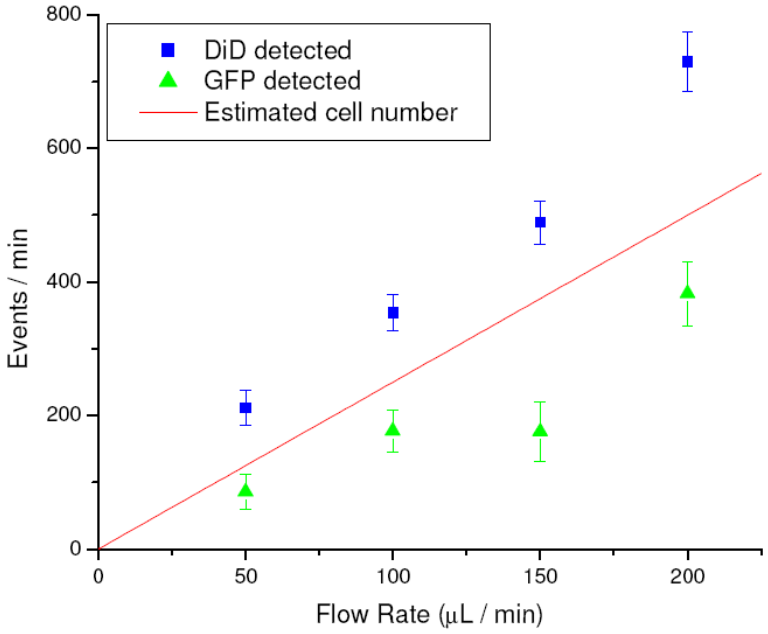

Figure 5.31 The detected number of cells per minute versus the flow rate. DiD-labeled GFP-transfected MCA-207 cells were flowed in a 500-μm plastic tube. The concentration of the cells is 1 x 10^6 /mL. The red line is the predicted number of cells to be detected using the average flow velocity and the cell concentration. The blue squares represent the number of events detected in the long channel (DiD). The green triangles represent the number of events detected in the short channel (GFP). The error bars are the standard errors of the measurements.

Figure 5.31 is the detection rate versus the flow rate. Higher numbers of DiD events were observed, compared to the prediction from the flow rate and cell concentration. This might be due to the fact that when we were conducting the estimation of detected cell numbers, we used the average flow velocity to calculate the detection

frequency. However, the flow velocity profile in the tube is not uniform and the maximum flow velocity at the center of the tube is two-fold higher than the average velocity according to the Hagen-Poiseuille flow profile in fluid mechanics. Therefore, the detection rate is higher when the fiber is closer to the center of the tube. To avoid measurement errors, the fiber and the tube were fixed so that the relative position between them would not change.

We observed a higher detection rate at a higher flow rate. This might be due to the higher momentum of the moving cells. They could get closer to the fiber core and were easier to detect. Otherwise, it might be only because the concentration of the flowing cells was higher at a higher flow rate since, when the cells flowed faster, the settling effect due to gravity was not as severe. Therefore, we detected more cells in a faster flow. However, the detection efficiency of GFP-expressing cells did not seem to change with flow velocity. As we have discussed early, the detection efficiency of GFP cells in fiber-optic flow cytometry is mainly determined by the background photon counts in the short channel. Although more cells are detected in the long channel, the percentage of corresponding short channel events remains about the same at different flow rates. This reveals the difficulty of using the number of cells detected to measure the sampled blood volume. It might be even more problematic for *in vivo* measurement. The viscosity of the blood and the non-uniform flow nature *in vivo* might increase the difficulty of acquiring the accurate sampled volume.

5.3.7 Flow speed measurement with FCS

Figure 5.32(a) shows the FCS curves of the DiD events recorded in the long channel. Figure 5.32(b) plots the mean dwell time of the cell passing though the probe area versus the flow speed. The red line is the theoretical prediction from the sizes of the probe volume and the cell as well as the flow rate. The dwell time was found inversely proportional to the flow rate, as predicted by the theory. We found that using FCS to

measure the speed of flow might be more reliable than cell counting. Although the value measured by FCS is an averaged flow speed, this is enough for us to estimate the sampled blood volume [22].

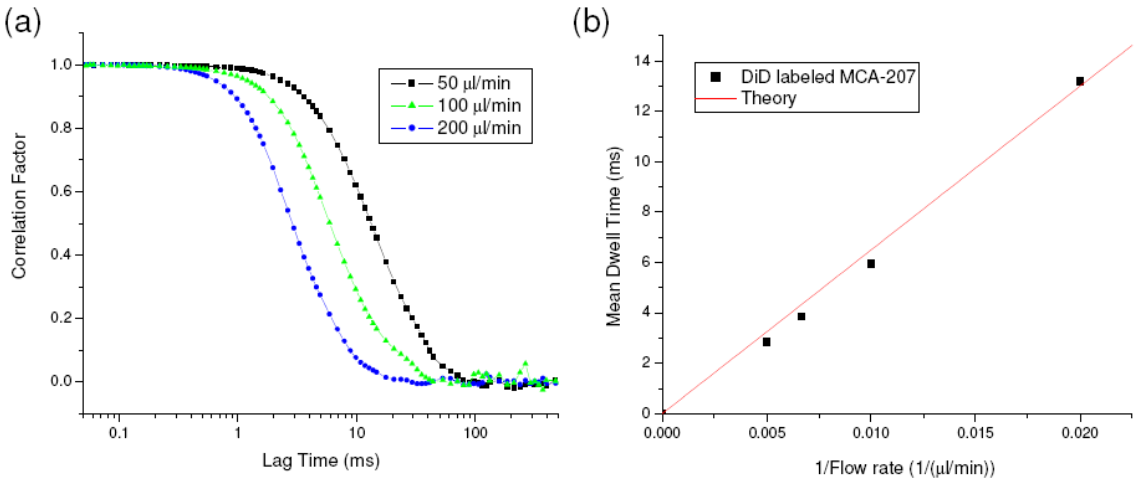

Figure 5.32 (a) Fluorescence correlation curves of detected events in the long channel under flow rates of 50 μL/min (black square), 100 μL/min (green triangle), and 200 μL/min (blue filled circle). (b) The mean dwell time (the lag time at which the correlation factor equals to 0.5) of the correlation curve versus the inverse of the flow rate.

5.4 *In vivo* study

5.4.1 Methods of *in vivo* study

The ultimate goal is to put the fiber probe in a large vein, as in an intravenous drip, to achieve real-time *in vivo* long-term monitoring of rare circulating cancer cells. For proof of principle, the double-clad solid fiber probe was inserted into the left lobe of the liver of the mice to monitor circulating cells in live mouse. The liver was chosen for the proof of principle experiment because of the high density of blood vessels and abundant blood flow in the liver. Male specific-pathogen-free CD1 30-32 mice were purchased from Charles River Laboratories (F38989, Portage, Michigan) and housed in a pathogen-free animal facility at the University of Michigan Medical Center. The handling of the mice was in accordance with the regulations of the University's Committee on the Use and Care of Animals as well as with federal guidelines, including the principles of Laboratory Animal Care [23].

The mice were anesthetized by inhalation of isoflurane before and during the measurements. DiD-labeled, untransfected or DiD-labeled GFP-transfected MCA-207 cells were injected through different places to monitor the circulating and depletion dynamics of the cells. The mice were unconscious but alive throughout the measurements. The mice were sacrificed after the experiments.

Before the injection of the labeled cells, the background signals in both the short and long channels were recorded as the control. The control traces are shown in Figure 5.33. The background trace in the long channel (DiD) was flat; no photon counts higher than 20 were recorded during a recording period of about 3 minutes. The mean photon counts were 2.7 with a standard deviation of 2 photons. However, in the short channel, we noticed periodic spiking with a period of about 2-3 seconds. The periodicity is the

same as the respiration rate of mice. If we blow up the spiking in the short channel, as shown in Figure 5.33(b), a repeatable pattern of the trace can be seen. The green fluctuation might be due to bleeding of the blood vessels in the liver caused by breathing motions. The fluctuations in the short channel make the identification of GFP cells *in vivo* more difficult. There are many kinds of intrinsic autofluorescent fluophores in the blood or tissue with a maximum emission wavelength around the emission wavelength of GFP. Fortunately, because of the capability of conducting dual-channel detection under two-photon excitation, we can use the long channel as the reference to confirm the arrival of a cell in the probe volume, then look for the corresponding signal in the short channel. Using the long channel signal as a reporter to tell us the existence of a cell at the probe volume makes it possible for us to do ratiometric measurements *in vivo*, even with the high background in the short channel.

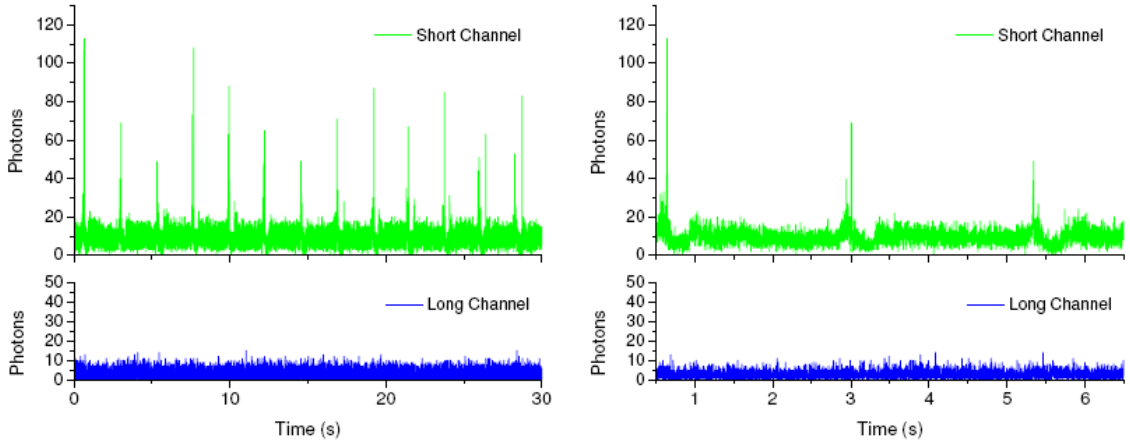

Figure 5.33 (a) Control traces of two-channel two-photon intravital fiber-optic flow cytometry when inserting the fiber probe into the left liver lobe of a mouse without injecting labeled cells in the mouse. Each time point is the number of photons detected by the TCSPC module in 1 ms. The green line represents the short wavelength channel (corresponding to the GFP emission wavelength). The blue line represents the number of photons collected in the long wavelength channel (corresponding to the DiD emission wavelength). (b) Magnified view of the control traces. The fluctuation in the short channel is due to the autofluorescence of the blood and the tissue.

5.4.2 Cell circulating dynamics monitored by fiber-optic *in vivo* cytometry

To demonstrate the ability of using the TPOFF probe to conduct cytometry *in vivo,* 50 μL of DiD-labeled MCA-207 normal cells with a concentration of 50 x 10^6 /mL were injected into the spleen of the mouse. The time traces were recorded right after the injection, as shown in Figure 5.34. We observed the absorption and depletion dynamics of the DiD-labeled cells in the mouse as shown in Figure 5.35. Because the spleen is an organ, the cells injected into the spleen had to be absorbed by the spleen then transported to other locations in the body. It took about 5 minutes for the concentration of the DiD-labeled cells to reach the maximum concentration in the liver; the cells were then quickly filtered out of the circulating system due to repellence.

The average peak maximum of the DiD events was found smaller than those in the *in vitro* measurements. The reason might be that the absorption and recirculation process in the mouse caused the dye stained on the membranes to be washed off. It is also possible that when the fiber was inserting into the liver, there was something attached to the fiber tip, hence reducing the signal strength.

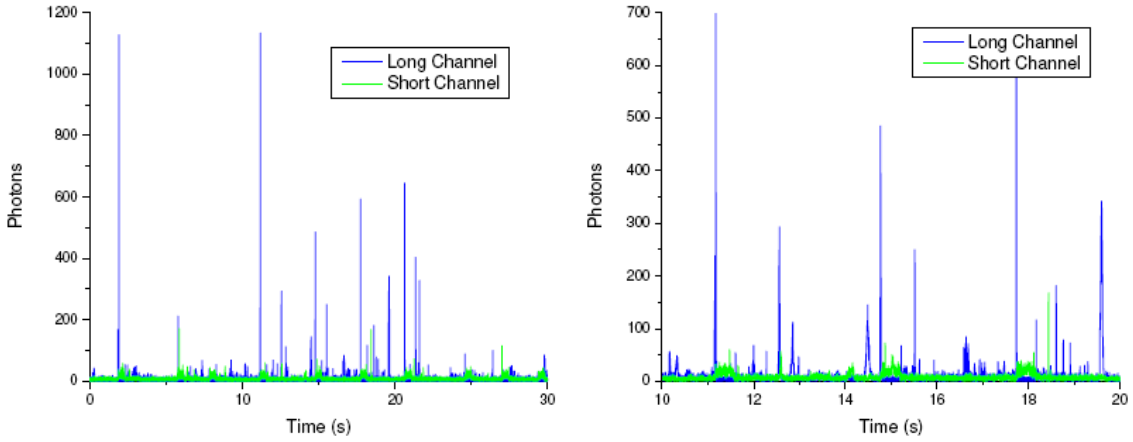

Figure 5.34 Two-photon fiber-optic flow cytometry photon counting traces. The fiber probe was put on the left liver lobe of the mouse and 50 μL of DiD-stained normal MCA-207 cells were injected into the spleen of the mouse. The blue line is the trace of the long channel, and the green line represents the short channel. DiD events can be clearly identified between the fluctuations in the short channel. **(a)** Representative

photon-counting time trace for the *in vivo* measurements in a 30-second period; the actual measurements were taken for more than 3 minutes for each data set. **(b)** The same time trace but only showing a time period of 10 seconds to illustrate the DiD events between the green fluctuation.

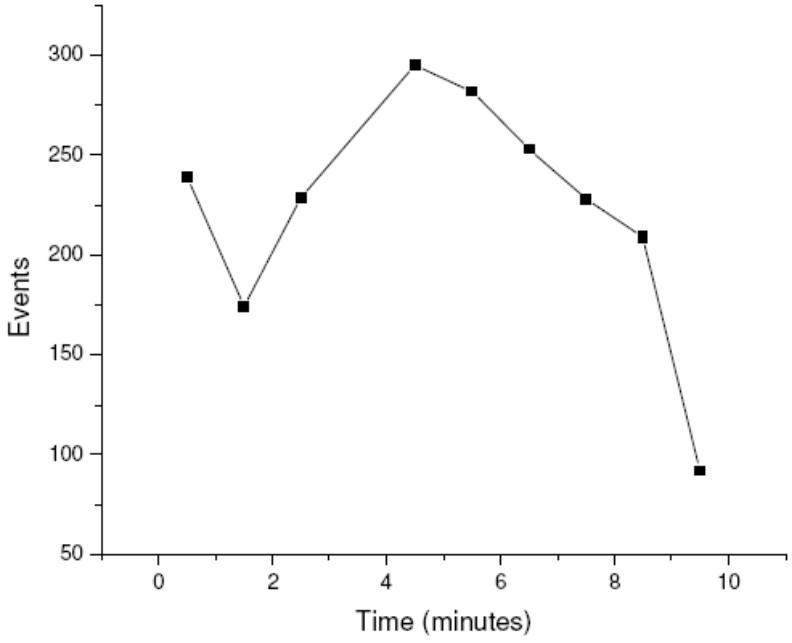

Figure 5.35 The absorption and depletion time course when injecting DiD-stained MCA-207 cells into the spleen of the mice.

To make sure the cells were in the circulation system, 100 μL of the cell suspension were injected through the tail vein of the mice. The cells injected through the tail vein entered the circulating system immediately. Figure 5.36 is the depletion time course when cells were injected through the tail vein. Because those cells did not need to be absorbed, we did not see the increase of the detected cell number in the first few minutes. The cells were only depleted gradually, as reported in the in literature [6, 19].

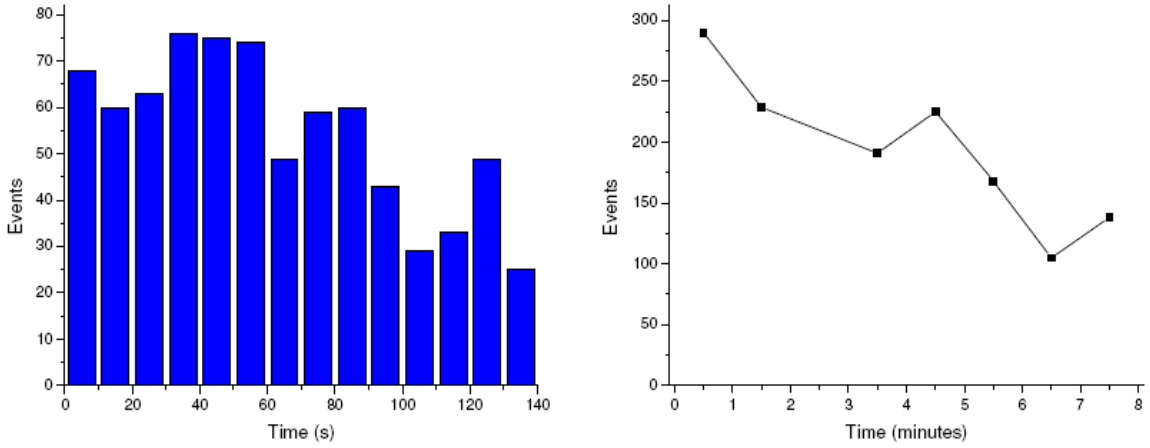

Figure 5.36 (a) Detected events time course in the long channel after injecting 100 μL of DiD-labeled MCA-207 cells at a concentration of 50 x10^6 /mL into the tail vein. Each bar represents the number of peaks counted in 10 seconds. **(b)** The depletion dynamics of the cell clear out from the circulation.

More cells were seen, compared to free space techniques under the same cell concentrations [13]. This might be because we were actually interrogating a larger blood vessel or we were measuring the bleeding through multiple blood capillaries. Compared to the free space scheme, we can only measure one blood vessel at a time. We envision that by putting the fiber probe in a larger blood vessel, we can detect more cells due to the vast blood flow and fast flow velocity.

5.4.3 Monitoring GFP-expressing cells *in vivo*

Because of the autofluorescence of the tissue and the blood, it was difficult to identify the GFP cell events. Fortunately, we could label the cells with the membrane-binding lipophilic dye DiD and use the signals in the long channel to register the coming of a cell of interest to the probe volume. Figure 5.37 shows representative time traces of the raw data where some of the peaks occurred at the same time in both channels, indicating dual-labeled cells. Because of the low background in the long channel and the high TPF brightness of DiD, we can use DiD events as a reporter to do ratiometric measurements as in the *in vitro* study.

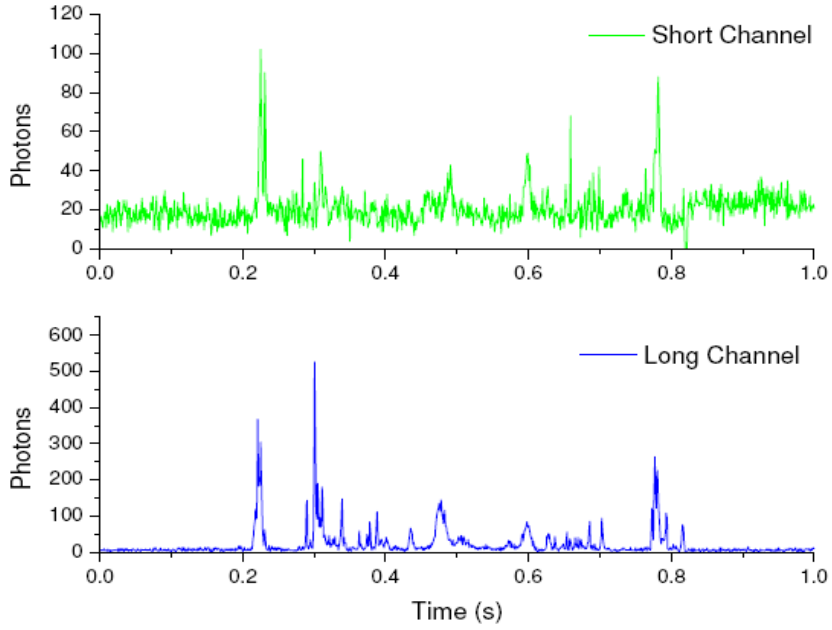

Figure 5.37 In vivo interrogating of dual-labeled cells in two channels.

The correlation of the peak widths in two channels is shown in Figure 5.38. The peak widths are somewhat correlated, but not as clear as those in the *in vitro* measurement. This is because that the fiber probe was not put in a freely flowing fluid but in an organ. The environment could be complicated around the fiber. Therefore when the cells move around the probe volume, many things could affect the path of the cells, hence affecting the peak widths. The energy distribution of the correlated peaks is shown in Figure 5.39. The energy distribution scatter plot is similar to what we have seen in the *in vitro* measurements.

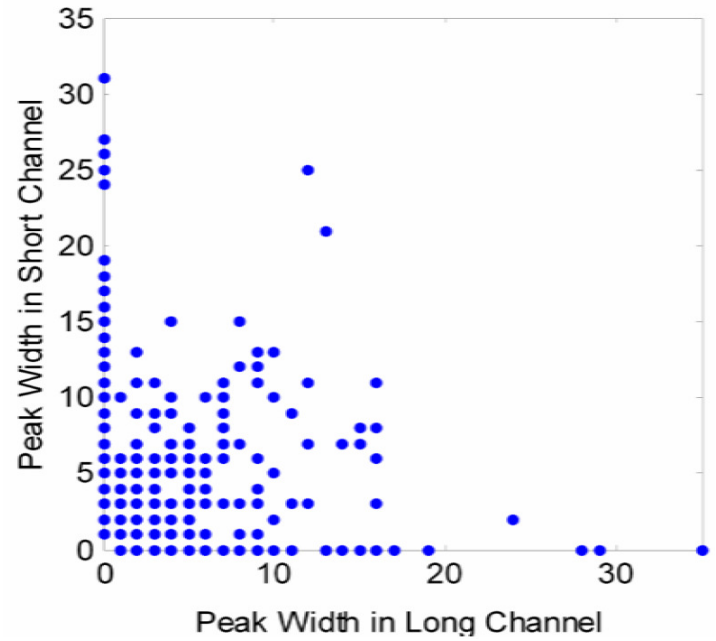

Figure 5.38 Scatter plot of the energy distribution of correlated peaks in the short channel and the long channel. Each dot in this graph represents a correlated peak between the short channel and the long channel.

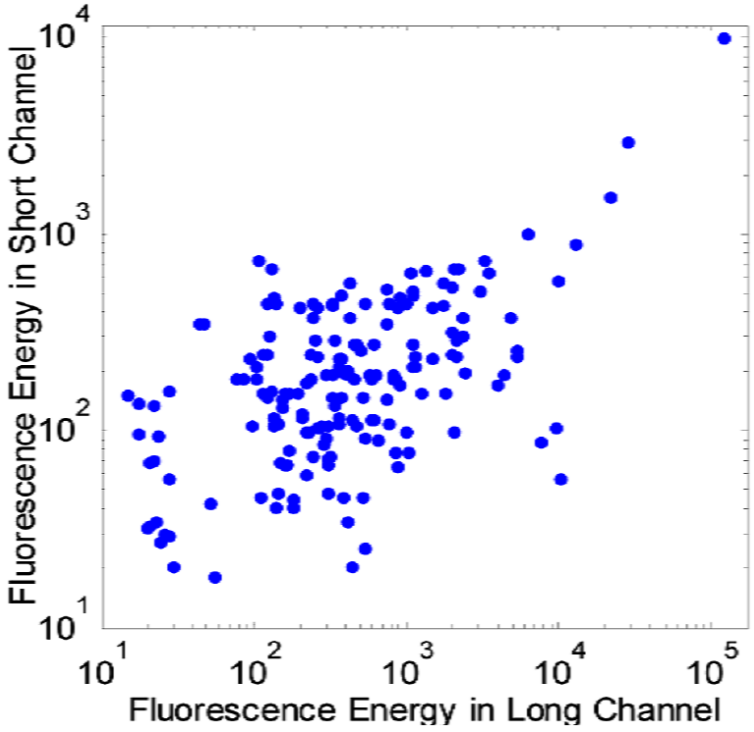

Figure 5.39 Scatter plot of the energy distribution of the correlated peaks.

Dual-labeled GFP-DiD cells were injected into the mice through multiple locations. The average numbers of detected events per minute in the two channels are illustrated in Figure 5.40. The red bars represent the number of cells detected in the long-wavelength channel, and the green bars are the number of events detected in both channels. Because of the sizes of the organs, the injected volumes of the cell suspensions were different. We injected 100 μL into the tail vein, 50μL into the right lobe of the liver, 50 μL into the spleen, and 30 μL into the heart. The values plotted in the figure are the numbers normalized by assuming the same injection volumes as in the tail vein injection case. The number of events detected for cells injected into the tail vein and heart are similar, as they both enter the circulating directly. The number of events detected for cells injected into the spleen is the fewest since the cells need to be absorbed before they can enter the circulation to reach the liver. In addition, the cells could be depleted or lodged in the organs before they can enter the circulation.

When a cell flows through the probe volume, we are supposed to see peaks occur in both channels at the same time if the TPF signals of both fluophores have the same magnitude. However, because of the lower TPF brightness of GFP, we have fewer events in the GFP corresponding channel. The overall possibility to have identifiable events occur simultaneously in both channels was 27%±7%. This value is consistent with the *in vitro* measurements in whole blood.

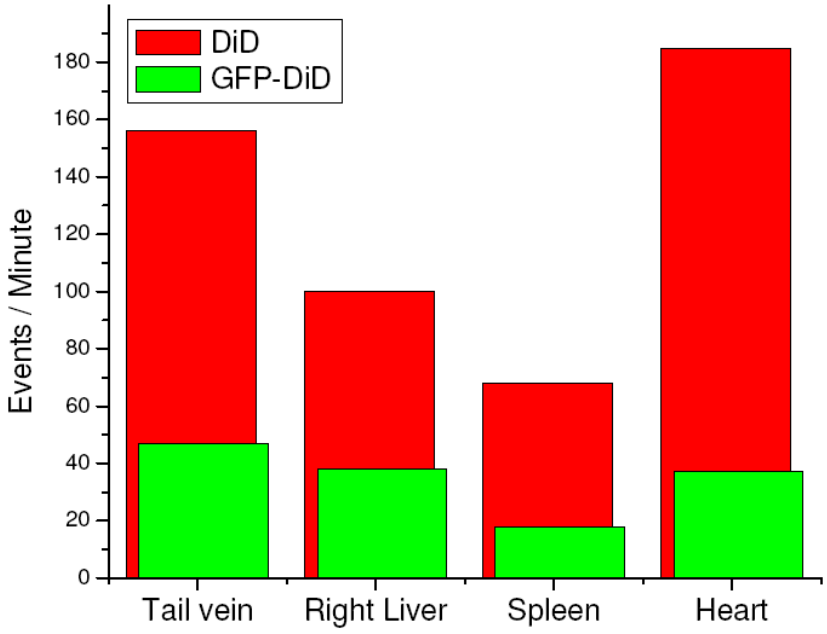

Figure 5.40 The number of detected events in the long channel (red bars, DiD) and in both channels (green bars, GFP-DiD) per minute in the *in vivo* measurements. The fiber probe was put on the left lobe of the liver and the dual-labeled cells were injected through different places: tail vein, right lobe of the liver, spleen, and the heart.

5.5 Conclusions

The use of a two-photon excitation fluorescence double-clad fiber probe to conduct flow cytometry has been demonstrated in this study. A proof of principle experiment to use the fiber probe to implement *in vivo* flow cytometry is demonstrated.

A big hurdle for applying *in vivo* flow cytometry to the clinical study of either one-photon or two-photon excitation is the difficulty of sampling a large volume of blood. For the purpose of detecting rare circulating tumor cells (CTCs) *in vivo*, a large volume of blood needs to be sampled. By using the TPOFF probe, we have demonstrated the enhanced sensitivity to detect cells *in vivo* while the signal-to-noise ratio is on the same order when compared with the free space scheme in *in vitro* studies. The high collection efficiency of the fiber-optic based system was due to the high numerical

aperture (NA) of the inner cladding of the fiber. This is the first demonstration of using a bare single double-clad fiber to conduct *in vivo* measurements in a living animal. The overall collection of the system was found to be about 0.5%, which is comparable to the 1% collection efficiency of a typical fluorescence microscope [24, 25].

High detection efficiency of the GFP-transfected cells has been demonstrated as well. The detection efficiency of GFP-expressing cells is about one order of magnitude higher than the free space scheme when measuring flowing cells in bovine whole blood *in vitro*. The enhancement is believed to be more significant if we compare the *in vivo* measurements.

For free space measurements, because of the scattering and absorption issue of the biological samples, the penetration depth is limited. Therefore, only peripheral blood vessels could be measured. The amount of blood sampled is thus limited.

Because of the high TPF brightness of DiD and the low background in its emission wavelength range (the long channel), the cells labeled with DiD showed high detection efficiency. The detected number of DiD cells was confirmed to be about the same as the predicted detectable cell numbers. If we assume the number of DiD events as the total number of cells interrogated, we can do a ratiometric measurement to determine the detection efficiency of GFP-expressing cells. The overall detection efficiency of GFP-expressing cells was found to be around 30% in whole blood or *in vivo*. This detection efficiency is higher than in a free space scheme, which has a detection efficiency of less than 5% in whole blood under comparable signal strength when flowing the cells in PBS buffer. The significantly higher sensitivity of detecting GFP-expressing cells *in vivo* makes the TPOFF probe a superior tool for studying cancer metastasis in animal models.

5.6 References

1. K. Pantel, R. H. Brakenhoff, and B. Brandt, "Detection, clinical relevance and specific biological properties of disseminating tumour cells," Nat Rev Cancer 8, 329-340 (2008).
2. R. Weissleder, and M. J. Pittet, "Imaging in the era of molecular oncology," Nature 452, 580-589 (2008).
3. M. Cristofanilli, G. T. Budd, M. J. Ellis, A. Stopeck, J. Matera, M. C. Miller, J. M. Reuben, G. V. Doyle, W. J. Allard, L. W. Terstappen, and D. F. Hayes, "Circulating tumor cells, disease progression, and survival in metastatic breast cancer," N Engl J Med 351, 781-791 (2004).
4. W. He, H. F. Wang, L. C. Hartmann, J. X. Cheng, and P. S. Low, "In vivo quantitation of rare circulating tumor cells by multiphoton intravital flow cytometry," Proceedings of the National Academy of Sciences of the United States of America 104, 11760-11765 (2007).
5. E. R. Tkaczyk, C. F. Zhong, J. Y. Ye, A. Myc, T. Thomas, Z. Cao, R. Duran-Struuck, K. E. Luker, G. D. Luker, T. B. Norris, and J. R. Baker, "In vivo monitoring of multiple circulating cell populations using two-photon flow cytometry," Optics Communications 281, 888-894 (2008).
6. C. F. Zhong, E. R. Tkaczyk, T. Thomas, J. Y. Ye, A. Myc, A. U. Bielinska, Z. Cao, I. Majoros, B. Keszler, J. R. Baker, and T. B. Norris, "Quantitative two-photon flow cytometry--in vitro and in vivo," J Biomed Opt 13, 034008 (2008).
7. J. Novak, I. Georgakoudi, X. Wei, A. Prossin, and C. P. Lin, "In vivo flow cytometer for real-time detection and quantification of circulating cells," Optics Letters 29, 77-79 (2004).
8. S. Boutrus, C. Greiner, D. Hwu, M. Chan, C. Kuperwasser, C. P. Lin, and I. Georgakoudi, "Portable two-color in vivo flow cytometer for real-time detection of fluorescently-labeled circulating cells," J Biomed Opt 12, 020507 (2007).
9. C. Alt, I. Veilleux, H. Lee, C. M. Pitsillides, D. Cote, and C. P. Lin, "Retinal flow cytometer," Opt Lett 32, 3450-3452 (2007).
10. T. P. Thomas, J. Y. Ye, Y. C. Chang, A. Kotlyar, Z. Cao, I. J. Majoros, T. B. Norris, and J. R. Baker, "Investigation of tumor cell targeting of a dendrimer nanoparticle using a double-clad optical fiber probe," J. Biomed. Opt. 13, 6 (2008).
11. T. P. Thomas, M. T. Myaing, J. Y. Ye, K. Candido, A. Kotlyar, J. Beals, P. Cao, B. Keszler, A. K. Patri, T. B. Norris, and J. R. Baker, Jr., "Detection and analysis of tumor fluorescence using a two-photon optical fiber probe," Biophys J 86, 3959-3965 (2004).

12. Y. C. Chang, J. Y. Ye, T. Thomas, Y. Chen, J. R. Baker, and T. B. Norris, "Two-photon fluorescence correlation spectroscopy through a dual-clad optical fiber," Opt. Express 16, 12640-12649 (2008).
13. C. F. Zhong, "Quantitative Two-photon Flow Cytometry - in vitro and vivo," in Applied Physics(University of Michigan, Ann Arbor, 2006).
14. D. P. a. R. Stovel, "Flow chambers and sample handling," in Flow cytometry: Instrumentation and Data Analysis, P. N. D. M.A. Van Dilla, O.D. Laerum, and M.R. Melamed, ed. (Academic, London, 1985).
15. M. G. Oelamed, Flow Cytometry (Pringer-Verlag, New York, 1999).
16. C. Xu, W. Zipfel, J. B. Shear, R. M. Williams, and W. W. Webb, "Multiphoton fluorescence excitation: new spectral windows for biological nonlinear microscopy," Proc Natl Acad Sci U S A 93, 10763-10768 (1996).
17. O. Shimomura, F. H. Johnson, and Y. Saiga, "Extraction, purification and properties of aequorin, a bioluminescent protein from the luminous hydromedusan, Aequorea," J Cell Comp Physiol 59, 223-239 (1962).
18. C. F. Zhong, E. R. Tkaczyk, T. Thomas, J. Y. Ye, A. Myc, A. U. Bielinska, Z. Cao, I. Majoros, B. Keszler, J. R. Baker, and T. B. Norris, "Errata: Quantitative two-photon flow cytometry-in vitro and in vivo," J Biomed Opt 13, 059801 (2008).
19. I. Georgakoudi, N. Solban, J. Novak, W. L. Rice, X. Wei, T. Hasan, and C. P. Lin, "In vivo flow cytometry: a new method for enumerating circulating cancer cells," Cancer Res 64, 5044-5047 (2004).
20. E. R. Tkaczyk, A. H. Tkaczyk, S. Katnik, J. Y. Ye, K. E. Luker, G. D. Luker, A. Myc, J. R. Baker, Jr., and T. B. Norris, "Extended cavity laser enhanced two-photon flow cytometry," J Biomed Opt 13, 041319 (2008).
21. W. R. Zipfel, R. M. Williams, and W. W. Webb, "Nonlinear magic: multiphoton microscopy in the biosciences," Nature Biotechnology 21, 1368-1376 (2003).
22. E. L. Elson, "Quick tour of fluorescence correlation spectroscopy from its inception," Journal of Biomedical Optics 9, 857-864 (2004).
23. T. P. Thomas, M. T. Myaing, J. Y. Ye, K. Candido, A. Kotlyar, J. Beals, P. Cao, B. Keszler, A. K. Patri, T. B. Norris, and J. R. Baker, "Detection and analysis of tumor fluorescence using a two-photon optical fiber probe," Biophysical Journal 86, 3959-3965 (2004).
24. J. Mertz, C. Xu, and W. W. Webb, "Single-molecule detection by two-photon-excited fluorescence," Optics Letters 20, 2532-2534 (1995).
25. J. Mertz, C. Xu, and W. W. Webb, "Single molecule detection by two-photon excited fluorescence," Biophysical Journal 70, Wamj1-Wamj1 (1996).

CHAPTER 6
Summary and Outlook

6.1 Summary

***In vivo* biosensing prior to this work:**

- Even with two-photon excitation by NIR lasers, the maximum penetration depth was only a few hundred micrometers in the tissue [1]. It was impossible to have quantitative measurements on tumors deep inside the body.
- The two-photon optical fiber fluorescence (TPOFF) probe system was developed in our group to conduct localized fluorescence detection in deep tissue. However, the single-mode fiber-based system did not have adequate sensitivity for quantifying low-level fluorescence signals, such as non-specific binding of nanoparticles or autofluorescence from endogenous fluorophores [2].
- The double-clad photonic crystal fiber (DCPCF) was introduced to increase the sensitivity of the probe. However, the uptake of liquid by the air holes in the fiber precluded its application in aqueous biological environments [3, 4].
- *In vivo* flow cytometry implemented by microscope-based free-space methods was demonstrated, but only peripheral blood vessels can be accessed, which limits the sampled blood volume [3]. In addition, anesthesia is required to stabilize the object, which precludes the possibility of long-tem monitoring. To practically enumerate rare circulating tumor cells, long-term monitoring is necessary to acquire enough blood volume.

Principal results of this work:

- Solid double-clad fibers were employed for TPOFF probe. High sensitivity TPOFF measurements were conducted in aqueous biological environments [4]. The fluorescence signal collection efficiency was comparable to a conventional objective-lens-based microscope.
- Fluorescence lifetime measurements were implemented *in situ* with TPOFF probe.
- Few-nanomolar concentrations of multiple fluorescent conjugates with different emission wavelengths and lifetimes were discerned simultaneously in the tumors.
- Two-photon-excitation fiber-based fluorescence correlation spectroscopy (2P-FFCS) was demonstrated [5].
- Fiber-optic two-photon excitation flow cytometry was performed *in vitro* and *in vivo*. Significantly higher detection efficiency of green fluorescent protein-expressing cells is achieved compared to free-space methods. The technique enables long-term real-time monitoring of circulating cells deep inside the body.

Publications related to works in this dissertation:

1. Y. C. Chang, J. Y. Ye, T. Thomas, Y. Chen, J. R. Baker, and T. B. Norris, "Two-photon fluorescence correlation spectroscopy through a dual-clad optical fiber," *Opt. Express* **16**, 12640-12649 (2008).
2. T. P. Thomas, J. Y. Ye, Y. C. Chang, A. Kotlyar, Z. Cao, I. J. Majoros, T. B. Norris, and J. R. Baker, "Investigation of tumor cell targeting of a dendrimer nanoparticle using a double-clad optical fiber probe," *J. Biomed. Opt.* **13**, 6 (2008).
3. Y. C. Chang, J. Y. Ye, T. P. Thomas, A. Kotlyar, E. R. Tkaczyk, J. R. Baker, and T. B. Norris, "Fiber-optic multiphoton *in vivo* flow cytometry," *Proceedings of SPIE* (2009).

Manuscripts in Preparation:

4. T. P. Thomas, Y. C. Chang, J. Y. Ye, S. Qin, A. Kotlyar, Z. Cao, T. B. Norris, and J. R. Baker, Jr., "In situ Quantification of Human Epidermal Growth Factor Receptor 2 using a Two-photon Optical Fiber Probe," to be submitted to J. Biomedical Optics.
5. Y. C. Chang, J. Y. Ye, T. P. Thomas, A. Kotlyar, E. R. Tkaczyk, J. R. Baker, and T. B. Norris, "Dual-channel fiber-optic multiphoton *in vivo* flow cytometry," to be submitted to Journal of Biomedical Optics.

In this dissertation, we first briefly reviewed the current methodologies and the difficulties inherent in deep-tissue biosensing. The need for practical and quantitative diagnostic tools for dealing with cancer or inflammation disease was addressed. The advantages of combining two-photon excitation and fiber-optics for fluorescence measurements provided an alternative avenue to conducting minimally invasive deep-tissue fluorescence biosensing.

The two-photon optical fiber fluorescence (TPOFF) probe system described in this dissertation employed the scheme where the same fiber is used for both the excitation and collection of the fluorescence. The instrumentation of the TPOFF probe system was described and characterized in detail in Chapter 2. The methods of delivering ultrafast optical pulses through fused glass fibers were discussed. Due to possible tissue damage of the *in vivo* measurements, the applied power was kept around or below 20 mW. This corresponds to a pulse energy of 0.25 nJ for the Ti:Sapphire oscillator in our system. The fiber nonlinearity was not a limiting factor at this power level; i.e., pulse broadening due to self phase modulation (SPM) in the fiber could be neglected. The trade-off between the high excitation efficiency of single-mode fibers (SMF) and the high fluorescence collection efficiency of high numerical-aperture (NA) multi-mode fibers (MMF) was discussed. It is desirable to maintain the high excitation efficiency by propagating the pulses through a single-mode core while using a high-NA multi-mode fiber for signal collection. A double-clad photonic crystal fiber (DCPCF) was employed previously to increase the detection sensitivity in our group [6]. It has a single-mode core and high NA multi-mode inner cladding surrounded by an outer cladding. The TPF can be collected by both the core and the inner cladding. The sensitivity of the DCF was found to be more than one order of magnitude higher than the SMF. However, the uptake of liquid due to capillary effect in the air holes limited the application of the DCPCF from *in vivo* applications. In this dissertation work, a solid core double-clad fiber (DCF) was used. The sensitivity was the similar to that of the DCPCF. There is no holes in the fiber, so it

can be inserted into biological tissues without any limitation. The enhanced sensitivity and the ability to conduct measurements in aqueous environments open up a range of new applications for the DCF-TPOFF probe system.

A time-correlated single-photon counting (TCSPC) detection module was integrated with the system to enable time-resolved measurements. The operating principle of a TCSPC system was described. With the ability to conduct time-resolved measurements through the TPOFF probe, fluorescence analytic techniques, such as fluorescence lifetime or fluorescence correlation spectroscopy (FCS), can be implemented *in situ*. Some disease-induced biochemical changes take place in the molecular level before the structural transformation can be identified by microscope [8, 9]. With these molecular spectroscopic analysis techniques, the TPOFF probe developed here can be used to detect these early diseases.

Biological applications with the TPOFF probe for *in vivo* and *in vitro* studies were presented in Chapter 3. SMF and the solid core DCF probes were used to measure the uptake of dendrimer nanoparticles in mouse tumors. Higher detection efficiency with the DCF probe has been demonstrated. The DCF probe showed the ability to detect and quantify few-nanomolar concentrations of dendrimers. In the *in vitro* studies, nanomolar concentrations of multiple fluorophores with different emission wavelengths or having different lifetimes were identified and quantified using the technique. In the *in vivo* studies, the DCF showed a 5-fold enhancement over the SMF. Threading the fiber through a 30-gauge needle (300-μm outer diameter) to implement optical biopsy in the tumors makes this probe a superior optical diagnostic tool in quantifying fluorescently tagged nanoparticles and in monitoring targeted drug delivery in deep tissues. Simultaneous detection of multiple *in vivo* targeted Herceptin conjugates with different emission wavelengths has also been demonstrated. We envision that this DCF-TPOFF probe will serve as a minimally invasive diagnostic tool for screening cancer signatures, such as the human EGF-receptor 2 (HER2) in breast cancer.

Because of its ability to conduct fluorescence measurements in aqueous solutions, it is feasible for the TPOFF probe to conduct FCS measurements. A fiber-optics-based two-photon fluorescence correlation spectroscopy system was demonstrated for the first time with our double-clad TPOFF system. The ability to detect fluorescent nanospheres as small as 12 nm in radius was demonstrated. We have also shown that a smaller detection size limit is achievable when quantum dots (7 nm in radius) are employed as the fluorescent probe because of its large two-photon excitation cross-section. Our study showed that it is critical to employ a double-clad fiber for a fiber-based two-photon FCS measurement to achieve adequate sensitivity for the measurement of fluorescent nanoparticles. With the pulsed 2PE scheme, multiple fluophores with different excitation maxima can be excited simultaneously, and fluophores with different lifetimes can also be discerned.

Because of its ability to conduct *in vivo* fluorescence measurements in deep tissue, the TPOFF probe is suitable for intravital flow cytometry in order to achieve the ultimate goal of long-term monitoring of circulating cells *in vivo* on a real-time basis. In Chapter 5, we first reviewed the need for and the current advance toward *in vivo* flow cytometry. The experimental results using a double-clad TPOFF probe for *in vitro* and *in vivo* studies were presented. In the *in vitro* studies, it was found that the corpuscular property of the whole blood had almost no effect on the detected signal strength, which was a big hurdle for the free-space detection scheme. A ~30% detection efficiency of GFP-expressing cells in whole blood was demonstrated. The lower detection efficiency of GFP-expressing cells was because of the higher autofluorescence background from the whole blood, which was discussed in Chapter 5. The fiber probe was then used to monitor circulating cells in mice *in vivo*. The probe was inserted into the liver of the mice for the proof-of-principle experiment due to the abundant blood flow in the liver. With the ability to simultaneously detect multiple fluorescence signals in different wavelength channels, we could monitor the circulation of GFP-expressing cells—even with the noisy

background in the GFP-wavelength channel. The event dynamics were studied. The detection efficiency was consistent with the *in vitro* studies. The ability to conduct multi-color detection of circulating cells *in vivo* on a real-time basis was demonstrated. The significantly higher sensitivity of detecting GFP-expressing cells *in vivo* makes the TPOFF probe an ideal tool for studies of cancer metastasis in mouse tumor models. Because no anesthesia is needed when applying the probe to intravenous measurements, with other technical advances, such as effective *in vivo* labeling of specific cells and enhanced brightness of shorter-wavelength fluorescent proteins, this technique can be adapted for clinical use in the ultimate goal of real-time, long-term monitoring of circulating cancer cells *in vivo*.

6.2 Future improvements and potential applications

6.2.1 Miniaturized probe for *in vivo* microscopy and endoscopy

Laser scanning microscopy has been an invaluable research tool in the field of ife science. However, because of the bulky optics in conventional microscope, such as the objective, it is difficult to conduct deep-tissue imaging *in vivo*. As is described previously, the use of a double-clad fiber (DCF) significantly increased the collection efficiency when using a fiber probe to conduct the microscopy. By combining a double-clad photonic crystal fiber (DCPCF) and a GRIN lens, a compact nonlinear microscope has been constructed in our group by J.Y. Ye *et al.*[7]. With the fiber scanning scheme, a large scanning area can be achieved. Imaging of GFP-transfected cells was demonstrated [7].

Although a GRIN lens is only 1.8 mm in diameter, however, the applicable locations of this probe for *in vivo* microscopy were limited. In order to miniaturize the probe size, we could fabricate a micro-lens on the core of the fiber tip by two-photon

polymerization [8, 9]. Femtosecond pulses can be delivered through the core of the fiber while the other end of the fiber is immersed in photosensitive material. By the process of two-photon polymerization, a micro-structure with a size comparable to the wavelength of the laser could be formed at the fiber tip. The shape of the micro-structure is determined by the two-photon excitation volume. Therefore, a lens-shaped structure can be formed on the core of the fiber. With the micro-lens at the output of the fiber, the output beam can be further focused down to a smaller spot on the order of the laser wavelength. Thus, we can use the fiber directly for scanning microscopy, and no additional optics are required. The size of the microscope probe is then only the size of a single-mode fiber, which greatly enhances the feasibility of conducting deep-tissue microscopy or endoscopy. Furthermore, because of the reduced focal spot size, the 2PE efficiency is enhanced because of the tighter focus. In addition, the collection efficiency now is determined by the NA of the micro-lens rather than by the NA of the single-mode core, so the collection efficiency is also improved.

In addition to microscopy, a reduced focal spot size implies a reduced two-photon excitation volume in fluorescence correlation spectroscopy (FCS). As is discussed in Chapter 4, the biggest difficulties of conducting fiber-optic-based 2PE FCS are the lower excitation efficiency compared to a high-NA objective lens-based system and the larger excitation volume which is determined by the size and the NA of the core. Those problems could be solved by fabricating a micro-lens on the core of the probing end, and the sensitivity of the fiber-optic 2PE FCS measurements can be enhanced.

6.2.2 FCS for cell measurements

We demonstrated that by applying FCS in flow cytometry, we can use the FCS technique to distinguish differently labeled cells. The membrane-tagged DiD-labeled cells and cytoplastic GFP-expressing cells showed different decay behaviors in the FCS curves. It is also possible to use FCS to monitor cell apoptosis [10]. With the ability to

conduct deep tissue biosensing *in vivo*, we can use the TPOFF probe to monitor the response of tumor cells to the drugs *in vivo* on a real-time basis as the diffusion rate might differ when the targeted durg binds to the receptor.

Because of the ability to detect multiple dyes with a single laser, we can label normal cells with one dye and the apoptotic cells with another. By comparing the ratio of change between the signals in two channels, we can monitor cell apoptosis in real time.

6.2.3 Use of low repetition rate, higher energy pulses to increase the two-photon fluorescence signal

In order to increase the two-photon fluorescence (TPF) signal, the easiest way is to increase the excitation power. However, from our observations, when the power at the SMF tip is higher than 20mW, tissue damage could be sensed. Therefore, it is not practical to increase the power. Instead, we can reduce the repetition rate of the laser while maintaining the average power. The increased pulse energy means higher peak intensity. Although the nonlinearity in the glass fiber would cause a sub-quadratic relation between the applied pulse energy and the TPF signal, it has been shown that as long as the increase of the pulse energy is faster than the pulse width, the TPF signal still increases [11]. There are multiple ways to reduce the repetition rate and increase the pulse energy, including using an extended cavity oscillator [12], cavity dumping [13], or using a regenerative amplifier [14].

Enhanced detection efficiency of GFP-expressing cells has been demonstrated in the free-space detection scheme by an extended cavity laser compared to the same 76-MHz seed oscillator used in the work of this dissertation by E. Tkaczyk [15]. He found that the fraction of detectable GFP-expressing cells in the total detected cells (determined by the signal in the long channel) versus the excitation pulse energy has a sigmoid shape. This nonlinear behavior of the detection efficiency on the pulse energy dependence

implies that if the pulse energy is higher than a critical threshold, a modest increase in the pulse energy can improve the detection sensitivity more than linearly [15].

6.2.4 Compact ultrafast fiber lasers to reduce system size

The ultimate goal would be to develop this technique as a portable system to enable long-term real-time monitoring for clinical use. It is possible to use a compact fiber laser to reduce the size of the system. The laser system we are using right now is a solid-state Ti:Sapphire mode-locked oscillator (Mira, Coherent Inc.). The laser itself takes up at least 3 square feet of space. Over the last decade, there has been a significant advancement in the development of ultrafast fiber lasers [16]. The fiber lasers provide sufficient power plus have advantages such as low cost, compact size, and maintenance-free. For example, the Femtolite Ultra series from IMRA America Inc. has a size of (14.5 x 10 x 4 cm) and generates pulse energy of the same order as we are using in fiber-optic biosensing [17]. In addition, with a fiber pigtailed output from a fiber laser, it can easily be combined with our fiber probe through splicing. By combining the wavelength division multiplexer (WDM) fiber coupler, the signal can be separated from the excitation laser at the detection end to reduce the background noise from autofluorescence and backscattering of the fiber while, at the probe end, the single fiber detection scheme can be maintained for efficient *in vivo* measurements. With a compact size and high sensitivity, the fiber laser-based TPOFF system can serve as a portable real time health monitoring device for therapeutic treatment surrveillance.

6.3 References

1. F. Helmchen, and W. Denk, "Deep tissue two-photon microscopy," Nature Methods **2**, 932-940 (2005).
2. J. Y. Ye, M. T. Myaing, T. B. Norris, T. Thomas, and J. Baker, "Biosensing based on two-photon fluorescence measurements through optical fibers," Optics Letters **27**, 1412-1414 (2002).
3. C. Alt, I. Veilleux, H. Lee, C. M. Pitsillides, D. Cote, and C. P. Lin, "Retinal flow cytometer," Opt Lett **32**, 3450-3452 (2007).
4. C. F. Zhong, E. R. Tkaczyk, T. Thomas, J. Y. Ye, A. Myc, A. Bielinska, Z. Cao, I. Majoros, K. Balazs, J. R. Baker, and T. B. Norris, "Quantitative Two-Photon Flow Cytometry – in Vitro and in Vivo," Journal of Biomedical Optics **13** (2008).
5. Y. C. Chang, J. Y. Ye, T. Thomas, Y. Chen, J. R. Baker, and T. B. Norris, "Two-photon fluorescence correlation spectroscopy through a dual-clad optical fiber," Opt. Express **16**, 12640-12649 (2008).
6. M. T. Myaing, J. Y. Ye, T. B. Norris, T. Thomas, J. R. Baker, W. J. Wadsworth, G. Bouwmans, J. C. Knight, and P. S. J. Russell, "Enhanced two-photon biosensing with double-clad photonic crystal fibers," Optics Letters **28**, 1224-1226 (2003).
7. J. Y. Ye, M. T. Myaing, T. P. Thomas, I. Majoros, A. Koltyar, J. R. Baker, W. J. Wadsworth, G. Bouwmans, J. C. Knight, P. S. J. Russell, and T. B. Norris, "Development of a double-clad photonic-crystal-fiber based scanning microscope," in *Conference on Multiphoton Microscopy in the Biomedical Sciences V*, A. S. P. T. C. Periasamy, ed. (Spie-Int Soc Optical Engineering, San Jose, CA, 2005), pp. 23-27.
8. J. Serbin, A. Egbert, A. Ostendorf, B. N. Chichkov, R. Houbertz, G. Domann, J. Schulz, C. Cronauer, L. Frohlich, and M. Popall, "Femtosecond laser-induced two-photon polymerization of inorganic-organic hybrid materials for applications in photonics," Opt. Lett. **28**, 301-303 (2003).
9. B. H. Cumpston, S. P. Ananthavel, S. Barlow, D. L. Dyer, J. E. Ehrlich, L. L. Erskine, A. A. Heikal, S. M. Kuebler, I. Y. S. Lee, D. McCord-Maughon, J. Q. Qin, H. Rockel, M. Rumi, X. L. Wu, S. R. Marder, and J. W. Perry, "Two-photon polymerization initiators for three-dimensional optical data storage and microfabrication," Nature **398**, 51-54 (1999).
10. M. Keese, M. Offterdinger, C. Tischer, A. Girod, P. H. Lommerse, V. Yagublu, R. Magdeburg, and P. I. Bastiaens, "Quantitative imaging of apoptosis commitment in colorectal tumor cells," Differentiation **75**, 809-818 (2007).

11. M. T. Myaing, J. Urayama, A. Braun, and T. B. Norris, "Nonlinear propagation of negatively chirped pulses: Maximizing the peak intensity at the output of a fiber probe," Optics Express **7**, 210-214 (2000).
12. S. H. Cho, F. X. Kartner, U. Morgner, E. P. Ippen, J. G. Fujimoto, J. E. Cunningham, and W. H. Knox, "Generation of 90-nJ pulses with a 4-MHz repetition-rate Kerr-lens mode-locked Ti:Al(2)O(3) laser operating with net positive and negative intracavity dispersion," Opt Lett **26**, 560-562 (2001).
13. M. Ramaswamy, M. Ulman, J. Paye, and J. G. Fujimoto, "CAVITY-DUMPED FEMTOSECOND KERR-LENS MODE-LOCKED TI-AL2O3 LASER," Optics Letters **18**, 1822-1824 (1993).
14. T. B. Norris, "FEMTOSECOND PULSE AMPLIFICATION AT 250 KHZ WITH A TI-SAPPHIRE REGENERATIVE AMPLIFIER AND APPLICATION TO CONTINUUM GENERATION," Optics Letters **17**, 1009-1011 (1992).
15. E. R. Tkaczyk, A. H. Tkaczyk, S. Katnik, J. Y. Ye, K. E. Luker, G. D. Luker, A. Myc, J. R. Baker, Jr., and T. B. Norris, "Extended cavity laser enhanced two-photon flow cytometry," J Biomed Opt **13**, 041319 (2008).
16. L. Shah, and M. Fermann, "High-power ultrashort-pulse fiber amplifiers," IEEE J. Sel. Top. Quantum Electron. **13**, 552-558 (2007).
17. http://www.imra.com.